Angewandte Chemie
Eine Zeitschrift der Gesellschaft Deutscher Chemiker

Supporting Information

Discovery of Cyanobacterial Natural Products Containing Fatty Acid Residues**

*Sandra A. C. Figueiredo, Marco Preto, Gabriela Moreira, Teresa P. Martins, Kathleen Abt, André Melo, Vitor M. Vasconcelos, and Pedro N. Leão**

anie_202015105_sm_miscellaneous_information.pdf

Contents

Supporting Data 1-5 can be accessed at https://bit.ly/3u2SUxX.

Materials and Methods

General experimental procedures

Stable-isotope labeled fatty acids (d_{11}-hexanoic, d_{15}-octanoic d_{23}-dodecanoic and d_{31}-hexadecanoic acids) were obtained from CDN Isotopes Inc. L-methionine-(methyl-^{13}C, d_3) and 2-keto-3-methylbutyric acid-$^{13}C_5$ sodium salt were obtained from Sigma-Aldrich. All solvents, purchased from VWR Chemicals, Thermo Fisher Scientific, Carlo Erba and Chem Lab NV were ACS grade, except for HPLC solvents (HPLC gradient grade) and LC-MS solvents (MS-grade). Deuterated solvents for NMR were purchased from Cambridge Isotope Laboratories and Alfa-Aesar. Thin layer chromatography (TLC) controls were performed on aluminium silica gel F254 TLC plates (Merck) and detection by UV absorption. LC-HRESIMS and LC-HRESIMS/MS analyses were obtained on a Thermo Scientific UltiMate 3000 HPLC system, which consists of the following components: LPG-3400RS pump, WPS-3000RS autosampler, TCC-3x00RS column compartment, and MWD-3000RS UV/VIS detector coupled to a Q Exactive Focus Hybrid Quadrupole Orbitrap Mass Spectrometer (Thermo Fisher Scientific), controlled by Q Exactive Focus (Exactive Series) 2.9 and Thermo Scientific Xcalibur 4.1.31.9 software. Optical rotations were obtained on a P-2000 polarimeter (Jasco). A 100 µL sample cell was used for compounds **10**, while a 1 mL sample cell was used for compounds **1**. The electronic circular dichroism (ECD) spectrum of **1** was acquired on a J-1500 Spectrometer (Jasco). UV spectra of **10** and **11** were acquired on a UV-1600PC spectrophotometer (VWR). The UV-Vis spectrum of **1** was acquired on a Synergi HT microplate reader (BioTek) equipped with a Take 3 plate and a 1 cm path length quartz cuvette. Infrared spectra were determined on a Thermo Scientific Nicolet™ iS™ 5 Fourier transform IR spectrometer controlled by OMNIC 9.8.372 software. NMR spectra were acquired using a DMSO-matched Shigemi tube on a Bruker Avance III HD, 600 MHz, equipped with a 5 mm cryoprobe and controlled by TopSpin 3.6.1., in the Materials Center of the University of Porto (CEMUP) and the NMR data were analyzed in MestReNova 12.0.3 (MestrelabResearch). The chemical shifts values (δ) are presented in parts per million (ppm) and the coupling constants (*J*) in hertz (Hz). The HPLC system for the purification of **10**-**12** was performed on a LC-4000 series HPLC (Jasco), coupled with a photometric diode array detector (monitored wavelengths: 204 nm and 250 nm) and fitted with ACE 5 C18 column (250 mm × 4.6 mm, 5 µm, 100 Å, ACE). For the purification of compound **1**, semipreparative HPLC was carried out using a Waters 1525 binary pump, coupled to a Waters 2487 detector (monitored wavelengths: 254 nm and 280 nm) and fitted with a Synergi Hydro-RP column (250 × 10 mm, 10 µm, Phenomenex).

Phylogenetic analysis

Cyanobacterial strains were assessed using KEGG Annotation[1] for the key enzymes involved in the beta-oxidation pathway (KEGG Pathway: *Fatty acid degradation - Reference pathway*), in order to assign their gene ontologies using the Microbial Nucleotide BLAST (tblastn) NCBI tool for genomes of cyanobacteria (n = 129). The hits were considered significant when score >80, E-value < $1x10^{-15}$. A 16S rRNA gene phylogenetic analysis for the 125 different cyanobacteria in the KEGG Genome database[2] (accessed in May 2020) was carried out. A 16S rRNA gene nucleotide sequence for each cyanobacterium was retrieved and aligned with MUSCLE 3.8.425[3] from within the geneious software package (Biomatters). The alignment was used to build an approximate maximum-likelihood phylogenetic tree using FastTree v2.1.11[4] (GTR model, Gamma20 likelihood optimization).

Plasmids, strains and culture conditions

The plasmid pET24d-*aas*7492 (pET24 plasmid with *Synechoccocus elongatus* PCC 7492 acyl ACP-synthetase encoding gene)[5] was kindly provided by Dr. Martin Fulda (Department for Plant Biochemistry Albrecht-von-Haller-Institute for Plant Sciences University of Goettingen, Germany). *E. coli* BL21(DE3) cells were transformed with either pET24d or pET24d-*aas*7492 plasmids, as follows. Chemically competent *E. coli* BL21(DE3) cells were transformed with plasmid DNA using the heat shock method. Briefly, *E. coli* BL21(DE3) were thawed, mixed with the plasmid (1 µL of purified plasmid DNA) and incubated on ice for 30 min. The cells were subjected to a heat shock at 42 °C for 40 seconds and the mixture was incubated on ice for 2 min. SOC medium was added to the mixture, and samples were incubated at 37 ºC for 1 h on an orbital shaker at 225 rpm. Cell suspensions (20µL) were then spread onto solid LB medium supplemented with 50 µg mL^{-1} kanamycin, and incubated overnight at 37 °C. Colonies were grown overnight in 5 mL LB medium to prepare 1 mL glycerol/LB medium (1:1, v/v) stocks, which were stored at – 80 ºC, and the remaining 4 mL of culture was used to isolate plasmidic DNA using the NZYtech Miniprep Kit. DNA was eluted in 30 µL H_2O. A 1 % agarose gel was loaded with 4 µL of each sample and with 1.5 µL of 1 kb plus ladder (ThermoFisher) and run at 80 V for 35 min, which confirmed the presence of DNA of the expected size (Fig. S40). The expression of the Aas protein was assessed by SDS-PAGE. For that, frozen *E. coli* pET24d-*aas*7492 or *E. coli* pET24d glycerol stocks were inoculated in 2 mL sterile LB medium. An overnight inoculum was used to prepare 150 mL cultures of sterile LB supplemented with kanamycin at 50 µg/mL and incubated at 37 °C with continuous shaking (100 rpm). After reaching an OD_{600} of ~0.4, cultures were supplemented with IPTG (1 mM) and cultured under the same conditions for five additional hours. The cells were then harvested by centrifugation at 4500 ×*g* for 20 min, rinsed with deionized water and centrifuged again. The cell pellets were resuspended in 1 mL of lysis buffer (50 mM Tris-HCl, pH 8.0). While on ice, the cells were lysed by sonication (2 × 20 sec pulses with 1 min rest in between each). The protein ladder (PageRuler Prestained Protein

Ladder, Bio-Rad, 5 µL) and the samples (10 µL) were loaded onto a Mini-PROTEAN TGX Precast Polyacrylamide Gel (4-15%, Bio-Rad). Following electrophoresis (100-200 V, ~ 40 min), the gels were stained (Coomassie G-250 Stain, Bio-Rad) for visualization of protein expression (Fig. S41). For the labeled-substrate incorporation experiments, test tubes with 2 mL sterile LB medium supplemented with 50 µg mL^{-1} kanamycin were inoculated from each of the frozen bacterial glycerol stocks. After overnight growth at 37 ºC and continuous shaking (50 rpm), a 150 mL culture of sterile LB with 50 µg mL^{-1} kanamycin was inoculated. After reaching an OD_{600} of ~0.4, IPTG (1mM) was added and the cultures were grown to an OD_{600} of ~0.65 before being split over test tubes (5 ml each) for the substrate incorporation experiments.

The cyanobacteria *Synechocystis sp.* PCC 6803, *Anabaena cylindrica* PCC 7122, *Kamptonema formosum* PCC 6407, *Fischerella sp*. PCC 9431, *Scytonema hofmanii* PCC 7110 were purchased from Pasteur Culture Collection of Cyanobacteria (PCC), Institute Pasteur (France). The cyanobacteria *Stanieria* sp. NIES-3757 and *Mastigocladus* sp. NIES-3754 were acquired from the NIES collection (Japan). The cyanobacteria *Microcystis aeruginosa* LEGE 91094, *Nodularia sp.* LEGE 06071, *Synechocystis salina* LEGE 06099, *Cyanobium* sp. LEGE 06135 and *Cuspidothrix issatschenkoi* LEGE 03285 were obtained from the Blue Biotechnology and Ecotoxicology Culture Collection (LEGEcc, Portugal). Cyanobacterial cultures were grown in Z8 medium with aeration, 25 ºC, 30 µmol photons m^{-2} s^{-1}, 16 h light / 8 h dark cycle).

Stable-isotope labeled substrate incorporation experiments

The initial supplementation of cyanobacteria and *E. coli* cultures with deuterated FAs to verify their lipidome labeling was performed as follows. The cyanobacteria *Synechocystis* sp. PCC 6803, *Anabaena cylindrica* PCC 7122 and *Kamptonema formosum* PCC 6407, small-scale (25 mL) cultures in Z8 medium in Erlenmeyer flasks, were inoculated with d_{11}-hexanoic (d_{11}-C_6), d_{23}-dodecanoic (d_{23}-C_{12})and d_{31}-hexadecanoic (d_{31}-C_{16}) acids to a final concentration of 0.1 mM from a 1000× concentrated solution of each acid in DMSO. After a seven-day growth period, cells were harvested by centrifugation at 5000 ×*g* for 15 min, rinsed with deionized water, centrifuged again and the supernatant was discarded. A similar procedure was used for the labeled-substrate incorporation experiments with *E. coli* pET24d or *E.coli* pET24d-*aas*7492 small-scale (5 mL) cultures in LB medium in test tubes (see "Plasmids, strains and culture conditions") that were supplemented with the same deuterated fatty acids as for cyanobacteria at a final concentration of 0.1 mM. After 4 h at 37 ºC, cells were harvested by centrifugation at 4000 ×*g* for 10 min at 4 °C, rinsed with deionized water, centrifuged again and the supernatant was discarded. In order to increase the levels of labeling of the FA-derived lipidome in cyanobacteria, distinct supplementation conditions were screened, namely different frequency patterns (one single dose with final concentration at day 1 or three pulses with 1/3 of the final concentration at day 1, 3 and 5), FA final concentrations (0.1, 0.3 or 0.5 mM), initial cell densities (estimated by a higher or lower chlorophyll *a* content [6]) and culturing times (24 h, 7 days, 30 days or 60 days). Based on this screening, optimized conditions were used for the ensuing labeled-substrate incorporation experiments with *Scytonema hofmanii* PCC 7110, *Stanieria* sp. NIES-3757, *Microcystis aeruginosa* LEGE 91094, *Fischerella* sp. PCC 9431, *Nodularia* sp. LEGE 06071 and *S. salina* LEGE 06099, namely: small-scale (25 mL) cultures in Z8 medium, with a chlorophyll *a* content of ~0.8–2.9 µg mL^{-1}, in Erlenmeyer flasks with three pulses of d_{11}-C_6 to a final concentration of 0.5 mM (from a 1000× concentrated solution in DMSO). After 7 days, cells were harvested by centrifugation at 5000 ×*g* for 15 min, rinsed with deionized water, and the supernatant was discarded after an additional centrifugation step. As part of the structure elucidation of hapalosins, precursor incorporation experiments were performed as follows. Small scale (25 mL) *Fischerella* sp. PCC 9431 cultures in Z8 medium were supplemented with L-methionine-(methyl-^{13}C, d_3), 2-keto-3-methylbutyric acid-$^{13}C_5$ sodium salt or d_{15}-octanoic acid (d_{15}-C_8) to a final concentration of 0.5 mM. After 7 days, cells were harvested by centrifugation at 5000 ×*g* for 15 min, rinsed with deionized water, and the supernatant was discarded after an additional centrifugation step. The precursor incorporation experiments were carried out in triplicate.

Organic extraction

To assess the labeling of PGs, MGDGs, DGDGs and SQDGs, total lipids from biomass were extracted following a previously described method [7], but with slight modifications, as follows. The biomass pellets were immersed in a mixture of CH_2Cl_2/MeOH (2:1, v/v), under continuous gentle agitation for 2 h. After filtration and transfer to new tubes, 1 mL of an aqueous solution of KCl (0.88%, w/v) was added with strong agitation, followed by centrifugation at 250 ×*g* at 4 ºC for 5 min. The aqueous upper phase was discarded, and the organic phase evaporated under vacuum. For the remaining experiments, the biomass pellets were extracted with CH_2Cl_2/MeOH (2:1, v/v) for 30 min. After being filtered, the organic solvents were evaporated under vacuum and the crude extracts were resuspended in MeOH (2 mg mL^{-1}) to be analyzed by LC-HRESIMS.

LC-HRESIMS and MS/MS analysis

HRESIMS data were obtained in Full Scan positive and negative mode with a scan range of *m/z* 150-2000, with a capillary voltage of HESI set to −3.5 kV and the capillary temperature to 263 °C. Sheath gas flow rate was set to 50 units. For LC-

HRESIMS analyses, separation was performed in an ACE UltraCore 2.5 SuperC18 column (75 x 2.1 mm) and maintained at a column temperature of 40 ℃. It was used a flow rate of 0.4 mL min^{-1} and a mobile phase of 0.1% formic acid in MeOH/H2O 1:1 (v/v) (eluent A) and in iPrOH (eluent B). The gradient program for the crude extracts was as follows: 10% B for 1 min, a gradient from 10% to 65% B over 5 min, held at 65% B for 12 min, then a gradient to 85% B over 2 min, and held again at 85% B for 9 min, before returning to the initial conditions.

For the LC-HRESIMS/MS analysis of compounds **3-9** from the organic extract under optimized separation conditions, the separation of these compounds was achieved in an ACE UltraCore 2.5 SuperC18 column (75 × 2.1 mm) and maintained at a column temperature of 40 ℃. A flow rate of 0.3 mL min^{-1} and a mobile phase of 0.1% formic acid in H_2O (eluent A), MeOH (eluent B) and in iPrOH (eluent C) were used. The program started with 100% A and increased linearly to 100% B over 20 min, was held at 100% B for 15 min, followed by a linear to reach 70% C over 5 min, and held at 70% C (30% B) for 7 min, before returning to the initial conditions. For the MS analysis, the parameters used were: resolution of 17 500, with a 3 *m/z* isolation window, a loop count of 1, AGC target of 5×10^4 and collision energy of 30 eV.

LC-HRESIMS/MS analysis of purified compound **10** was performed using the same LC program for organic extracts (0.5 mg mL^{-1}) and a resolution of 35 000, with a 1 *m/z* isolation window, a loop count of 1, AGC target of 2×10^5 and collision energy of 15 eV.

To obtain an in-source fragment of **10** that matched the parent ion of **1** and that could be further fragmented (*de facto* MS^3), the parameters used were: in-source collision induced dissociation (CID) energy set to 70 eV, resolution of 35 000, with a 1 m/z isolation window, a loop count of 3, AGC target of 8×10^3 and collision energy of 10 eV. The parameters used for fragmentation of the in-source fragment of **10** corresponding to **1** or for pure **1** itself were: resolution of 35 000, with a 1 *m/z* isolation window, a loop count of 3, AGC target of 2×10^5 and collision energy of 10 eV.

Metabolomics analysis

Processing and analysis of LC- HRESIMS data from the stable-isotope labeled substrate incorporation experiments was carried out using MZmine 2.53.[8] The raw files obtained from the Orbitrap mass spectrometer were directly imported to MZmine without previous conversion. The data processing followed a standard workflow for processing mass spectrometry data, namely: generation of mass lists (noise level set to 5 x 10^5); detection of chromatograms; deconvolution of chromatograms into individual peaks using the local minimum search algorithm; removing of isotopes; identification of adducts and peak complexes; alignment of triplicate features from the control and the supplementation experiments using the Join aligner option. In order to simplify our search for secondary metabolites, we created a custom database with positive- and negative-mode lists for exclusion of labeled metabolite features found in phylogenetically diverse strains: *Synechocystis* sp. PCC 6803, *Anabaena cylindrica* PCC 7122 and *Kamptonema formosum* PCC 6407 (Supporting Data 2 and 3). After identifying these common labeled features using the Custom Database Search tool, we used the Adduct Search module to identify the labeling of different secondary metabolites with deuterium-labeled hexanoic acid (d_{11}-C_6). For this purpose, the following parameters were used in the Adduct Search module: mass difference = 11.0681 *m/z* for d_{11} labeling; mass difference = 22.1369 *m/z* for d_{22} labeling; mass difference = 10.0627 *m/z* for d_{10} labeling; mass difference = 9.0564 *m/z* for d_9 labeling; mass difference = 8.0502 *m/z* for d_8 labeling; mass difference = 7.0439 *m/z* for d_7 labeling, all with 5 ppm tolerance. These mass differences consider not just the direct labeling with d_{11}, but also the double labeling (d_{22}) in case of incorporation of two fatty acyl moieties, and the incomplete labeling (d_{10}, d_9, d_8, d_7), resulting from dehydrogenations or substitutions at the fatty acyl moieties. The data from the peak lists were filtered for peaks found only in at least two out of the three supplemented replicates (i.e. not found in the controls or in other strains), to account for some inefficiency in feature detection. For a systematic analysis, the peaks were sorted by area and the raw data verified in Xcalibur 4.1.31.9 to validate the labeling and the correspondent non-labeled metabolite features. Finally, the accurate masses from the validated hits selected for isolation were dereplicated using several databases (LipidMaps,[9] Dictionary of Natural Products v29.1 (CRC Press) and PubChem). The comparative metabolomics datasets are available under MassIVE Accession MSV000086325 and MSV000086329.

For GNPS analysis,[10] raw LC-HRESIMS/MS data were converted to .mzML format with MSConvert (version: 3.0.19092-b4abc4e88)[11] and uploaded to the GNPS server . A molecular networking was created with feature-based molecular networking analysis on GNPS and was visualized in Cytoscape 3.8.0.[12] The GNPS datasets are available under MassIVE Accession MSV000086326 and MSV000086327.

Isolation of nocuolactylates A-C (10-12)

Extraction of the freeze-dried biomass (77.7 g, d.w.) from 140 L culture of *Nodularia* sp. LEGE 06071 in Z8 medium was achieved by repeated percolation using organic solvents (CH_2Cl_2/MeOH, 2:1 v/v). The resulting crude extract (7.8 g) was fractionated by normal phase Vacuum Liquid Chromatography (VLC) (Silica gel 60, 0.040-0.063 mm, Merck KGaA) using a gradient of increasing polarity from *n*-hexane to EtOAc to MeOH, yielding eleven fractions (1-11). By LC-HRESIMS analysis,

fractions 4-6 showed to contain *m/z* 551.4055, 585.3665 and 619.3275 (compounds **10-12**, $[M+H]^+$). Accordingly, these fractions were pooled (1.326 g) and further fractionated by normal phase Flash Chromatography (FC) (Silica gel 60, 0.015-0.040 mm) using a gradient of increasing polarity from hexane to EtOAc to MeOH, yielding fifteen subfractions (1-15) that were pooled according to their TLC profiles. After LC-HRESIMS analysis, FC subfractions 08 and 09 (eluting with 1:2 EtOAc/hexane, 129.53 mg), were further fractionated by reversed phase Solid Phase Extraction (RP-SPE) (Strata ® C18-E, 55 µm, 70 Ă, 70g / 60 mL, Phenomenex), using a gradient of decreasing polarity from MeOH:H_2O 1:1 to iPrOH, yielding six subfractions (1-6). RP-SPE subfractions 2 and 3 (16.22 mg), eluting with 1:1:2 MeOH:H_2O/ iPrOH, contained compound **10-12** (551.4055, 585.3665 and 619.3275 *m/z* $[M+H]^+$) as verified by LC-HRESIMS analysis, and were further fractionated by RP analytical HPLC (ACE 5 C18, 250 × 4.6 mm, 5 µm, 100 Å, ACE), using MeOH/H_2O 1:1 (v/v) (eluent A) and in iPrOH (eluent B). The gradient program started with 10% B, held for 1 min and increased linearly to 60% B over 2 min, was held at 60% B for 13 min, followed by a linear to reach 85% B over 1 min, and held at 85% B for 5 min, before returning to initial conditions for 3 min. The HPLC fractionation afforded 4 subfraction. HPLC subfraction 3 (compound **10**, 320 µg, t_R ~ 11.2) and HPLC subfraction 2 (compound **11**, 240 µg, t_R ~ 12.1) were spectroscopically pure (~95%, 1H NMR).

Nocuolactylate A (10) (white amorphous solid): $[\alpha_D^{24}]$ +84.5 (*c* 0.01, MeOH); IR (thin film) υ_{max} 3445, 2953, 2924, 2851, 1744, 1698, 1683, 1651, 1557, 1456, 1404, 1202, 1160, 1132, 1100, 968 cm−1; UV (MeOH) λ_{max} (log ε) 204 (1.2), 250 (1.5); ^{1}H and ^{13}C NMR data, SI Table 3; HRESIMS *m/z* 585.3663 $[M+H]^+$ (calcd. for $C_{31}H_{53}N_2O_6Cl$ 585.3665).

Nocuolactylate B (11) (white amorphous solid): IR (thin film) υ_{max} 3445, 2953, 2924, 2851, 1744, 1698, 1683, 1651, 1557, 1456, 1404, 1202, 1160, 1132, 1100, 968 cm−1; UV (MeOH) λ_{max} (log ε) 204 (0.6), 248 (0.5); ^{1}H and ^{13}C NMR data, SI Table 5; HRESIMS *m/z* 619.3278 $[M+H]^+$ (calcd. for $C_{31}H_{52}N_2O_6Cl_2$ 619.3275)

Isolation and structure elucidation of nocuolin A (1)

Extraction and isolation of nocuolin A (1)

Multiple 4 L cultures of *Nodularia* sp. LEGE 06071 were grown to late exponential stage in Z8 medium,[13] at 25 ºC, under a 14:10h light (30 µmol photons m^{-2} s^{-1})/dark regime. The resulting biomass was harvested and lyophilized until further use. 15.1 g of lyophilized biomass were repeatedly extracted by immersion on a 2:1 mixture of CH_2Cl_2/MeOH (< 40º C). The resulting slurry was evaporated under reduced pressure yielding 2.7 g of crude extract. The extract was fractionated by normal-phase (Si Gel 60, 0.015-0.040 mm, Merck) Vacuum Liquid Chromatography (VLC). A gradient of increasing solvent polarity, from *n*-hexane to EtOAc to MeOH, resulting in nine fractions (A – I). Fraction F (53.3 mg), eluting with a 1:4 *n*-hexane/EtOAc mixture, was further separated using normal-phase gravity column chromatography (Si Gel 60, 0.040-0.063 mm, Merck) using a gradient of increasing polarity from 1:1 *n*-hexane/EtOAc to MeOH. Collected samples were pooled on the basis of their TLC profiles, resulting in 11 sub-fractions (FA – FK). Sub-fraction FE (6.7 mg) was submitted to semi-preparative reversed-phase HPLC, under isocratic conditions (MeCN/H_2O, 7:3, 2 mL min^{-1}), to yield **1** (0.7 mg, 0.0046% d.w., t_R = 20.2 min).

Nocuolin A (1) (white amorphous solid): $[\alpha]^{20}D$ +35.4 (*c* 0.025, MeOH). UV−Vis (MeOH) λ_{max} (log ε): 206 (3.31), 252 (3.51) nm. For ^{1}H and ^{13}C NMR please see SI Table 4. HRESIMS *m/z* 299.2329 $[M+H]^+$ (calcd. for $C_{16}H_{31}N_2O_3^+$ 299.2329); 321.2148 $[M+Na]^+$ (calcd 321.2149); 619.4408 $[2M+Na]^+$ (calcd 619.4405).

HRESIMS and HRESIMS/MS conditions used in the structure elucidation of nocuolin A (1). HRESIMS and HRESIMS^2 data were acquired on an LTQ Orbitrap XL spectrometer, controlled by LTQ Tune Plus 2.5.5. and Xcalibur 2.1 (Thermo Fisher Scientific). The capillary voltage of the ESI was set to 3000 V. The capillary temperature was 275 ºC. The sheath gas flow rate (nitrogen) was set to 5 (arbitrary unit as provided by the software settings). The capillary voltage was 36 V and the tube lens voltage 110 V. Samples were injected at 0.1 mg mL^{-1} and selected ions were fragmented using collision-induced dissociation (CID) with a normalized collision energy of 35% (Fig. S26). For comparison of HRESIMS/MS data of **1** with 1*H*-pyrazol-1-ol (**s1**) and an extract containing 1*H*-pyrazol-1-yl propionate (**s2**), samples were injected at 0.1 mg mL-1 in a Q Exactive Focus Hybrid Quadrupole Orbitrap Mass Spectrometer (Thermo Fisher Scientific). The ESI spray voltage was 3800 V, the capillary temperature 300 ºC, the sheath gas flow rate (nitrogen) was set to 5 (arbitrary unit as provided by the software settings). Selected ions were fragmented using higher-energy collisional dissociation (HCD) with a normalized collision energy of 10%.

Synthesis of 1*H*-pyrazol-1-yl propionate (s2) for HRESIMS/MS analysis. To a 5 mL RB flask**,** 1*H*-pyrazol-1-ol (**s1**, 50 mg, 0.12 mmol, acquired from Enamine, Ltd.), propionic acid (1 mL, 13.40 mmol, p.a., Sigma-Aldrich) and 0.1 mL of concentrated sulfuric acid (>=95%, Fisher Scientific) were added. The flask was placed at 141 ℃ and stirred for 20 h. The resulting solution was extracted with hexane (3 × 20 mL). The extract was washed with water (10 mL) and brine (10 mL). The obtained organic phase was dried over anhydrous Na_2SO_4, filtered, and evaporated under reduced pressure to give a colourless solution which was diluted in methanol and analysed by direct injection by HRESIMS, which showed *m/z* values ($[M+H]^+$ and $[M+Na]^+$) ions for the predicted Fisher-Speier esterification product **s2**. Fragmentation of the $[M+H]^+$

ion (**s2**) was consistent with the predicted product, namely by the prominent neutral loss of propionaldehyde (see Figure below).

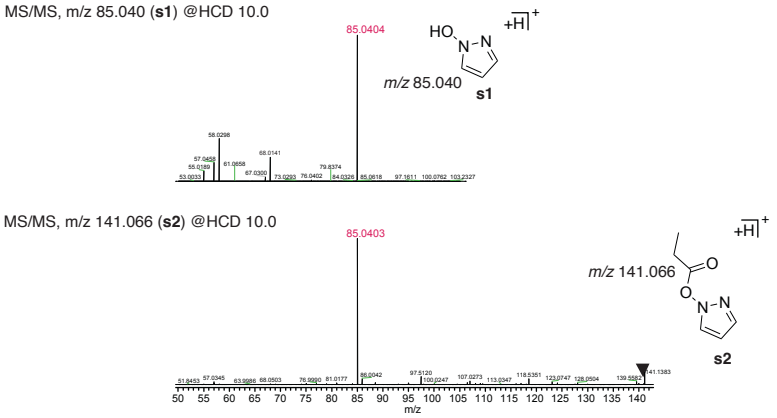

Comparative HRESIMS/MS analysis of s1, s2, 1 and of an in-source fragment of 1. The commercially available **s1**, an extract containing the synthetic product **s2**, and metabolite **1** were analyzed by direct infusion into the qExactive instrument

UV-Vis spectroscopy computational simulations. The most stable structures found for each enantiomer of a putative pyrazoline-containing structure for **1** were calculated. There were obtained after minimization using MM-FF94, followed by a further optimization at a B3LYP/6-31G* quantum level and their UV-Vis spectra simulated using TDDFT (B3LYP/6-311G++(2d,2p), as detailed for the ECD calculations of the proposed 1,2,3-oxadiazine structure of **1** (see *ECD computational simulations* below). The UV-Vis spectra for the"pyrazoline" enantiomers and the "oxadiazine" enantiomers (simulated as detailed in *ECD computational simulations* below) were plotted using GaussSum[14] and compared to the experimental UV-Vis spectrum of **1** reported in this study.

NMR chemical shift predictions. NMR chemical shift predictions were carried out with SPINUS[15] (^{1}H), nmrdb[16] (^{13}C) or Mnova Lite CDE software (^{1}H and ^{13}C, NMR predict plug-in, Mestrelab Research S.L) and compared to the experimental values reported here.

Genome sequencing and identification of the *noc* locus

Genomic DNA from an exponentially growing culture of *Nodularia* sp. LEGE 06071 was extracted according to Singh et al.,[17] slightly modified by including an RNAse A (Life Technologies, 50 µg mL^{-1}) treatment step. The isolated gDNA was sequenced using an illumina MiSeq (2 × 300 bp reads) technology, quality filtered (FASTQC), assembled using SPADES v3.8[18] and the assembly quality assessed using QUAST.[19] The assembled data was used to populate a local BLAST database with the geneious software package. tBLASTn searches against this database, using several previously reported *noc* genes as queries, revealed the *noc* locus from *Nodularia* sp. LEGE 06071 (NCBI Accession number: MW071172), within a 98.5 kb contig. Manual annotation of the Noc/Cly proteins was performed using BLASTp searches against the NCBI nr database.

ECD computational simulations

In order to establish the absolute configuration of nocuolin A (**1**), Monte Carlo (MC) conformational searches (MM-FF94 force field)[20] for the two possible enantiomers were performed using the TINKER package.[21,22] The five most stable conformers for each enantiomer were identified. These were further optimized, at a B3LYP/6-31G* quantum level as implemented in Gaussian 09 software package.[23] Analytic harmonic frequencies were additionally calculated, for all optimized structures, for ensuring correspondence to genuine minima without any imaginary frequency. Each optimized structure was checked in order to confirm its chiral carbon conformation and to avoid duplicate structures. During the optimization (from MM-FF94 to B3LYP) some of the conformers changed configuration to the other enantiomer and thus were reassigned accordingly. Following reassignment, five conformers of each enantiomer were obtained. All structures had their ECD spectra simulated, using TDDFT (B3LYP/6-311G++(2d,2p), as implemented in Gaussian 09. The simulation data was processed using the GaussSum software,[14] resulting in the ECD spectra for each simulated conformer. The final simulated ECD spectra for each enantiomer were obtained after weight-averaging of the respective individual conformers, using normalized Boltzmann populations as weight factors.

Cytotoxicity assays

Compounds **1**, **10** and **11** were stored at -20 °C as stock solutions of 5 mM in DMSO. The stock solutions were diluted in culture medium just before the start of each experiment to obtain the working solutions with the defined final concentrations. Paclitaxel was obtained from Enzo Biochem, Inc. In all conditions assayed, the final concentration of DMSO was lower than 0.5%. Four different cell lines were used: three tumor (MCF7, MG-63 and HCT116), obtained from the American Type Culture Collection (ATCC), and one non-tumor (hCMEC/D3), kindly donated by Dr. P. O. Courad (INSERM, France). The human osteosarcoma cell line MG-63, the human breast adenocarcinoma cell line MCF7 and the human cerebral microvascular endothelial cell line hCMEC/D3 were maintained in Dulbecco's Modified Eagle Medium (DMEM), from Gibco, while the human colorectal carcinoma cell line HCT116 was grown in McCoy's 5A modified medium (Roth). These two media were supplemented with 10% of fetal bovine serum (FBS, Biochrom), 1% of penicillin/streptomycin (Biochrom) and 0.1% amphotericin B (GE Healthcare). All the cell lines were maintained in 75 cm^2 culture flasks with 10 mL of the respective complete medium and kept in the incubator at 37 °C in 5% CO_2. The viability of all cell lines in the presence of different concentrations of the compounds was evaluated by the IC_{50} and the GR_{50} values determined by the 3-(4,5-dimethylthiazol-2-yl)-2,5-diphenyltetrazolium bromide (MTT) assay. MCF7, MG-63 and HCT116 were seeded at 9×10^4 cells per mL, while hCMEC/D3 was seeded at 5×10^4 cells per mL in 96 wells plates, at 100 µL per well and allowed to attach for 24 h. To determine the initial cell density (time 0) for the GR_{50} determination, 20 µL of MTT was added to three wells. After 3 hours in the incubator at 37 °C the solution was removed, and 100 µL of DMSO was used to dissolve the formazan crystals and allow the absorbance measurement at 550 nm (Synergy HT, BioTek). At time 0, the growth medium was removed in the other wells and the compounds were added, in triplicate, at increasing concentrations. After 48 h of incubation, the MTT assay was performed as above. Subsequently, GR_{50} and IC_{50} values were determined using the Online GR Calculator.[24] Two independent experiments were performed in triplicate for each compound and cell line.

Antimicrobial assays

The antimicrobial activity of compounds **10** and **11** was tested by the method of agar disk diffusion against two gram-negative bacterial strains (*Escherichia coli* ATCC 25922 and *Salmonella typhimurium* ATCC 25241), two gram-positive bacterial strains (*Staphylococcus aureus* ATCC 29213 and *Bacillus subtilis* ATCC 6633), and one yeast strain (*Candida albicans* ATCC 10231). The bacterial strains were plated in Mueller-Hinton Agar (MH, BioKar diagnostics) and the yeast strain was plated in Sabouraud Dextrose Agar (BioKar diagnostics) from glycerol stocks and incubated overnight at 37 °C. Microbial colonies were then picked and suspended in 2 mL of liquid medium (Mueller-Hinton, Alliance Bio Expertise, for bacteria and Sabourad Dextrose, Liofilchem, for yeast), the OD_{600} was read and the turbidity adjusted to 0.1 for bacteria and 0.5 for *C. albicans* and the agar plates were seeded with the resulting inoculum.

Next, blank disks (Ø 6mm, Oxoid) were placed in the inoculated agar plates and impregnated with 15 µL of each compound with a final concentration of 1 mg mL^{-1}. As a negative control, a disk with 15 µL of DMSO was used. Positive controls were disks with Kanamycin for bacteria and Nystatin for the fungus. The plates were allowed to dry for 30 min at room temperature after being incubated overnight at 37 °C for 24 h. Finally, the diameter (mm) of any inhibition halos were measured as an indication of antimicrobial activity.

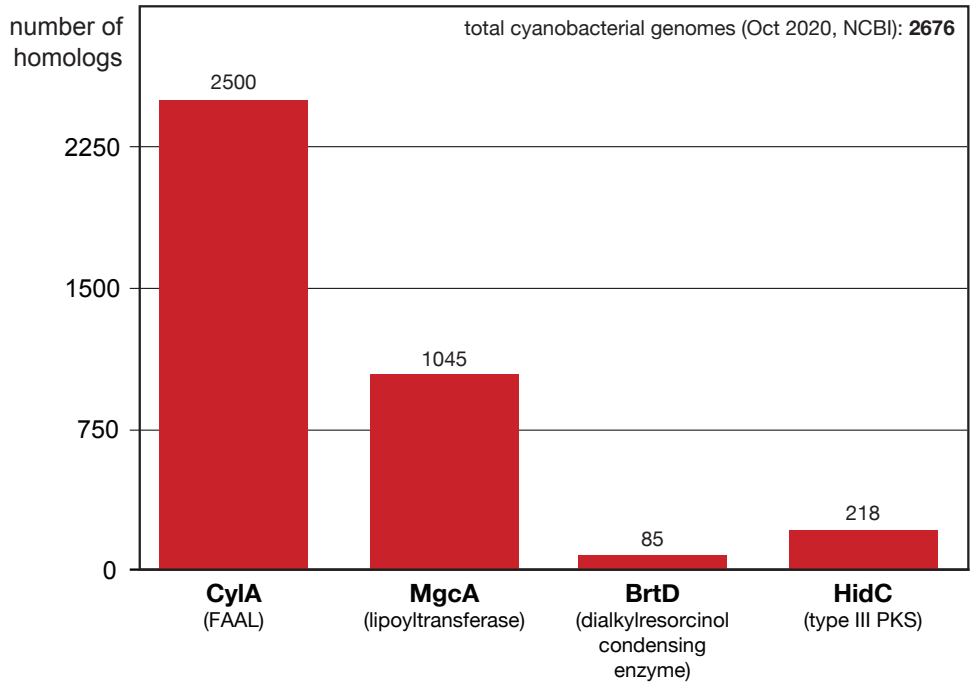

Figure S1. Abundance of selected FA-incorporating enzymes in cyanobacteria. Number of homologues per cyanobacterial genome deposited in the NCBI, for enzymes known to incorporate FAs into cyanobacteria metabolites, namely fatty acyl-AMP ligases (FAALs), lipoyltransferases, dialkylresorcinol condensing enzymes and type III PKSs. A cyanobacterial homolog of each enzyme class (CylA – GenBank: ARU81115, MgcA – GenBank:RQH10635, BrtD – GenBank:AKV71849 and HidC – GenBank: QBC65480, respectively) was used in a BlastP search against cyanobacterial (taxid:1117) sequences in the NCBI nr database, accessed in October 2020. At the time of accession, 2676 genomes from cyanobacteria were deposited in the NCBI genome database.

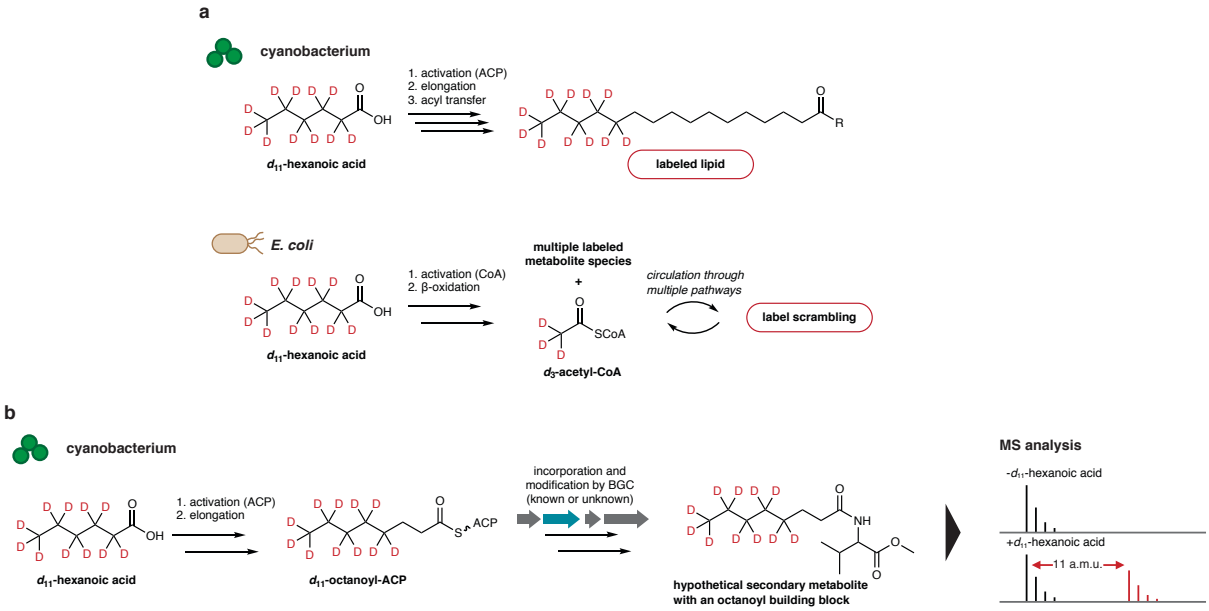

Figure S2. Overview of the FA-supplementation strategy for NP discovery. a) Cyanobacteria can elongate exogenous small- and medium-chain FAs and do not appear to carry out beta-oxidation; therefore, supplementation with deuterium-labeled hexanoic acid (as an example) will result in retention of the label in lipids incorporating longer-chain FAs, while in other bacteria (such as *E. coli*), exogenous FAs are not elongated and undergo beta-oxidative degradation. The resulting labeled acetyl-CoA is then circulated among multiple pathways, leading to scrambling of the deuterium label. b) Cyanobacteria cultures with active BGCs that incorporate FAs will produce stable-isotope labeled NPs (shown is a hypothetical NP that contains an octanoic acid derived moiety), enabling their detection by MS analysis.

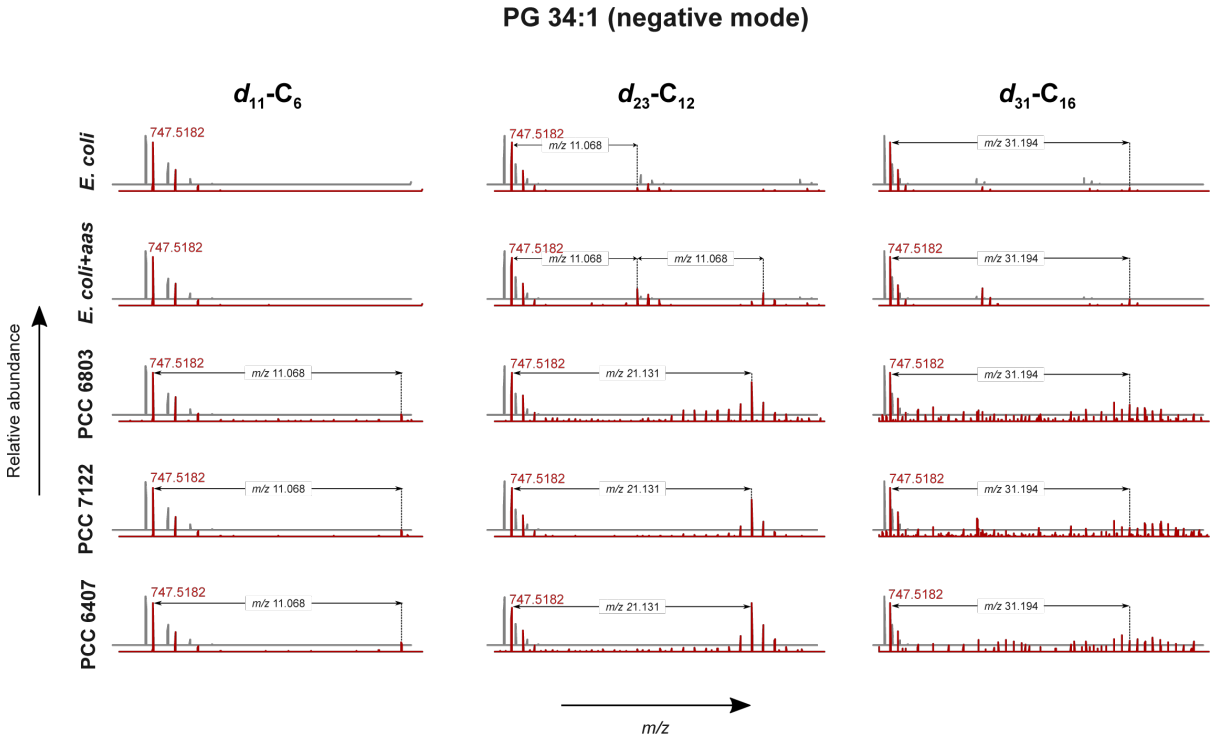

Figure S3. Comparison of the labeling pattern of PG 34:1 lipids in *E. coli* and cyanobacteria. Shown are HRMS spectra corresponding to the $[M-H]^-$ ion for PG 34:1 lipids in *E .coli* pET24d, *E. coli* pET24d-aas7942, *Synechocystis* sp. PCC 6803, *Anabaena cylindrica* PCC 7122 and *Kamptonema formosa* PCC 6407 strains, when their cultures were supplemented with d_{11}-C_6, d_{23}-C_{12} or d_{31}-C_{16}.

Table S1. Quantification of stable-isotope labeling in different lipid groups following supplementation of cultures of *Anabaena cylindrica* PCC 7122 with d_{11}-C6 for different time periods.

	Negative mode ionization								
	PG34:2			**SQDG 32:1**			**SQDG 32:0**		
Growth period	**non-labeled $[M-H]^-$** *m/z* 745.5042	**+d_{11} $[M-H+d_{11}]^-$** *m/z* 756.5721	**%labeling**	**non-labeled $[M-H]^-$** *m/z* 791.5003	**+d_{11} $[M-H+d_{11}]^-$** *m/z* 802.5688	**%labeling**	**non-labeled $[M-H]^-$** *m/z* 793.5159	**+d_{11} $[M-H+d_{11}]^-$** *m/z* 804.5848	**%labeling**
15 days	2.96E+09	1.88E+08	6.37%	8.63E+08	1.07E+08	12.41%	7.68E+08	9.93E+07	12.92%
30 days	4.96E+09	1.48E+08	2.98%	1.09E+09	8.97E+07	8.21%	8.85E+08	4.78E+07	5.40%
60 days	1.04E+10	1.57E+08	1.51%	2.79E+09	1.10E+08	3.93%	1.97E+09	6.64E+07	3.37%
	Positive mode ionization								
	MGDG 36:0			**MGDG 34:0**			**DGDG 36:7**		
Growth period	**non-labeled $[M+H]^+$** *m/z* 786.6000	**+d_{11} $[M+H+d_{11}]^+$** *m/z* 797.6692	**%labeling**	**non-labeled $[M+H]^+$** *m/z* 758.5691	**+d_{11} $[M+H+d_{11}]^+$** *m/z* 769.6384	**%labeling**	**non-labeled $[M+H]^+$** *m/z* 935.5689	**+d_{11} $[M+H+d_{11}]^+$** *m/z* 946.6380	**%labeling**
15 days	3.69E+08	4.71E+07	12.79%	5.51E+08	1.71E+08	31.10%	6.78E+08	2.10E+07	3.10%
30 days	3.83E+08	3.58E+07	9.33%	5.05E+08	1.36E+08	26.88%	6.13E+08	3.44E+07	5.61%
60 days	7.28E+08	5.05E+07	6.94%	1.69E+09	3.03E+08	17.95%	7.07E+08	1.87E+07	2.64%

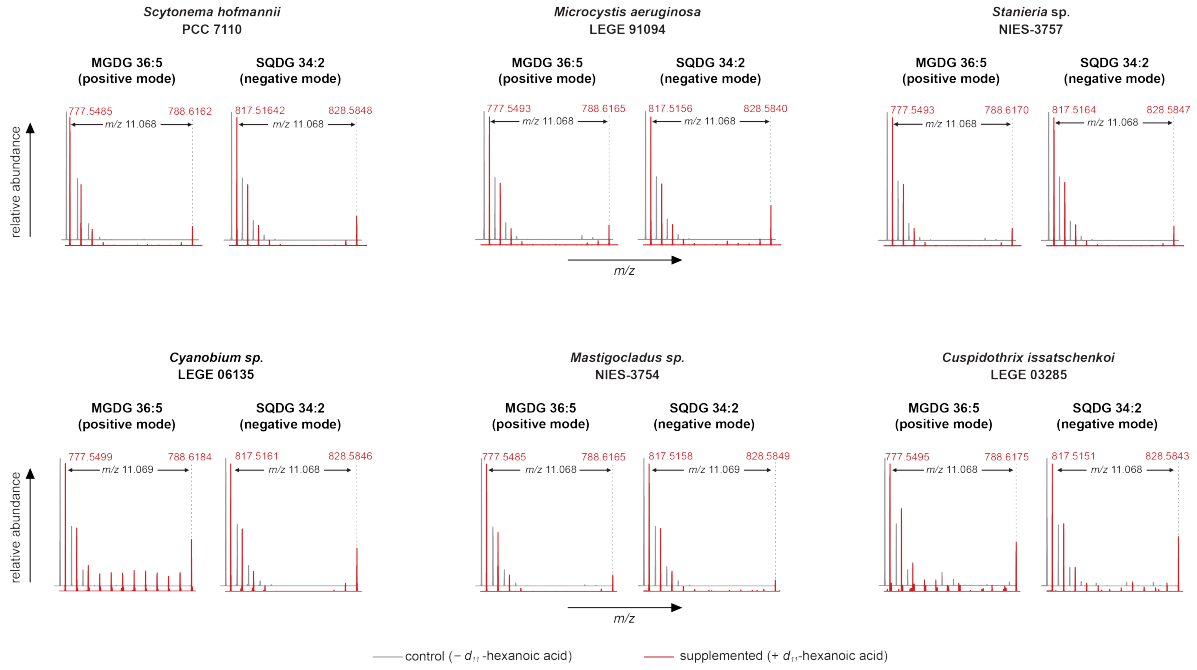

Figure S4. Common lipid species in cyanobacteria are abundantly labeled with deuterium following supplementation of a set of cyanobacterial strains from different taxonomic orders with d_{11}-C_6. Shown are MS spectra in the region of the $[M+H]^+$ or $[M-H]^-$ ions of unsaturated glycolipids, contributing to the pool of monogalactosyldiacylglycerols 36:5 and sulfoquinovosyldiacylglycerols 34:2.

Table S2. Qualitative assessment (from "+": lowest, to "+++": highest) of the stable-isotope labeling of lipids under different culture and supplementation frequencies. The trials were carried out with d_{11}-C_6 supplementation and with strains *Synechocystis sp.* PCC 6803 and *Anabaena cylindrica* PCC 7122. The 60-day trial was only carried out for *Anabaena cylindrica* PCC 7122 (see Table S1).

Time of harvest after initial supplementation (days)	**1**	**7**	**15**	**30**	**60**
% labeling	+	+++	++	+	+

[FA] (mM)	**0.1**	**0.3**	**0.5**
% labeling	+	++	+++

Supplementation frequency	**single pulse**	**3 pulses**
% labeling	+	+++

Inoculum: chlorophyll *a* (µg mL^{-1})	**< 4**	**> 4**
% labeling	+++	+

Shaking	**No**	**Yes**
% labeling	+	+++

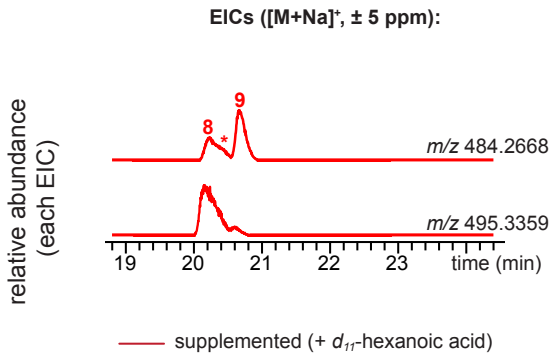

Figure S5. Detection of compounds **8** and **9** under an optimized LC gradient. Extracted Ion Chromatograms (EICs) for the $[M+Na]^+$ adduct *m/z* values corresponding to metabolites **8** and **9** (484.2668) and d_{11}-**8** and -**9** (*m/z* 495.3359) under optimized gradient separation conditions, indicating that both metabolites incorporate the deuterium labels from supplemented of the culture of *Fischerella* sp. PCC 9431 with d_{11}-hexanoic acid.

Text S1. Structure elucidation of hapalosin congeners.

Compound **4** showed an $[M+H]^+$ peak at *m/z* 504.3317 under HRESIMS conditions, corresponding to a molecular formula of $C_{29}H_{45}NO_6$ (calcd. 504.3320, $[M+H]^+$), a $+CH_2$ difference to **3**. LC-HRESIMS/MS analysis indicated that the additional methylene in **4** was present in the alpha-ketoacid derived unit. According to the proposed hapalosin biosynthesis,[25] this unit could derive from 3-methyl-2-oxovaleric acid, in which case **4** would correspond to the previously reported hapalosin B.[26] However, other structural

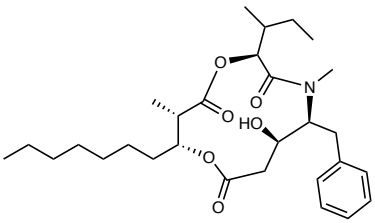

hapalosin B

possibilities cannot be entirely ruled out (e.g. a 4-methyl-2-oxovaleric derived unit), so we present only a tentative identification.

Compound **5** exhibited an $[M+H]^+$ ion at *m/z* 488.3004, corresponding to a molecular formula of $C_{28}H_{41}NO_6$ (calcd. 488.3007, $[M+H]^+$), a $-H_2$ difference to **3**. From LC-HRESIMS/MS data, this difference could be mapped to the N-methylated and oxygenated 5-phenylpentanoic moiety. The absence of a water loss for the precursor ion and also for this key fragment, both prominently observed for all other congeners, led us to propose that **5** is an 8-oxo version of **3** (Fig. 3c).

Compounds **6** and **7** showed *m/z* values for the $[M+H]^+$ ion of 476.3005 and 476.3004, respectively. These corresponded to a molecular formula of $C_{27}H_{41}NO_6$ (calcd. 476.3007, $[M+H]^+$), i.e. a $-CH_2$ difference to **3**. The LC-HRESIMS/MS data for **6** indicated that the difference could be ascribed to the methylated/oxygenated decanoic acid moiety in **3** (Fig. 3c). In the biosynthesis of **3**, this substructure is proposed to be built from the condensation of a malonyl-CoA monomer with octanoyl-ACP, with its 3-methyl group is provided by S-adenosyl-L-methionine.[25] To clarify whether **6** lacks a 3-methyl group or, alternatively, features a shorter aliphatic chain, we supplemented *Fischerella* sp. PCC 9431 with either L-methionine-(*methyl*-^{13}C,d_3) or d_{15}-octanoic acid. The resulting LC-HRESIMS data for **6** and **3** showed that a single methionine-derived methyl group is present in **6**, while two are present in **3**. Deuterium incorporation from d_{15}-octanoic acid was observed for both compounds. Hence, **6** is proposed to be a 3-desmethyl version of **3**. In the isobaric metabolite **7**, the CH_2 difference was associated with the alpha-ketoacid derived fragment, from LC-HRESIMS/MS data. In agreement with this observation, supplementation of a *Fischerella* sp. PCC 9431 culture with $^{13}C_5$-2-ketoisovaleric acid (the precursor for the 2-hydroxyisovalerate unit in **3**)[25] resulted in the expected incorporation of the $^{13}C_5$ label in **3**, but not in **7**. Based on these results, we propose that **7** contains a 2-hydroxybutyrate moiety.

The molecular formula of compounds **8** and **9** was found to be $C_{26}H_{39}NO_6$ on the basis of the LC-HRESIMS data for the respective $[M+H]^+$ ions, *m/z* 462.2845 and 462.2846 (calcd. 462.2850, $[M+H]^+$). Compound **3** has a $+C_2H_4$ difference to **8** and **9**. Comparison of LC-HRESIMS/MS data with those for other hapalosins, and analysis of LC-HRESIMS data for culture supplementations with the previously mentioned stable-isotope labeled precursors, formed the basis for our proposal that **8** has a hexanoic acid-derived alkyl chain, while **9** features a lactate unit. Because **5**-**9** are expected to be produced by the same hapalosin (*hap*)[25,27] BGC, we propose that the configuration for all chiral centers is the same as in **3**.

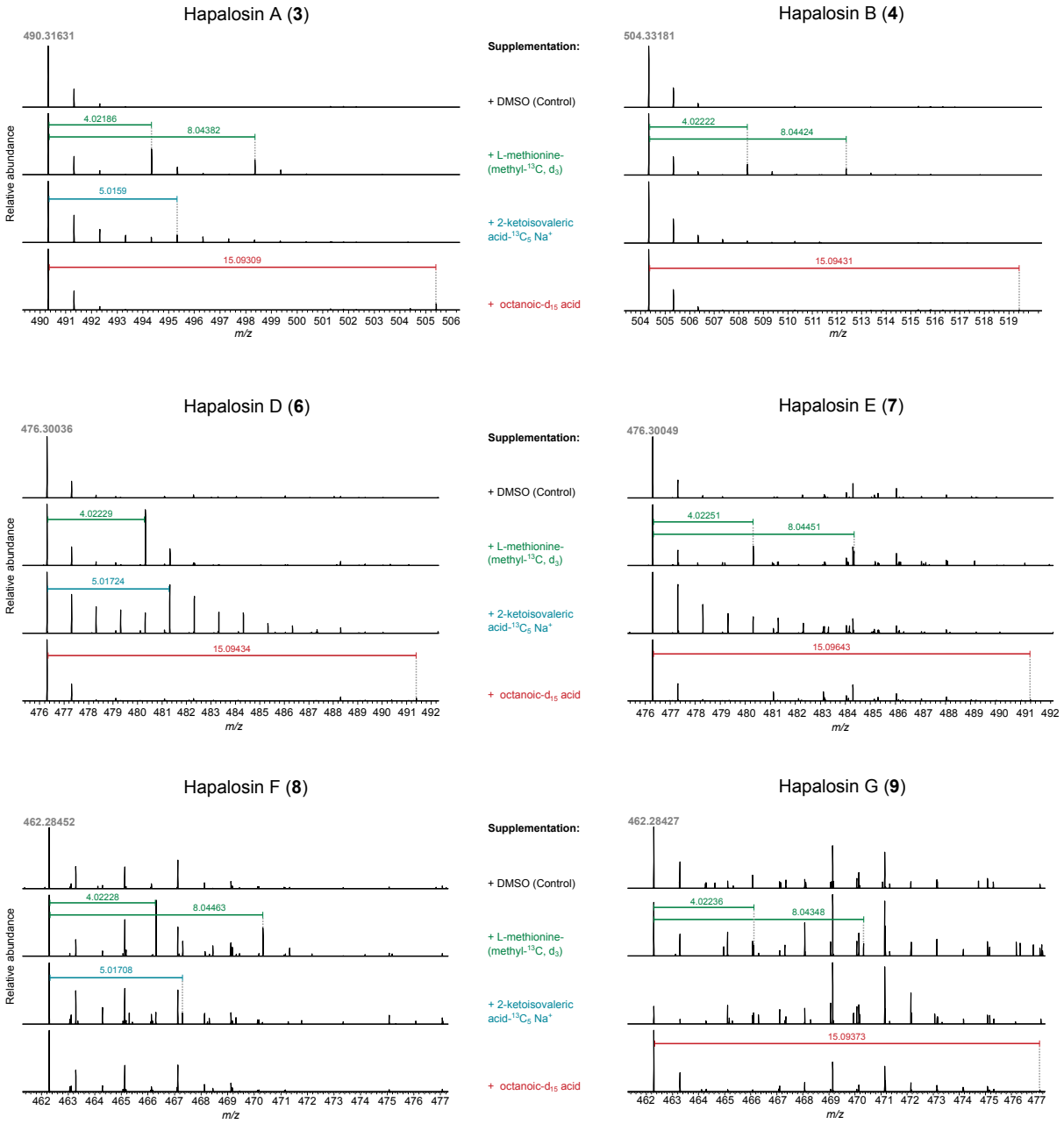

Figure S6. LC-HRESIMS spectra of the different hapalosin congeners and their annotation, following supplementation with different biosynthetic precursors.

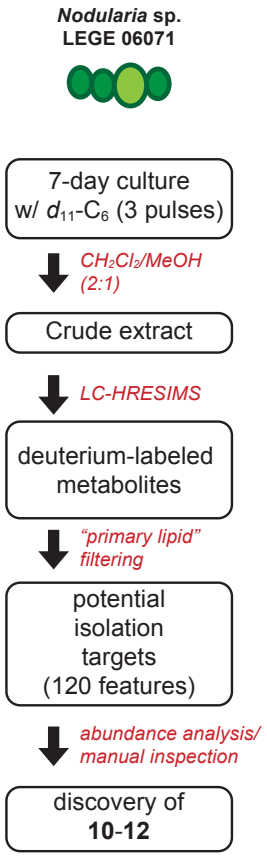

Figure S7. Schematic overview of the strategy leading to the discovery of **10**-**12**.

Table S3. NMR Spectroscopic Data (^{1}H 600 MHz, ^{13}C 150 MHz, DMSO-d_6) for nocuolactylate A (**10**).

Position	C	Type	H	mult. *J*(Hz)	HMBC[a]	H2BC[a]	HSQC-TOCSY[a]	COSY	NOESY	ROESY
1	163.5	C								
2	32.4	CH_2	2.87	m	163.5, 60.6	60.6	60.6, 32.4	4.36, 4.28		4.36, 4.28
3	60.6	CH_2	4.36/4.28	dt, 11.6, 6.0 / dt, 11.3, 6.1	170.8, 163.5, 32.4	32.4	60.6	4.36, 4.28, 2.87	4.36, 4.28, 2.87	4.36, 4.28, 2.87
4	75.0	CH	4.02	s		33.1, 30.7	75.0, 33.1, 30.7	2.39, 2.17, 1.50	1.50, 1.27	2.40, 1.50
5	30.7	CH_2	2.39/2.17	m	150.8, 75.0, 33.1	75.0	33.1, 30.7	4.01, 2.40, 2.17	2.39, 2.17	4.01, 2.40, 2.17
6	150.8[b]	C								
7	36.1	CH_2	2.22	m	150.8, 31.0, 23.8		36.1, 23.8	1.50	1.50	1.50, 0.87
8/13	23.8	2 × CH_2	1.35	m	31.00		31.2-31.0, 36.8, 32.0-28.2, 22.0, 13.9	1.50, 1.35, 1.27, 0.87	1.50, 1.35, 0.87	1.50, 0.87
9/14	31.0	2 × CH_2	1.27	m	32.0-28.2, 22.0, 16.5, 13.9	32.0-28.2, 22.0, 13.9				
10/15	22.0	2 x CH_2	1.28	m	32.0-28.2, 22.0, 16.5, 13.9	32.0-28.2, 22.0, 13.9	32.0-28.2, 22.0, 13.9	1.50, 1.27, 0.87	1.50, 0.87	1.50, 0.87
11/16	13.9	2 × CH_3	0.87	m	31.0-31.2, 23.8, 22.0	22.0	36.1, 33.1, 31.0-31.2, 23.8, 22.0, 13.9	1.51, 1.27	1.27	1.50, 1.27
12	33.1	CH_2	1.50	m	75.0, 31.2-31.0, 23.8	31.2-31.0, 23.8		4.01, 2.22, 1.35, 1.27, 0.87	2.22, 0.87	4.01, 2.22, 0.87
17	170.8	C=O								
18	68.4	CH	4.95	q. 7.0	170.8, 16.5	16.5	68.4, 16.5	1.35	1.35	1.35
19	16.5	CH_3	1.36	d. 7.1	170.8, 68.4	68.4	68.4	4.95	4.95	4.95
20	170.2	C=O								
21	36.8	CH_2	3.08	d. 6.6	170.2, 134.2, 121.5	121.5	134.2, 121.5, 36.8, 28.7-28.2	5.57, 5.43, 1.99		5.57, 5.43, 1.27
22	121.5	CH	5.57	dt, 14.7, 6.8	134.2, 36.8, 32.0	134.2, 36.8	121.5, 36.8	5.57, 3.08, 1.99		3.08, 1.99
23	134.2	CH	5.43	dt, 14.1, 6.7	121.5, 36.8, 32.0	121.5	121.5, 36.8	5.43, 3.08, 1.99		3.08, 1.99
24	31.8	CH_2	1.99	q, 7.0	134.2, 121.5, 28.7	134.2, 28.7	134.2, 121.5, 36.8, 32.3, 28.7-28.2	5.57, 5.43, 3.08, 1.99		5.43, 1.99
25-28	28.7-28.2	4 × CH_2	1.27	m	32.0-28.2, 22.0, 16.5, 13.9	28.7-28.2, 26.2	45.4, 36.8, 32.0-28.7, 26.2	1.99, 1.37, 1.27	1.99, 1.37	1.98
29	26.2	CH_2	1.37	m		32.0, 28.2	45.4, 32.0, 28.7, 26.2	1.99	1.70	
30	32.0	CH_2	1.70	p, 6.8	45.4, 26.2	45.4, 26.2	45.4, 32.0, 28.7-28.2, 26.2		1.27	1.37, 1.27
31	45.4	CH_2Cl	3.62	t, 6.7	32.0, 26.2		32.0, 28.7-28.2, 26.2			1.37, 1.27

[a]from proton to indicated carbon, [b]extracted from HMBC.

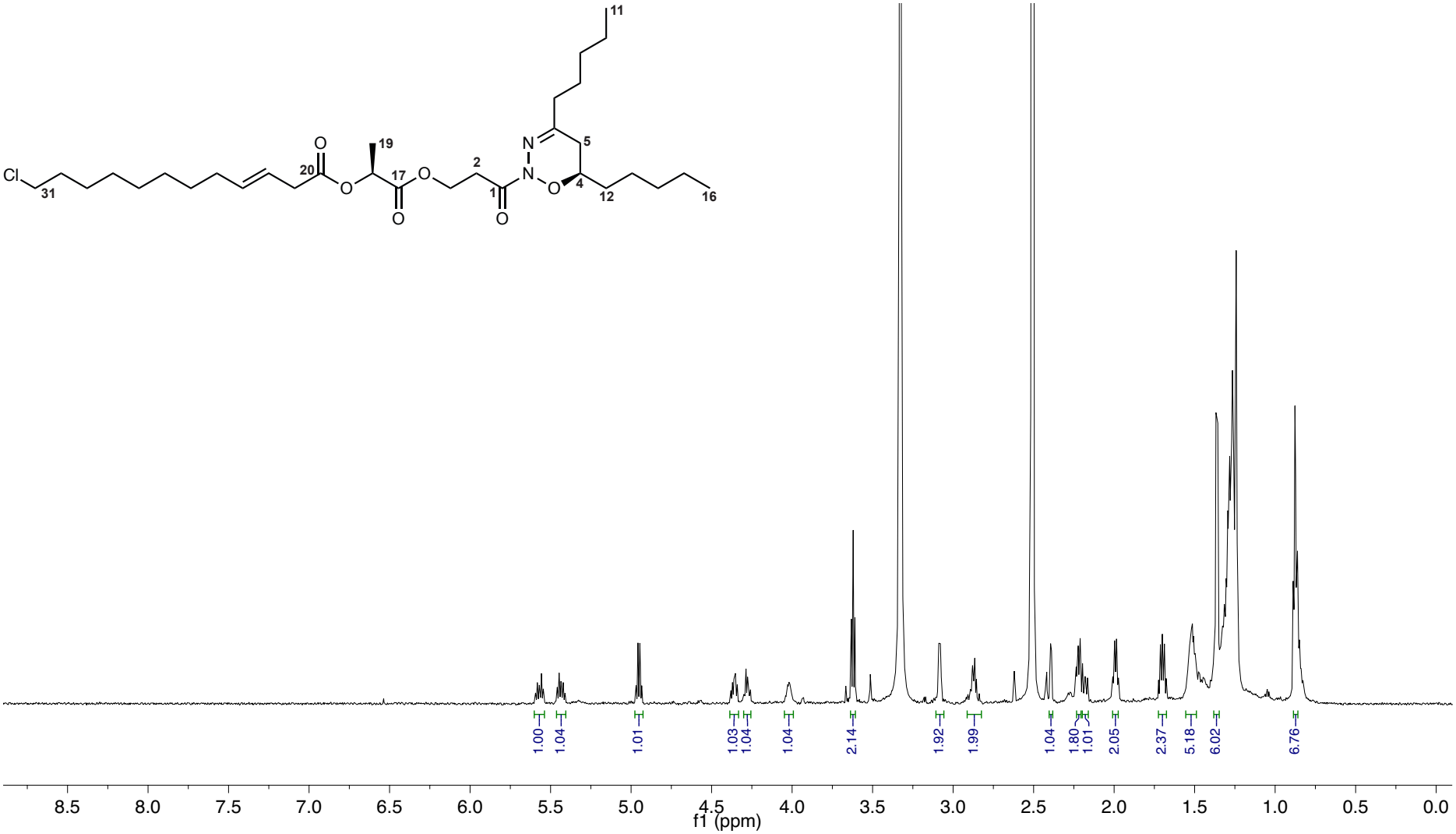

Figure S8. ^{1}H NMR (DMSO-d_6, 600 MHz) spectrum of compound **10**.

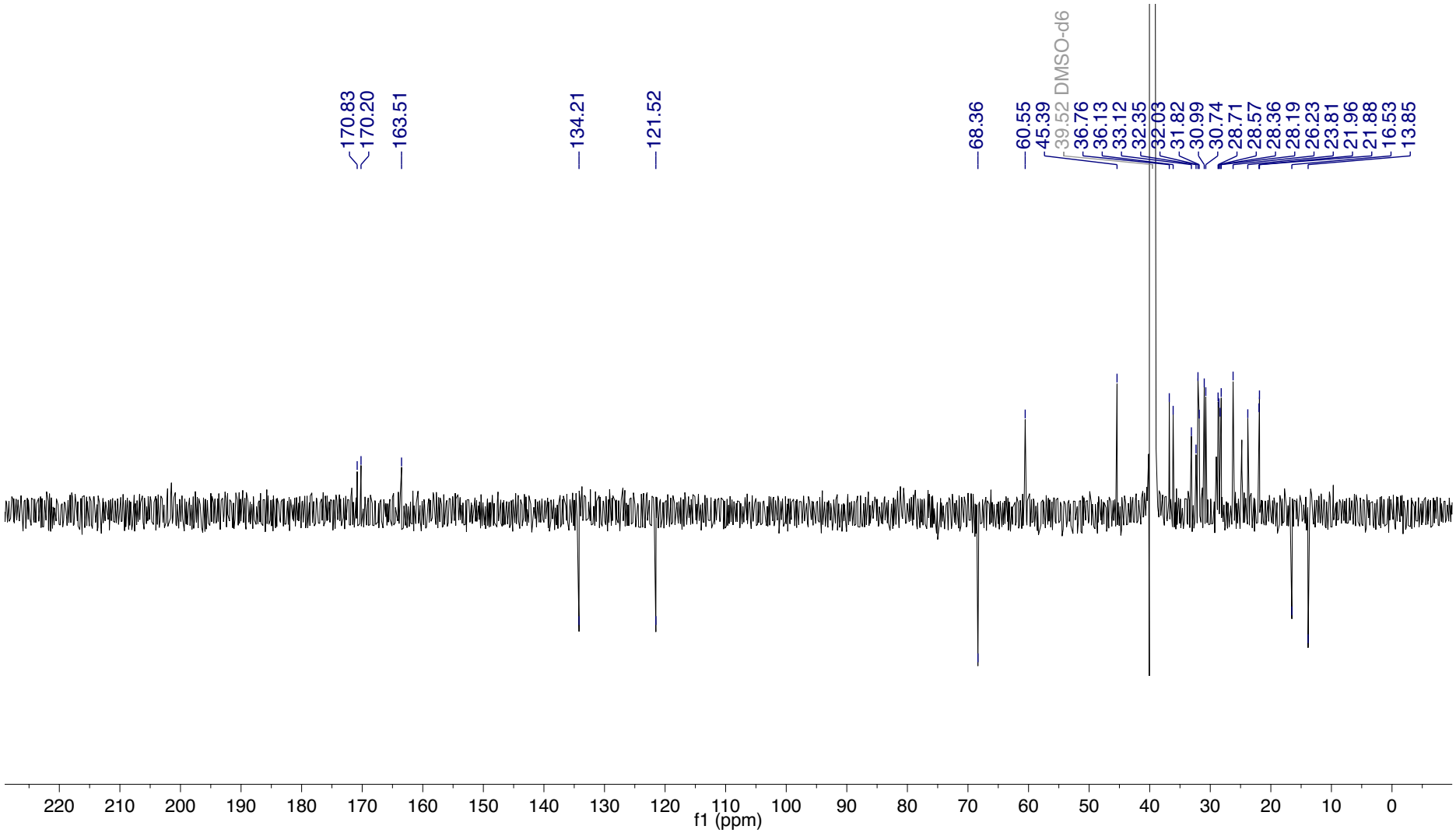

Figure S9. ^{13}C NMR (APT, DMSO-d_6, 150 MHz) spectrum of compound **10**.

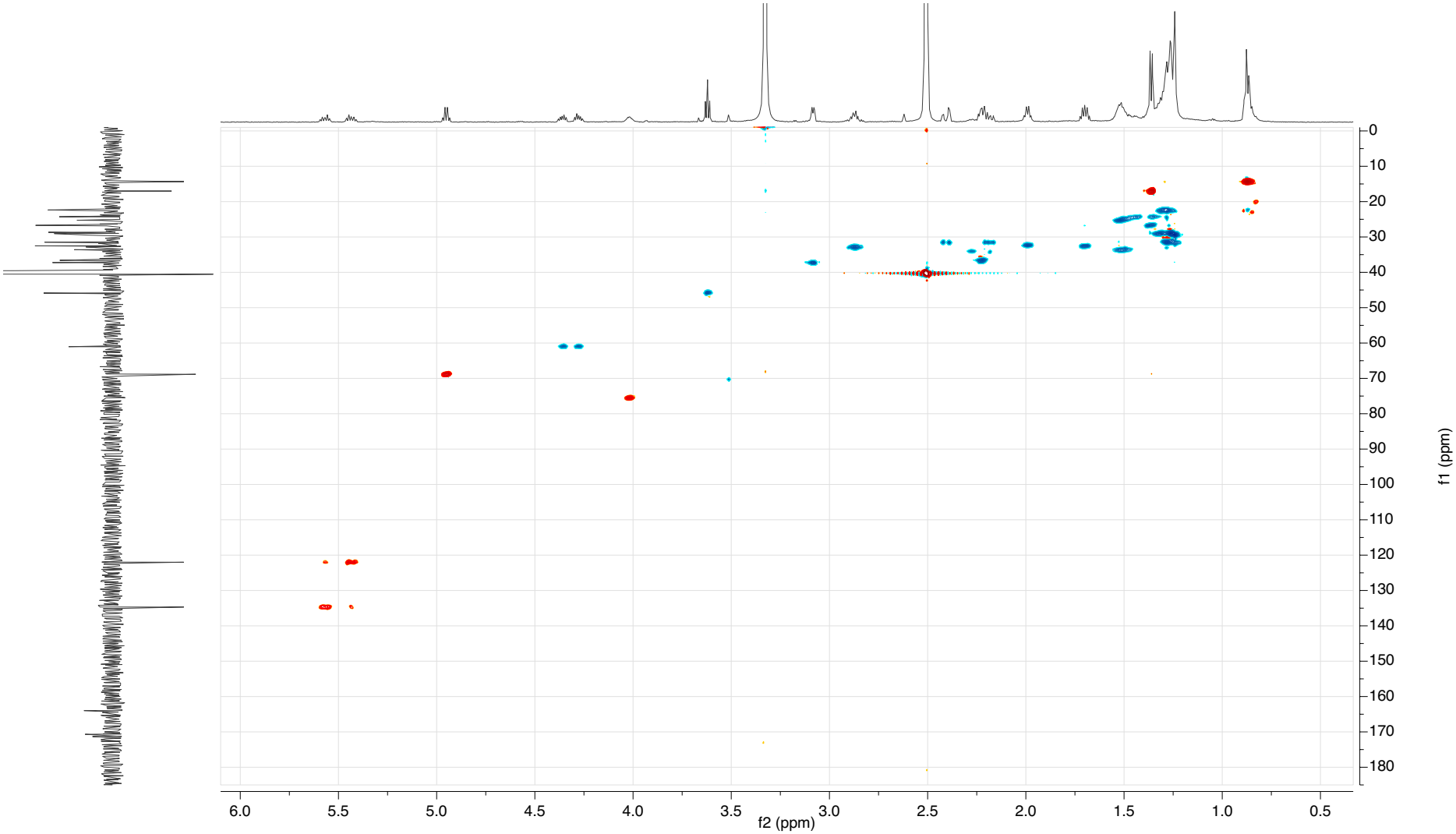

Figure S10. HSQC (DMSO-d_6, 600 MHz) spectrum of compound **10**.

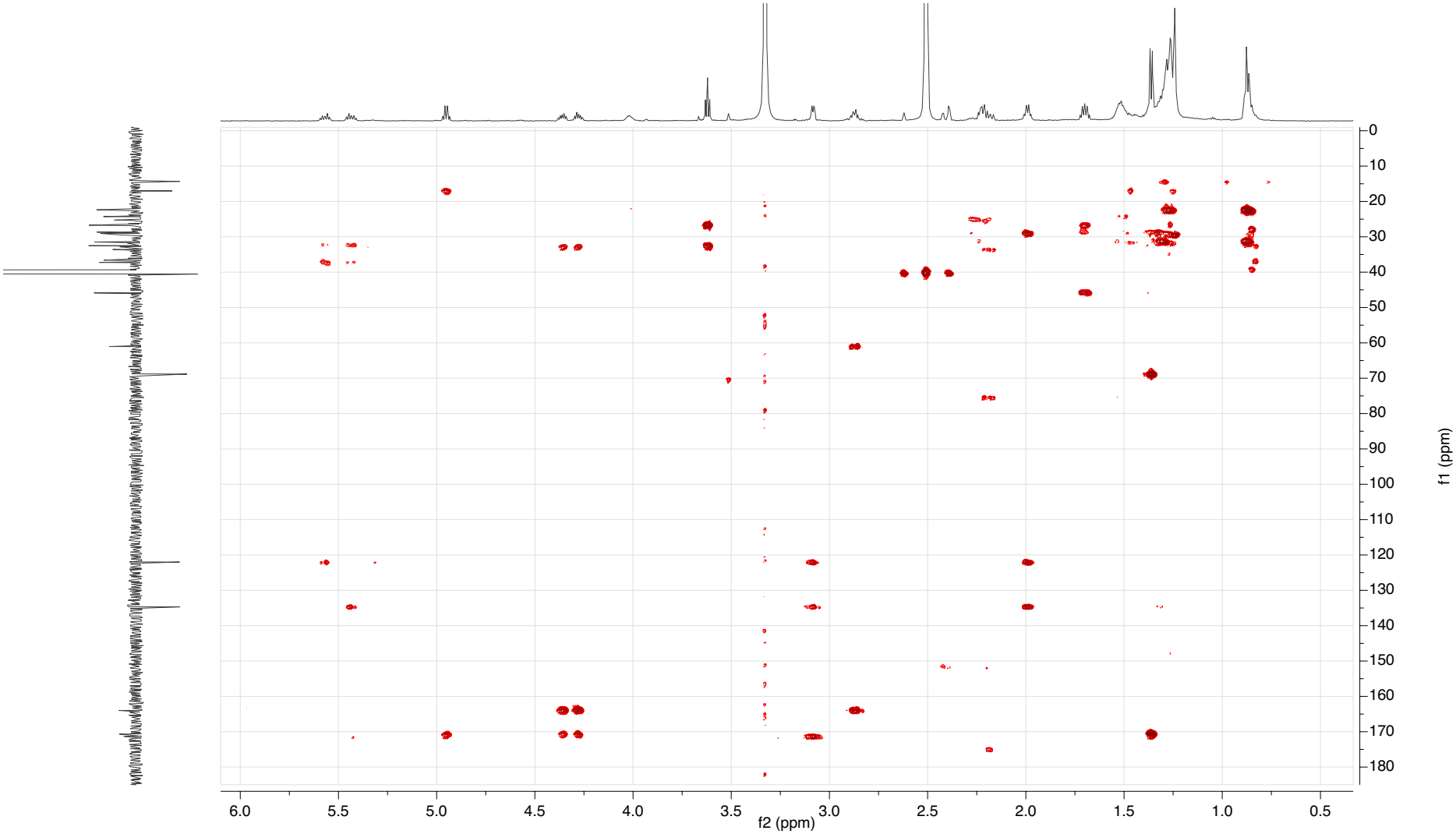

Figure S11. HMBC (DMSO-d_6, 600 MHz) spectrum of compound **10**.

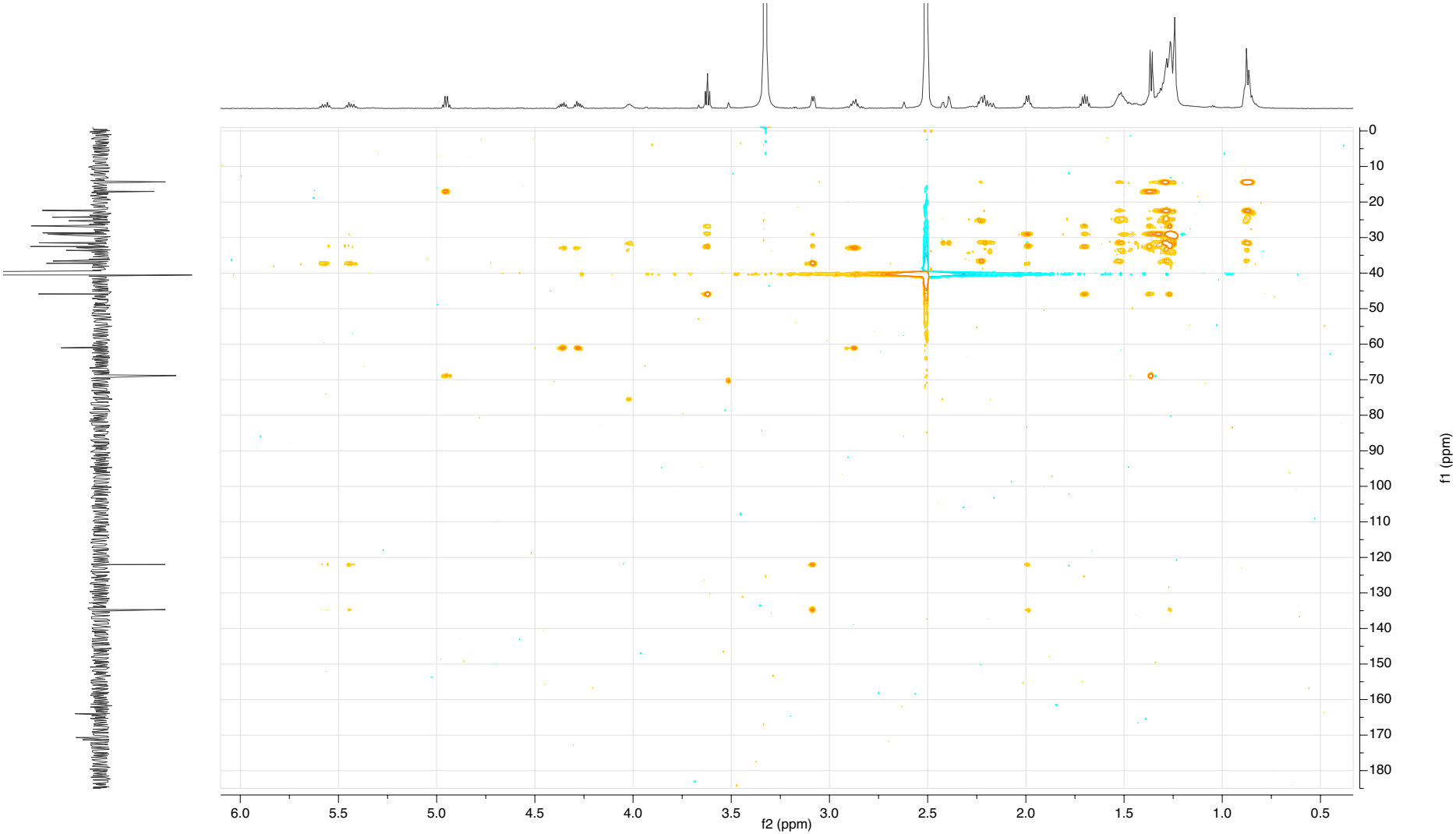

Figure S12. HSQC-TOCSY (100 msec mixing time, DMSO-d_6, 600 MHz) spectrum of compound **10**.

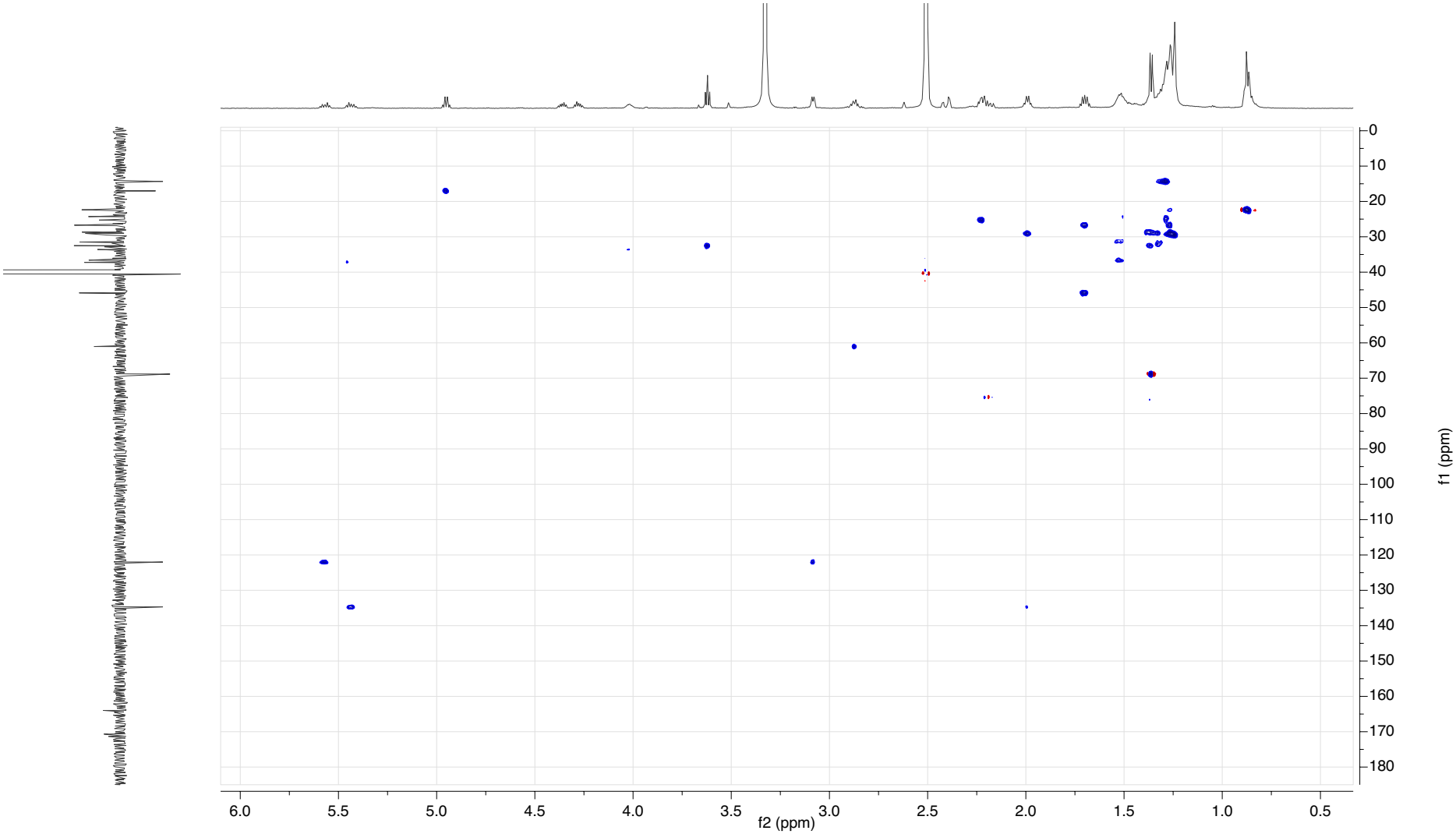

Figure S13. H2BC (DMSO-d_6, 600 MHz) spectrum of compound **10**.

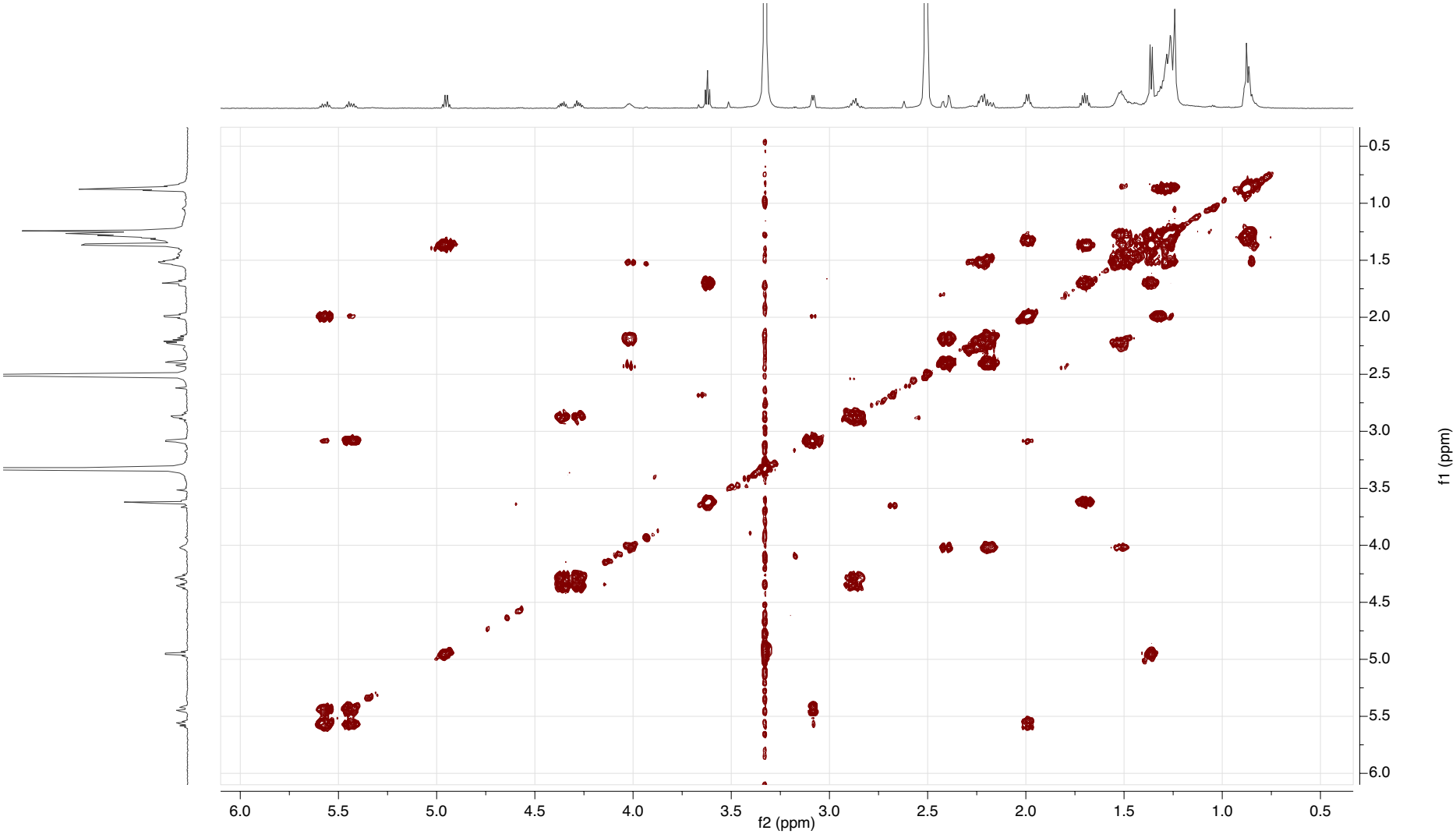

Figure S14. COSY (DMSO-d_6, 600 MHz) spectrum of compound **10**.

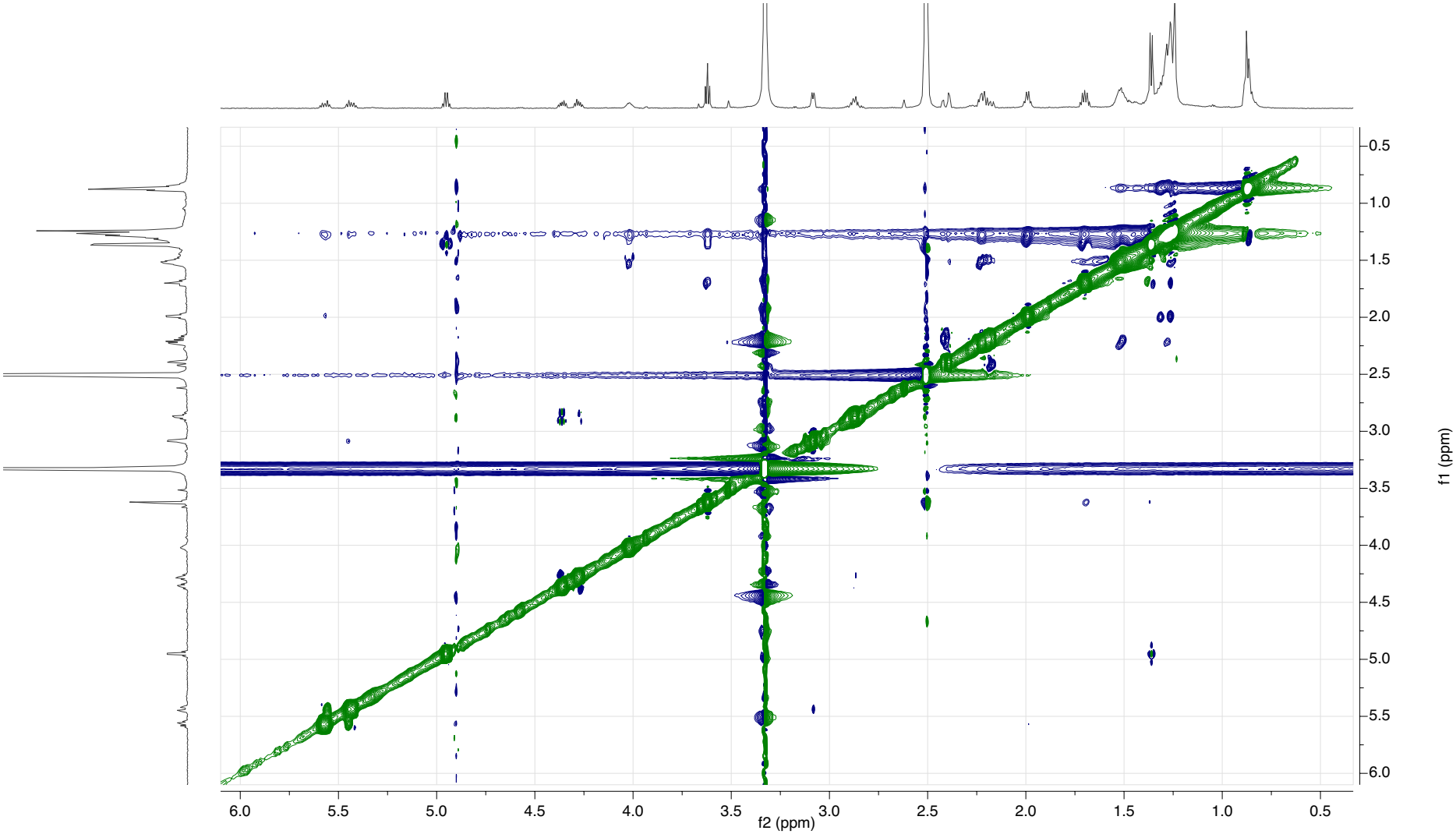

Figure S15. NOESY (DMSO-d_6, 600 MHz) spectrum of compound **10**.

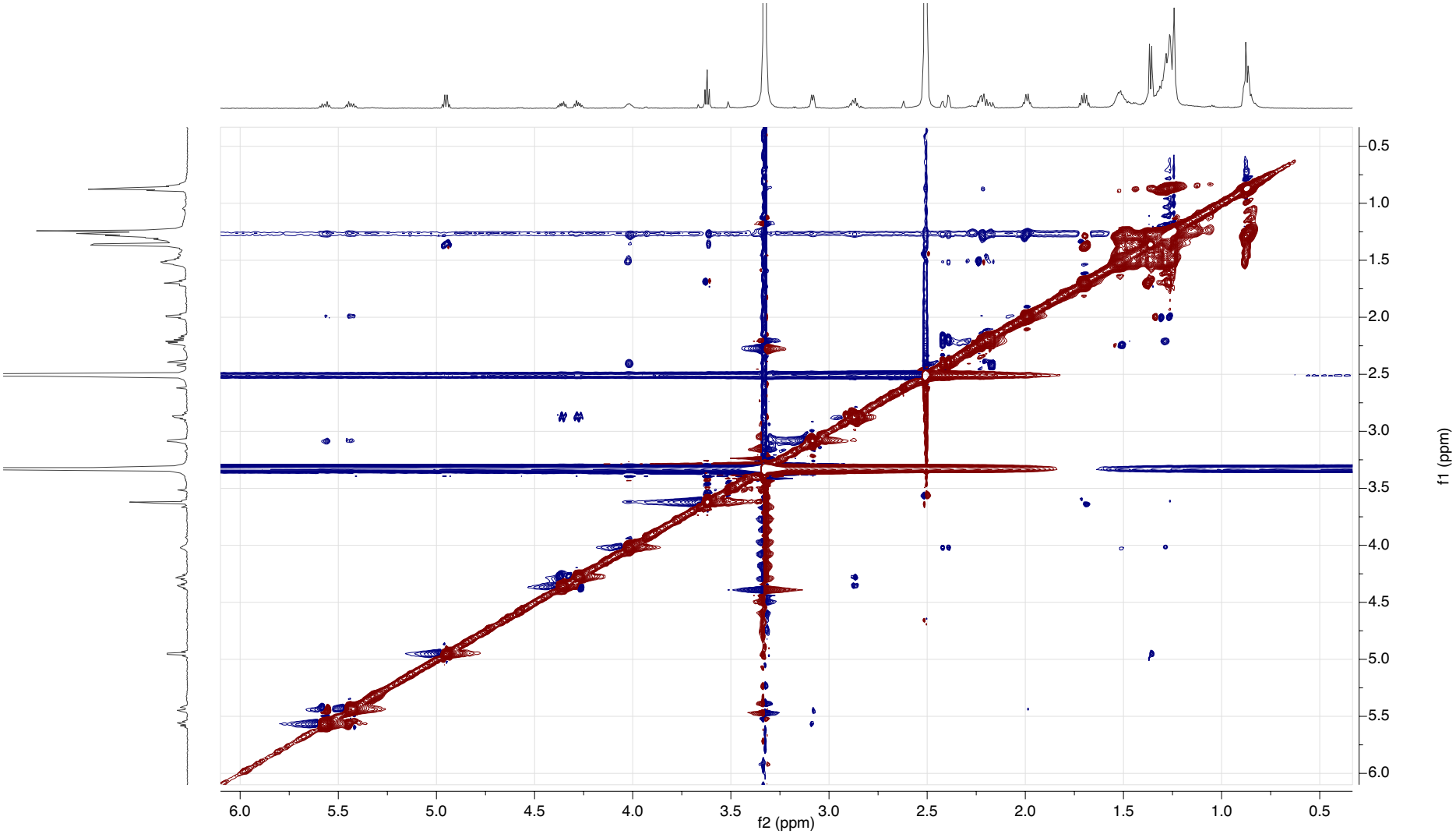

Figure S16. ROESY (DMSO-d_6, 600 MHz) spectrum of compound **10**.

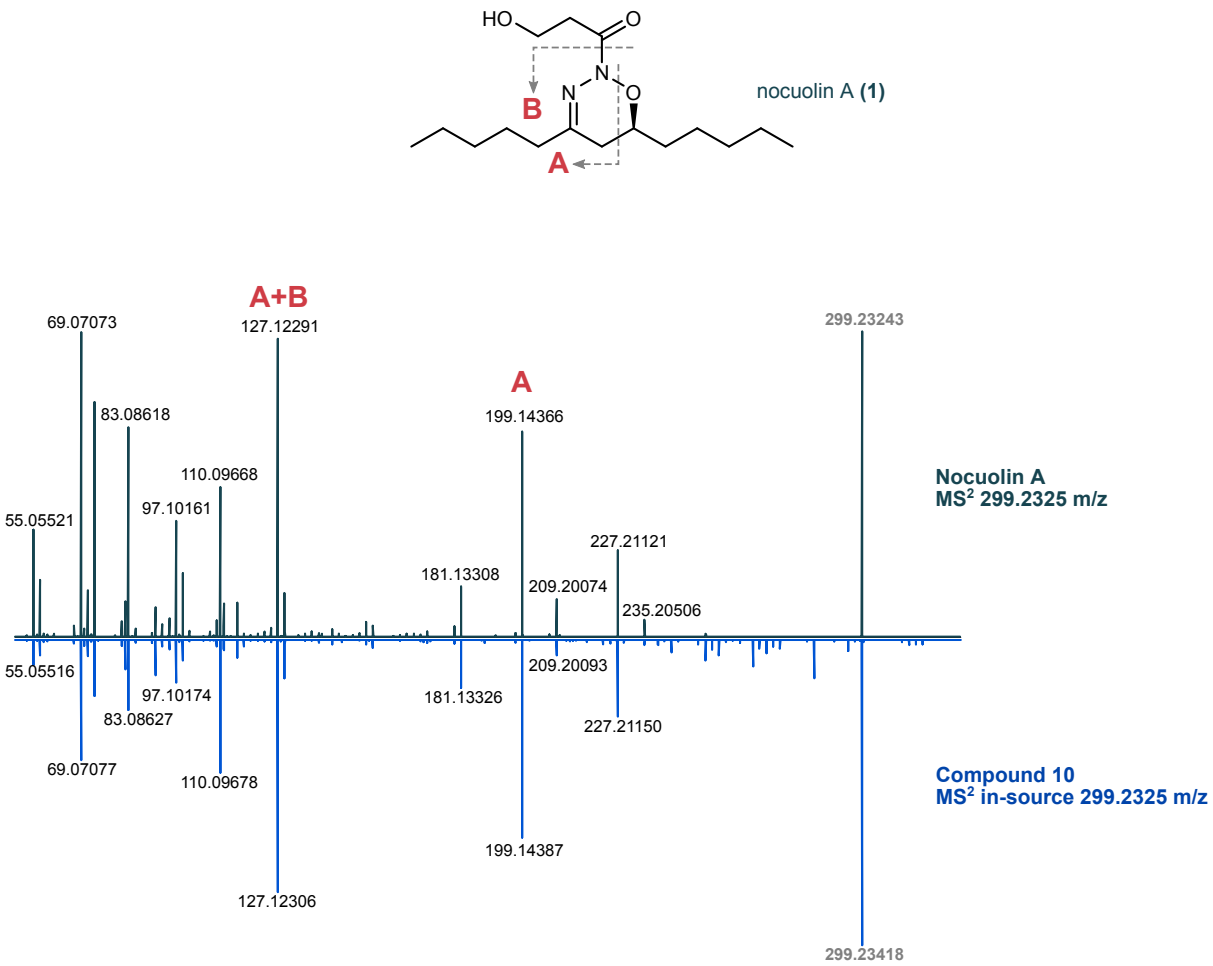

Figure S17. HRESIMS/MS confirmation of the presence of a nocuolin A (**1**)-derived moiety in compound **10**. Comparison of the HRESIMS/MS spectrum of pure **1** and of the 299.233 ion isolated in-source from **10**.

Text S2. Structure elucidation of nocuolin A (**1**) from *Nodularia* sp. LEGE 06071.

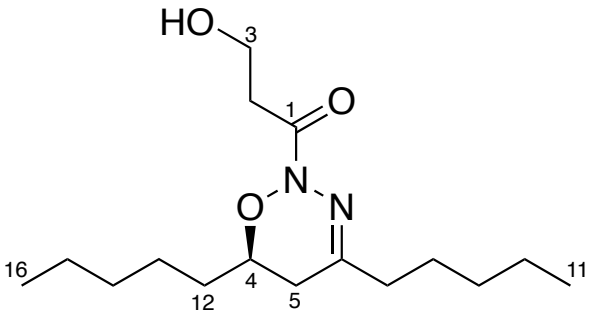

High-resolution electrospray ionization mass spectrometry (HRESIMS) data for nocuolin A (**1**) were consistent with a molecular formula of $C_{16}H_{30}N_2O_3$ (*m/z* 299.2329 $[M+H]^+$, calcd. 299.2329) with three degrees of unsaturation. The combination of the APT and HSQC NMR data indicated the presence of one carbonyl, one methine, 11 methylenes and two methyl groups. An additional deshielded and non-protonated carbon was evident from HMBC correlational data (Table S4) and corroborated the MS-derived molecular formula.

The planar structure of nocuolin A (**1**) was proposed from the analysis of 1D and 2D NMR data in DMSO-d_6 (Table S4) and supported by HRESIMS/MS data (Fig. S26). COSY correlations from H_2-3 to both H_2-2 and a single exchangeable proton (OH-3), taken together with HMBC correlations from this moiety to carbonyl C-1, allowed for the straightforward establishment of a 3-hydroxypropionyl moiety (see figure below). Loss of this acyl group was a favored fragmentation in the HRESIMS^2 spectrum of **1** (see Fig. S26). Two identical aliphatic three-carbon long chain termini were evident from the overlapping carbon and proton resonances of the COSY and/or HMBC correlated CH_3-11/16, CH_2-10/15 and CH_2-9/14. One of the chains could be further extended by two carbons through COSY correlations between H_2-8 and both H_2-9 and H_2-7, leaving only one methine, three methylenes and a non-protonated carbon to be assigned.

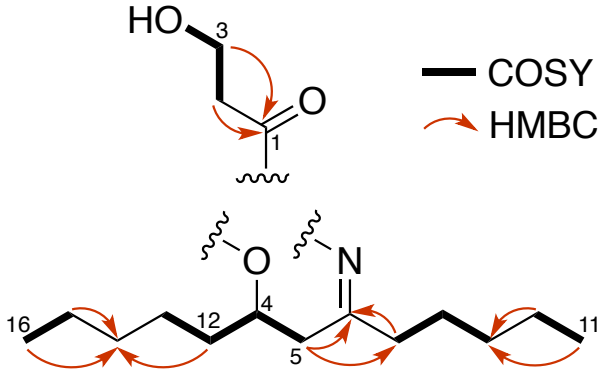

The single methine in the molecule (CH-4) was connected to a heteroatom (δ_C 74.9, δ_H 3.99) and correlated in the COSY spectrum with two methylene groups (H_2-5, H_2-12). In turn, the H_2-12 protons (δ_H 1.50) were COSY-correlated to a diastereotopic proton (H_b-13, δ_H 1.34) and HMBC-correlated to a methylene from one of the chain termini moieties (C-14, δ_C 31.0). Assignment of the two remaining carbons was based on HMBC correlations between the deshielded non-protonated C-6 (δ_C 150.3) and both the diastereotopic protons in position 5 and the H_2-7 protons. This left two N atoms and one O atom to be assigned. The possibility of a ketone functionality at C-6 was dismissed by its upfield carbon resonance. Instead, the ^{13}C NMR data were supportive of an N-substituted imino group at this position (see above figure). Regarding CH-4, the NMR data (δ_C 74.9, δ_H 3.99) were characteristic of an oxymethine and not of N-substitution. Finally, to satisfy the three degrees of unsaturation, it would be required that the single unassigned N atom fully connected the two substructures (via three σ bonds), thereby establishing the cyclic structure of **1**. HRESIMS^2 data for **1**

supported our structure proposal (see Fig. S26). It is noteworthy that the assignment of a N atom as a substituent at CH-4 would lead to either: i) an alkyl-substituted 4,5-dihydropyrazolyl moiety connected to 3-hydroxypropionate or ii) an *N*-acylated 1,2,6-oxadiazine (see figure below).

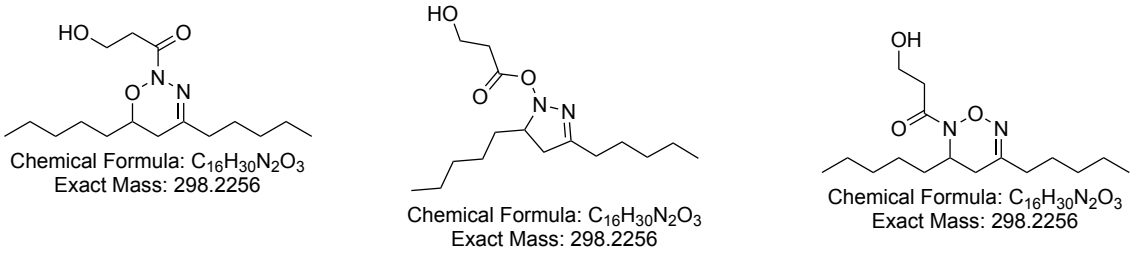

The latter alternative would require extensive rearrangements in the gas-phase to yield most fragments observed in HRESIMS² (Fig. S26). We thus focused on the remaining structure alternatives, namely the oxadiazine and the pyrazoline. Assuming gas-phase rearrangements involving ring-opening, both structures are compatible with most MS/MS-generated fragments. However, the prominent fragments "B" and "F", and minor fragments "D" and "E" (Fig. S26) support a direct linkage between the hydrazone and the 3-hydroxy-propionyl moieties and would require extensive rearrangement/bond breakage to be generated in the case of the pyrazoline. To better scrutinize the two structure alternatives, and in the absence of a synthetic route to a 1,2,3-oxadiazine,[28] we carried out HRESIMS/MS analysis on both the commercially available 1*H*-pyrazol-1-ol (**s1**) and its propionate ester (**s2**) (see Materials and Methods for the synthesis details). The HRESISMS/MS fragmentation patterns of these compounds and those of **1** and of its in-source-isolated fragment corresponding to the neutral loss of the 3-hydroxypropionic acid-derived moiety (carbonyl-heteroatom bond breakage) were compared (see figure below).

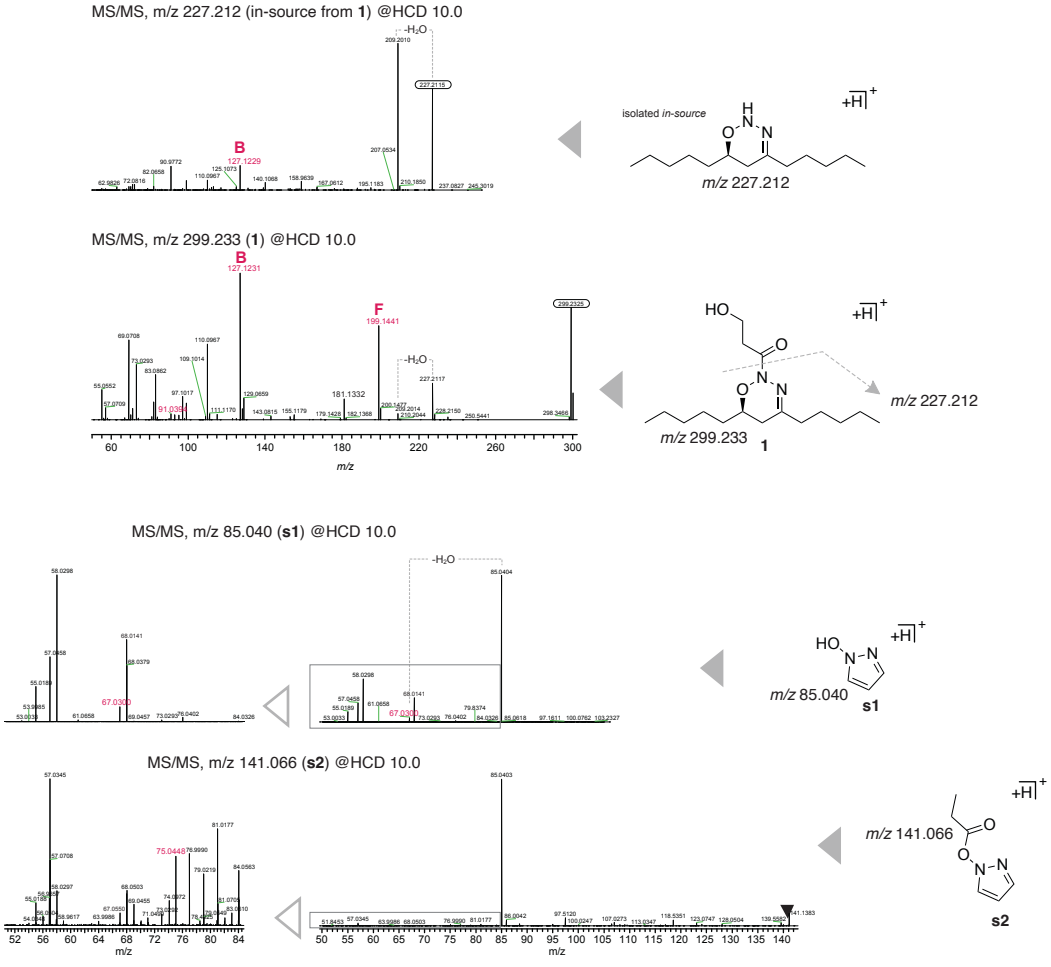

Overall, after analysis of the fragmentations of **s1** and **s2** most fragments observed for **1** can be reconciled with both structure alternatives (with considerable rearrangements). The fragmentation of **s2** yielded protonated **s1** in high abundance, but the subsequent loss of H_2O (*m/z* 67.030) was not prominent in the spectrum for **s2**. The opposite was observed for the HRESIMS/MS of **1** and its in-source isolated fragment; the latter showed a more prominent H_2O neutral loss (*m/z* 209.201). A minor fragment of **s2**, likely corresponding to the loss of protonated propionate moiety (*m/z* 75.044) had a counterpart in the HRESIMS/MS spectrum of **1** (*m/z* 91.039, $C_3H_7O_3^+$, compatible with a simple fragmentation of the entire 3-hydroxypropionate moiety), which was better explained by a pyrazoline structure. Still, the abundant fragments that correspond to losses of alkyl groups plus an oxygen atom, notably "B" (*m/z* 127.123), and "F" (*m/z* 199.144) in Fig. S26 and figure above are better explained by the oxadiazine structure. In particular, the most abundant fragmentation for **1**, "F, *m/z* 199.144", would require extensive rearrangement in the case of a pyrazoline system, while a simple ring opening, as expected for the 1,2,3-oxadiazine[28], would result in the fragmentation (see below).

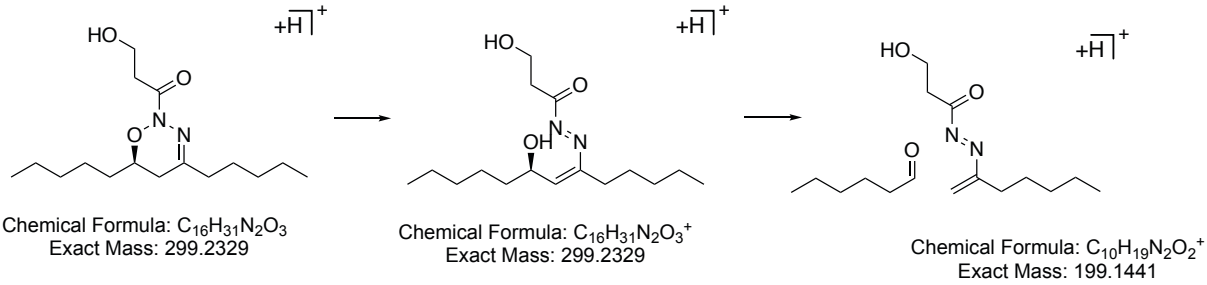

In line with this, HRESIMS/MS analysis of **10** also provided clues as to the nature of **1**. The sodium adduct was more stable than the protonated ion (see figure below) and fragmented through a different pathway, namely through a prominent N_2 loss (confirming the N-N bond in **1**) and also through a neutral loss of hexanal, which can be reconciled with the opening of the oxadiazine ring following ionization (see figure below), as previously proposed for **1**.[28] This prominent neutral loss would require extensive rearrangement if the structure of the **1**-derived portion in **10** was of the pyrazoline type.

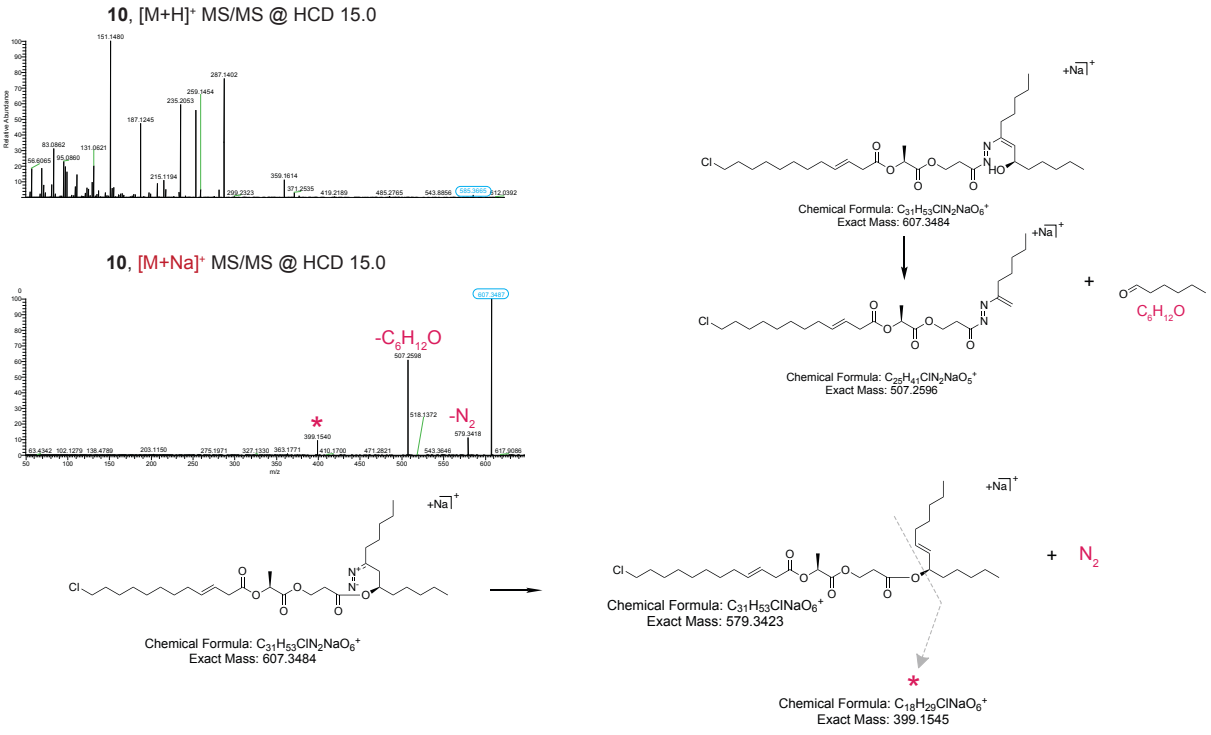

Computational UV-Vis spectra simulations predictions also support the oxadiazine structure (see figure below). While simulations of NMR data using different methods were compatible with both structures for ^{1}H NMR chemical shifts, ^{13}C NMR chemical shifts predictions, in particular those for the ring system, were much closer to the experimental values in the case of the oxadiazine structure (see figure below).

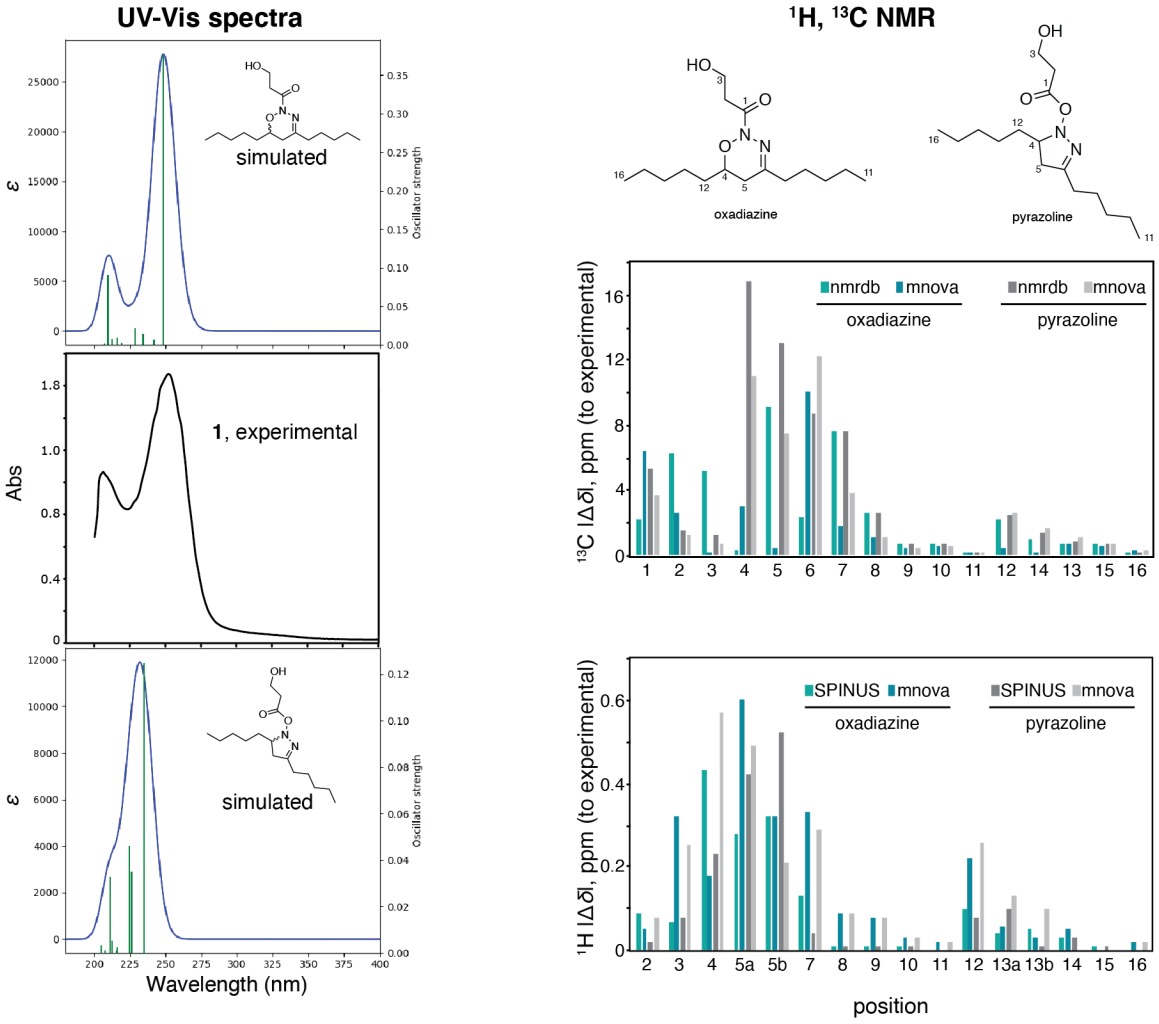

Overall, MS/MS data and computer simulations for UV/Vis and ^{13}C NMR data support the previous structural proposal by the Hrouzek group and co-authors.[28] Due to the novelty of the 1,2,3-oxadiazine ring in synthetic molecules or natural products,[28] the large number of consecutive heteroatoms in the structure and the fact that the original report of the structure of **1** was also based on NMR and MS/MS data analysis,[28] it would be desirable to obtain structural confirmation through total synthesis or partial synthesis of the ring system. To the best of our knowledge, 1,2,3-oxadiazines have not been synthesized to date.[28,29] NMR-independent methods such as the crystalline sponge method[30] or MicroED[31] could also be used for structure confirmation.

Table S4. NMR Spectroscopic Data (^{1}H 600 MHz, ^{13}C 150 MHz, DMSO-d_6) for nocuolin A (**1**).

Position	C	H (*J* in Hz)[b]	HMBC[a]	COSY	NOESY
1	165.1, C=O				
2	36.8, CH_2	2.67, td (2.2, 6.5)	56.9, 165.1,	3.64	3.64, 4.57
3	56.9, CH_2	3.64, td (5.4, 6.5)	36.8, 165.1	2.67, 4.57	2.67, 4.57
3-OH		4.57, t (5.4)	36.8, 56.9	3.64	2.67, 3.64
4	74.9, CH	3.99, m		1.50, 2.16	1.51, 2.38
5a	30.7, CH_2	2.38, dd (4.0, 18.3)	36.1, 150.3	2.16	1.50, 2.16, 3.99
5b		2.16, dd (8.8, 18.3)	33.2, 74.9, 150.3	2.38, 3.99	1.50, 2.38
6	150.3[b], C=N				
7	36.1, CH_2	2.21, td (2.7, 7.3)	24.8, 31.0, 150.3	1.51	1.27, 1.51
8	24.8, CH_2	1.51, m		1.27, 2.21	2.21, 3.99
9	31.0, CH_2	1.27, m	21.9, 24.8	1.51	2.21
10	21.9, CH_2	1.29, m	13.8, 31.0	0.87	0.87
11	13.8, CH_3	0.87, t (6.5)	21.9, 31.0	1.29	1.29
12	33.2, CH_2	1.50, m	23.8, 31.0, 74.9	1.34, 3.99	1.34, 1.43
13a	23.8, CH_2	1.43, m		1.34	
13b		1.34, m		1.43, 1.50	
14	31.0, CH_2	1.27, m	21.9		
15	21.9, CH_2	1.29, m	13.8, 31.0	0.87	0.87
16	13.8, CH_3	0.87, t (6.5)	21.9, 31.0	1.29	1.29

[a]from proton to the indicated carbon; [b]extracted from HMBC.

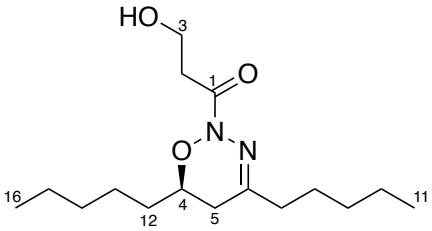

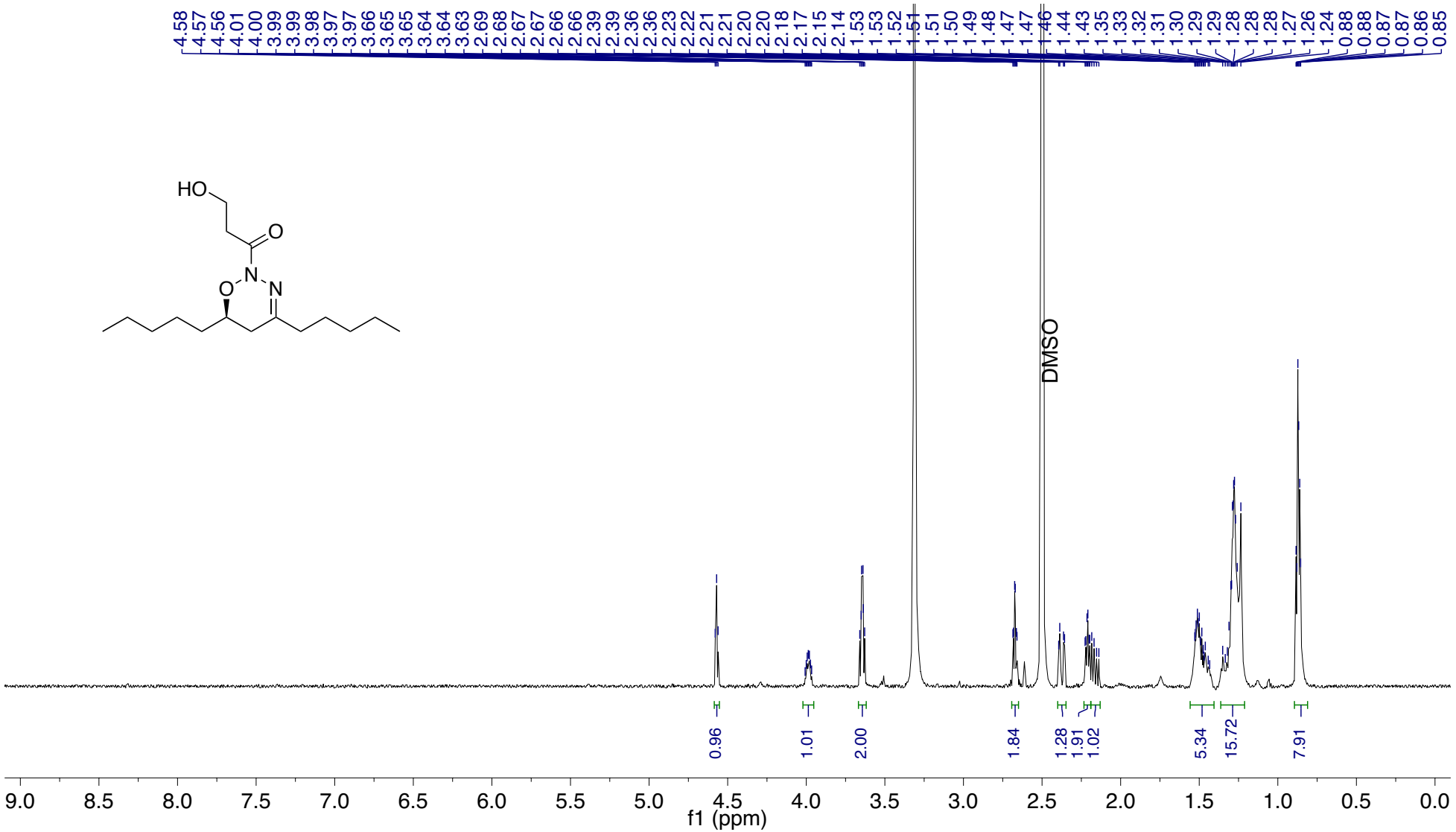

Figure S18. ^{1}H NMR spectrum of nocuolin A (**1**), recorded at 600 MHz in DMSO-d_6.

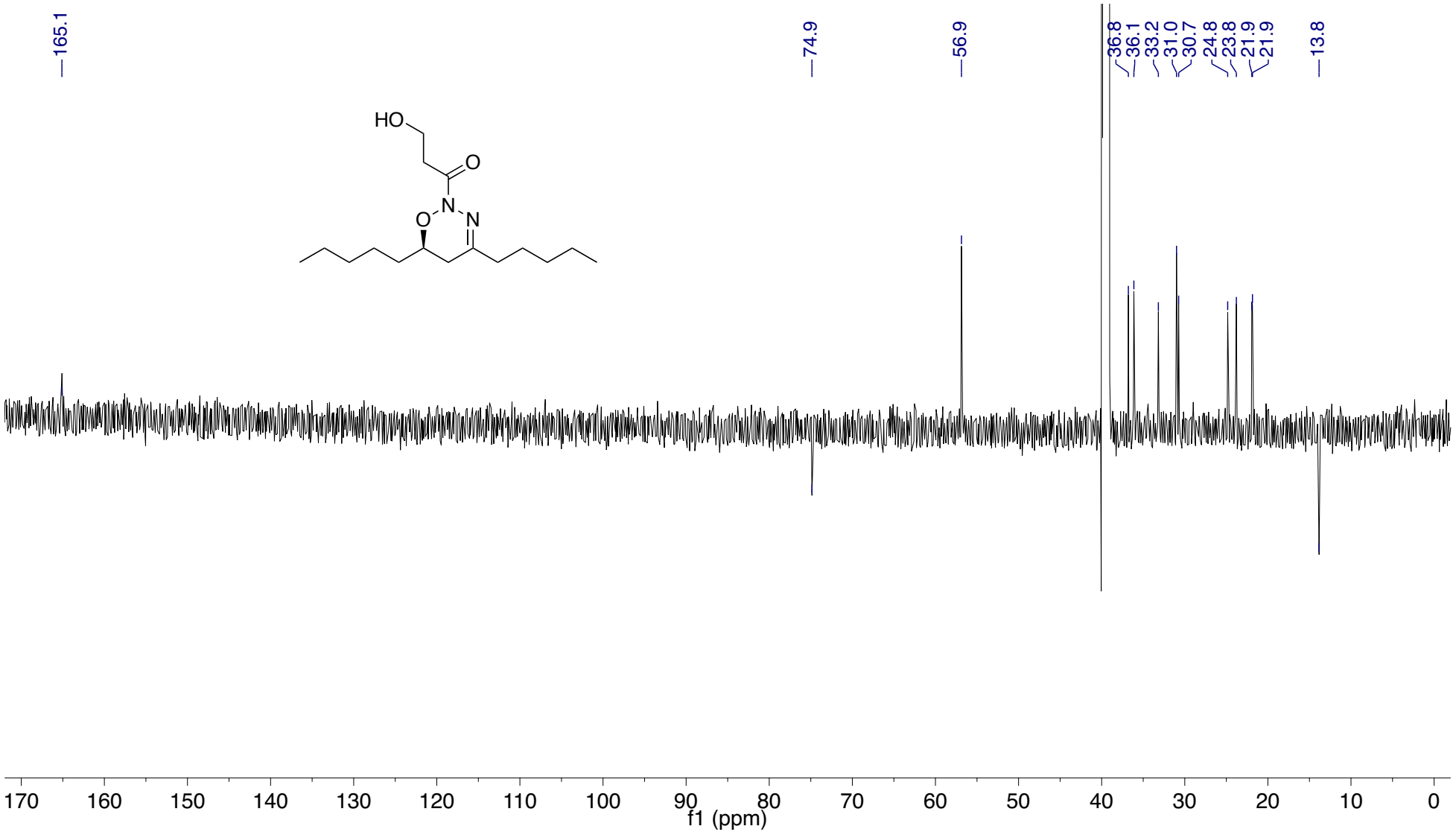

Figure S19. ^{13}C APT spectrum of nocuolin A (**1**), recorded at 150 MHz in DMSO-d_6.

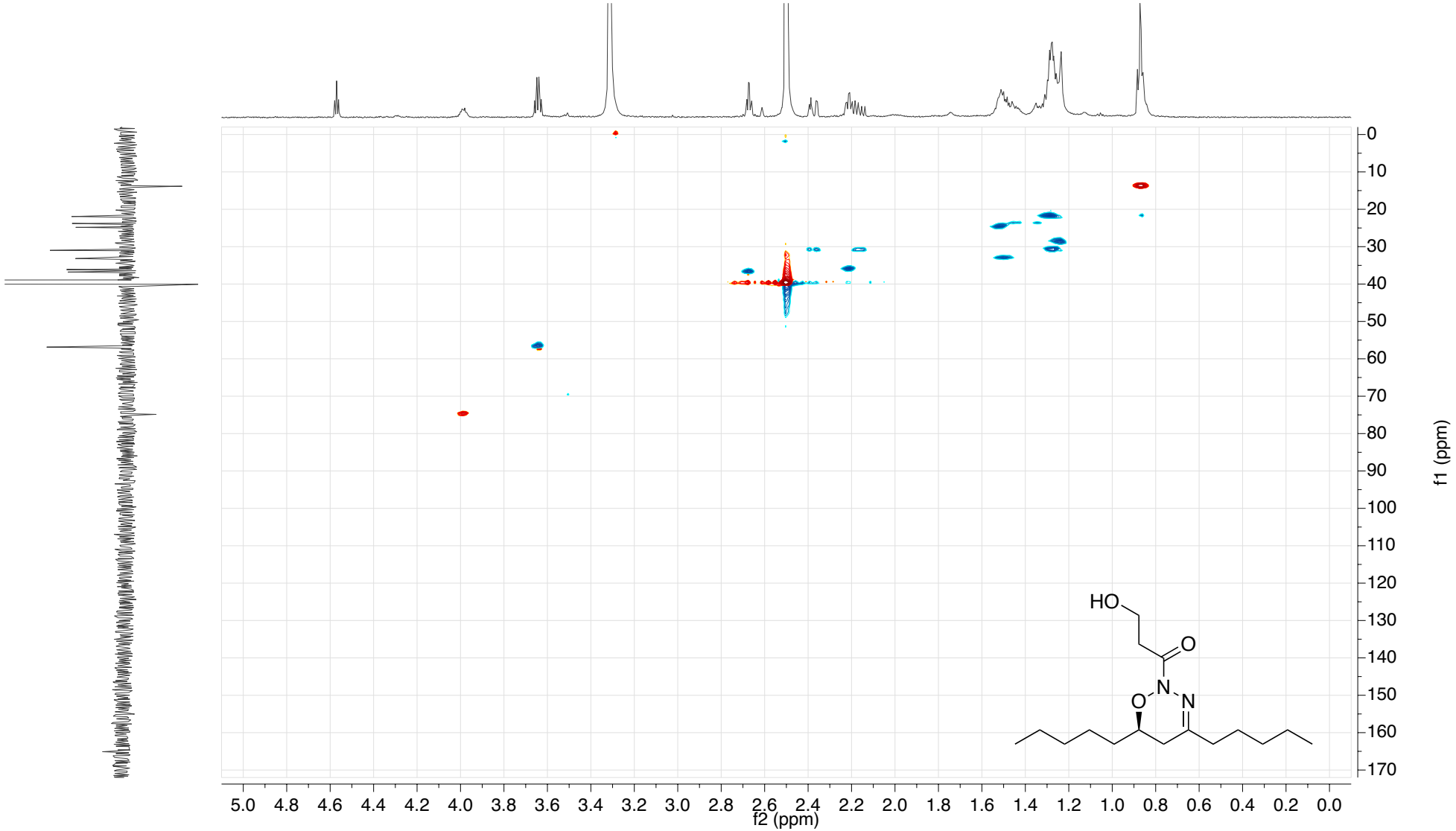

Figure S20. HSQC spectrum of nocuolin A (**1**), recorded at 600 MHz in DMSO-d_6.

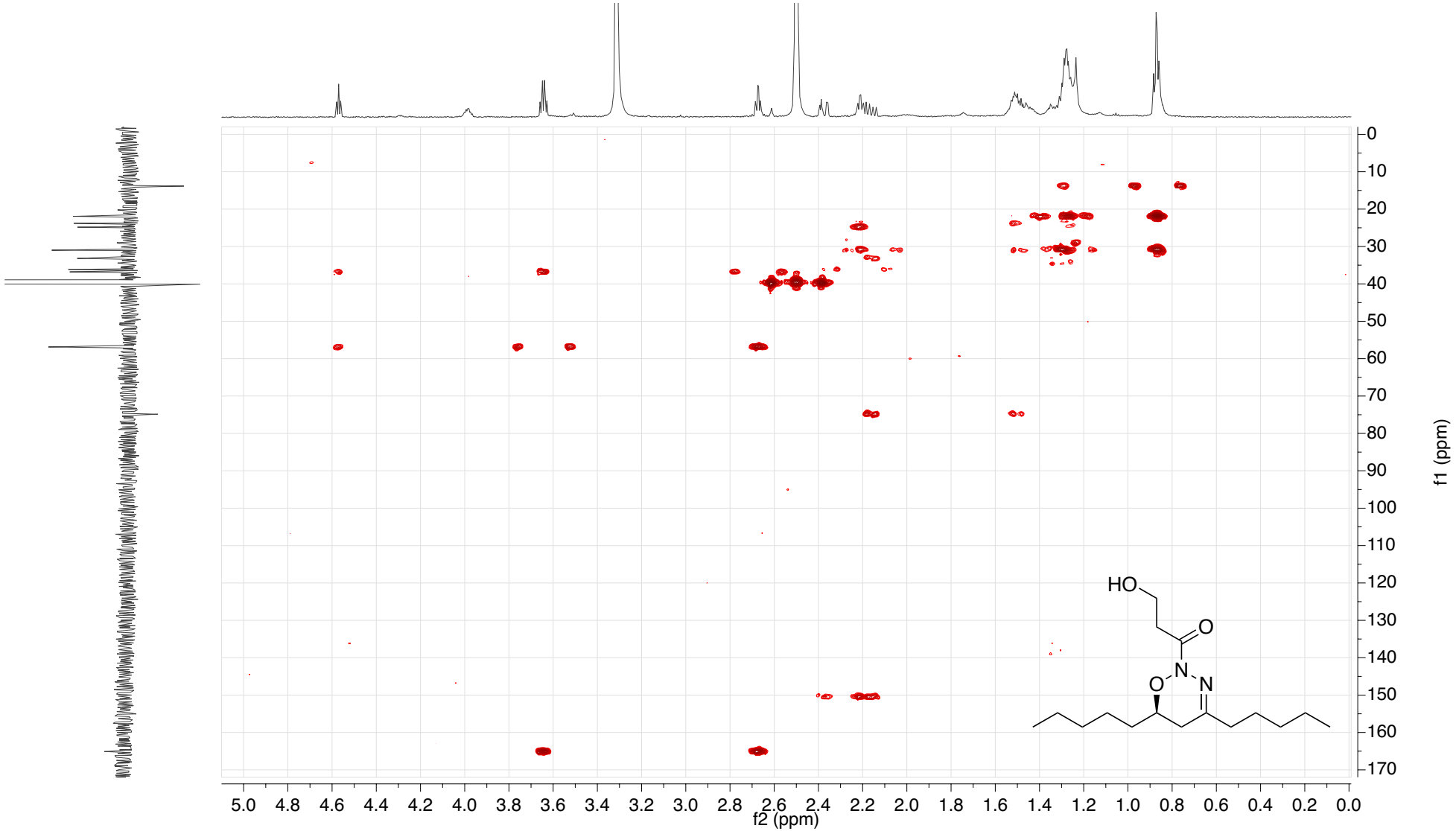

Figure S21. HMBC spectrum of nocuolin A (**1**), recorded at 600 MHz in DMSO-d_6.

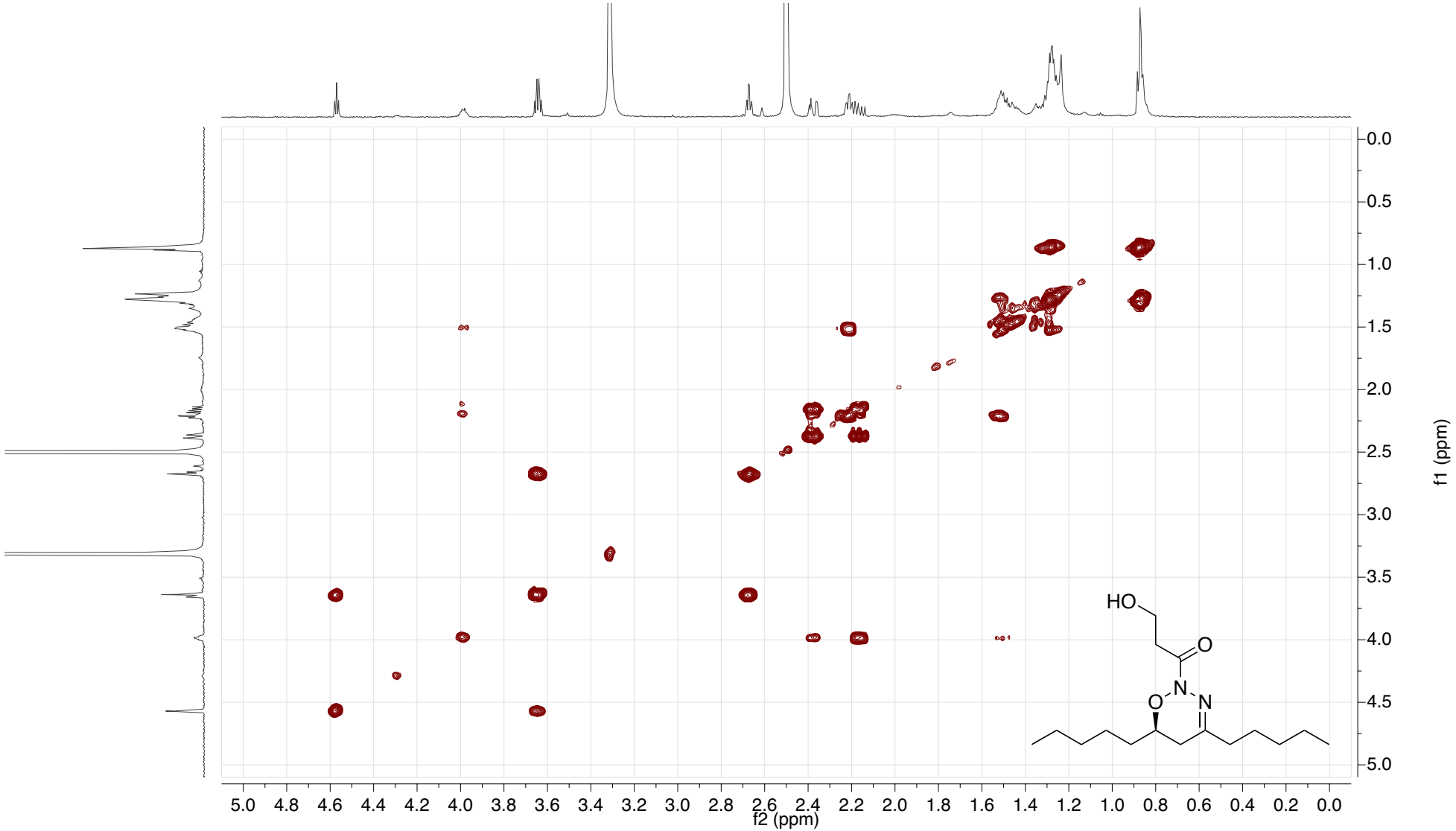

Figure S22. COSY spectrum of nocuolin A (**1**), recorded at 600 MHz in DMSO-d_6.

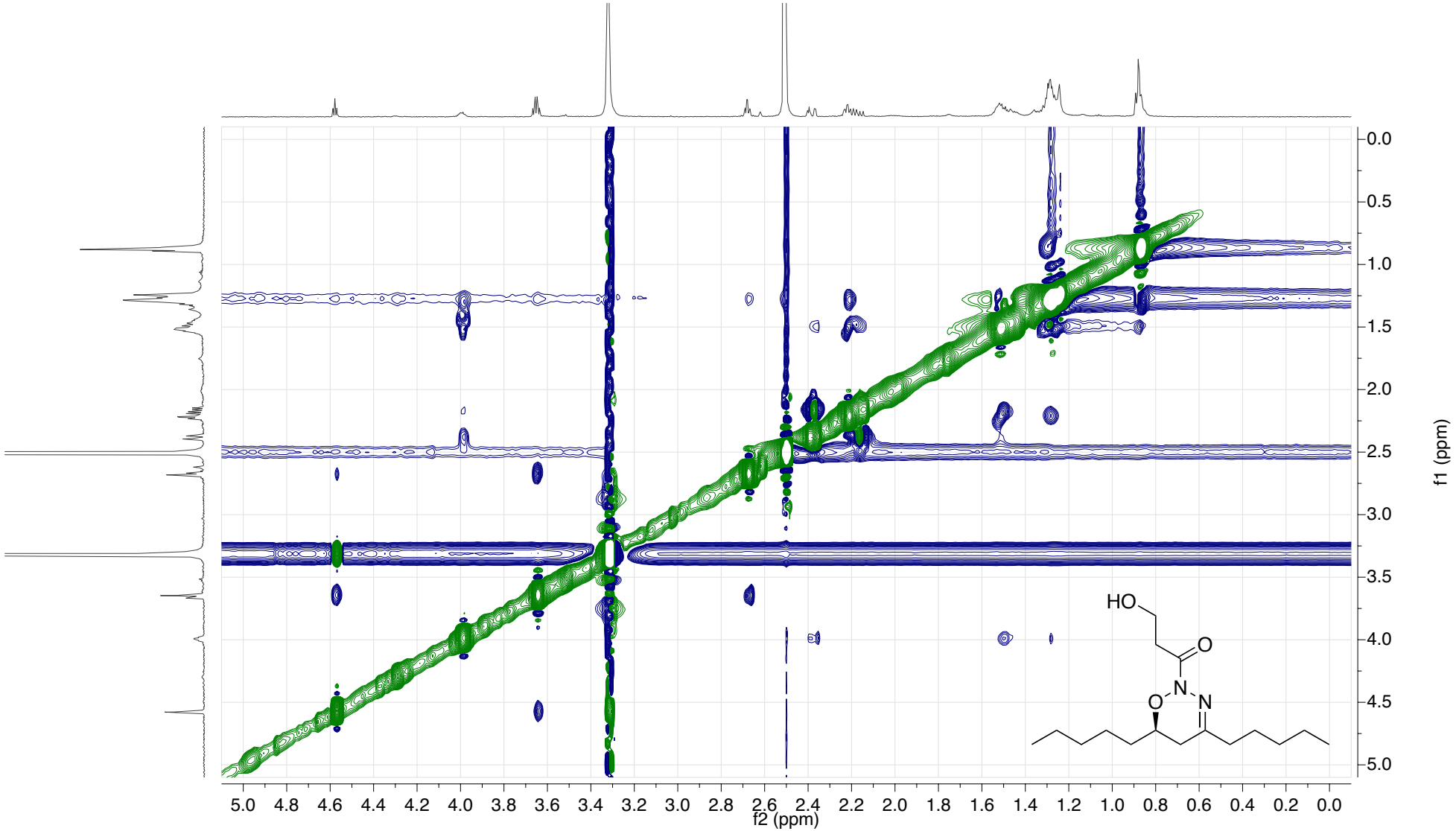

Figure S23. NOESY spectrum of nocuolin A (**1**), recorded at 600 MHz in DMSO-d_6.

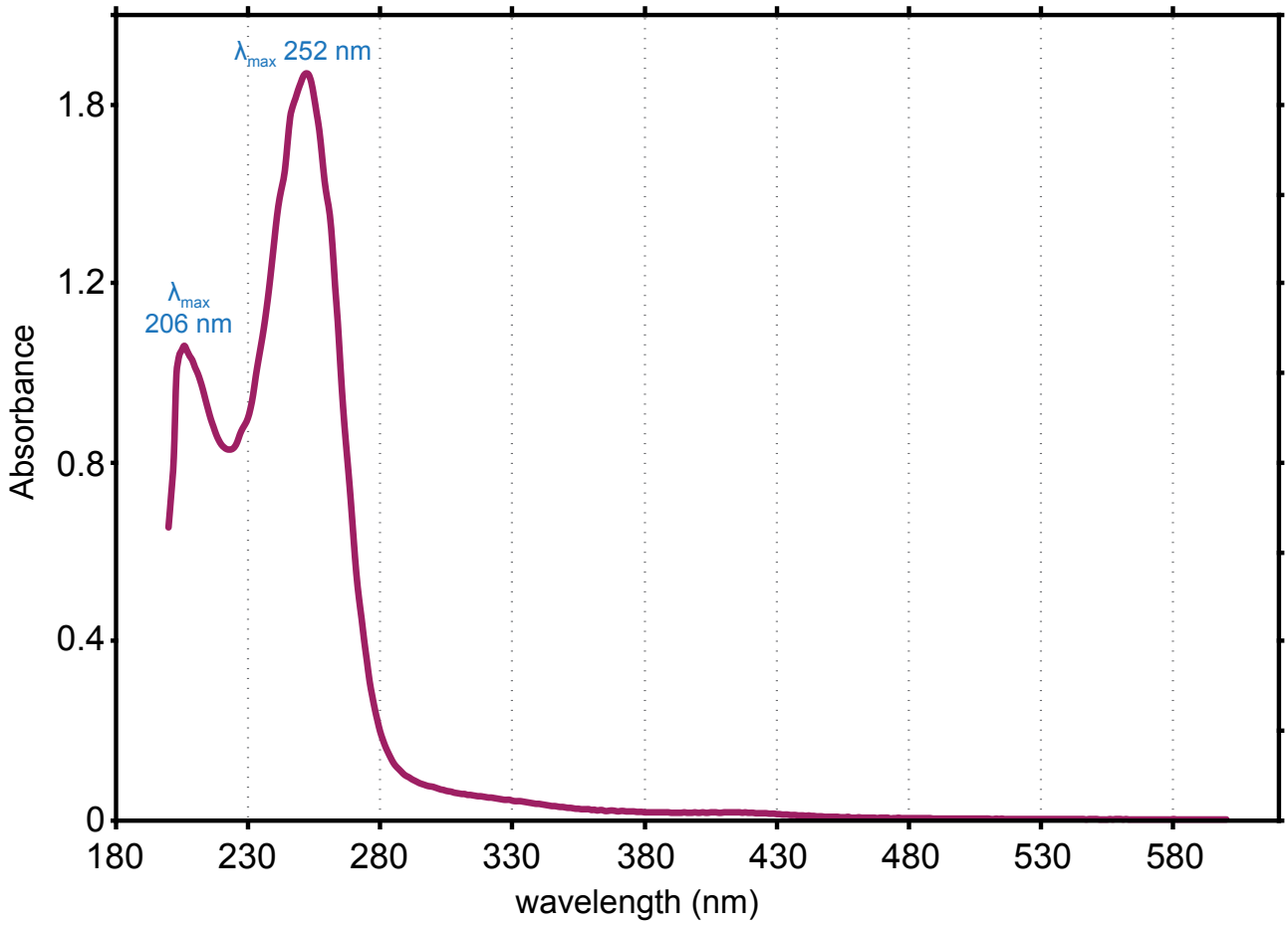

Figure S24. UV-Vis spectrum of nocuolin A (**1**) in MeOH (0.16 mg mL^{-1}).

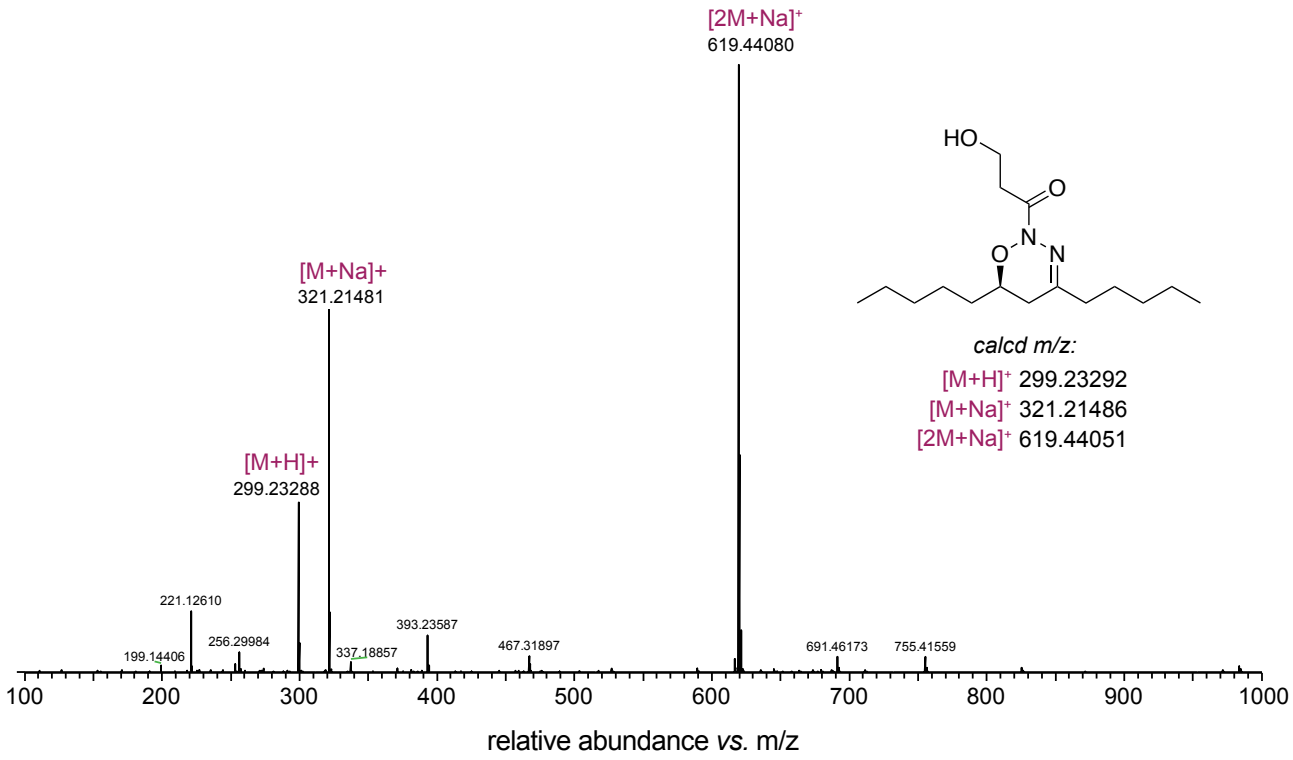

Figure S25. HRESIMS spectrum of nocuolin A (**1**).

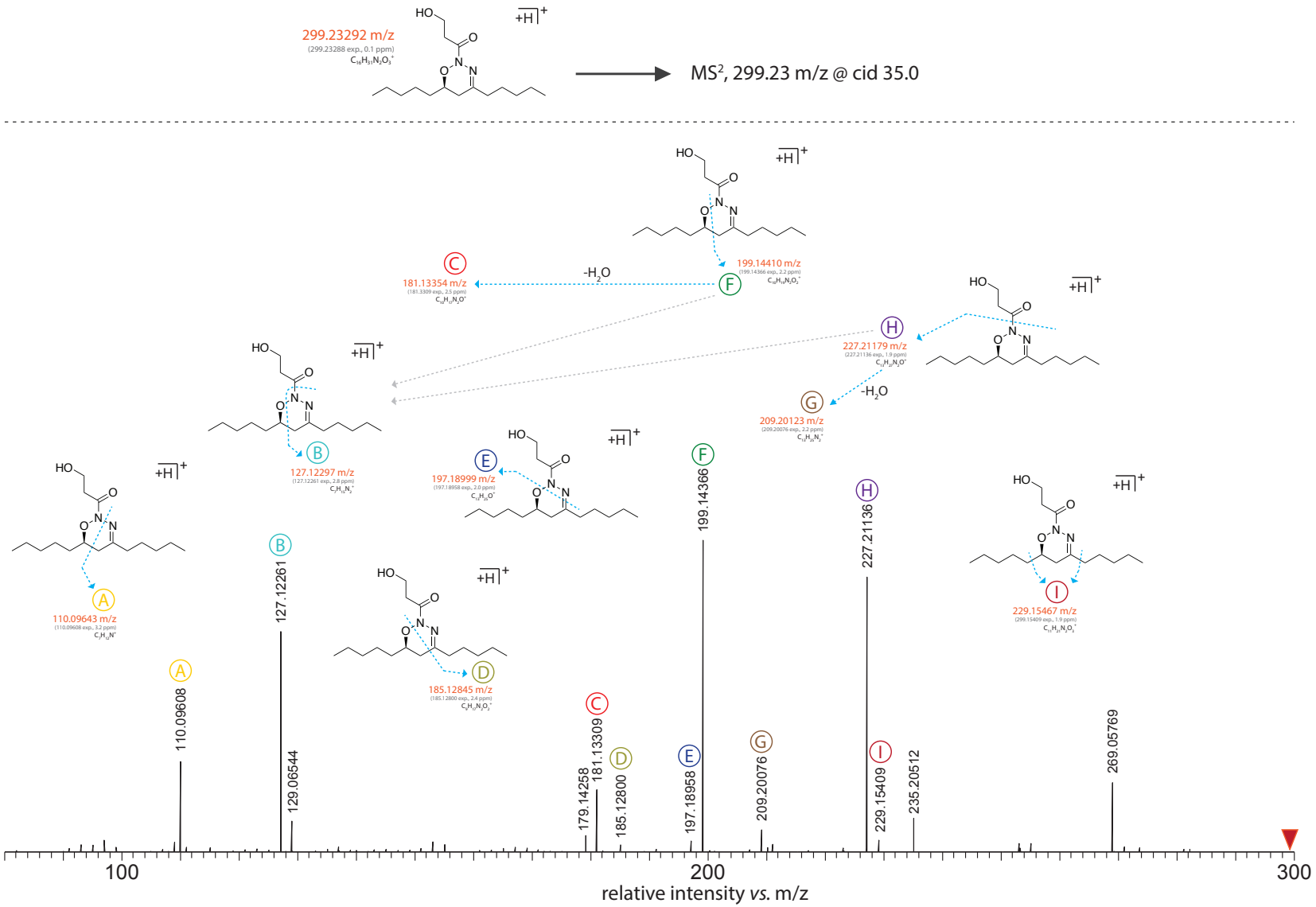

Figure S26. Annotated, positive-mode HRESIMS² (Collision-Induced Dissociation, CID) spectrum of the $[M+H]^+$ ion of nocuolin A (**1**).

Table S5. NMR Spectroscopic Data (^{1}H 600 MHz, ^{13}C 150 MHz, DMSO-d_6) for nocuolactylate B (**11**).

Position	C	Type	H	mult. *J*(Hz)	HMBC[a]	COSY
1	163.5	C				
2	32.4	CH_2	2.86	m	163.5, 60.6	4.35, 4.27
3	60.6	CH_2	4.35/4.27	dt, 10.8, 6.2/11.2, 6.0	170.8, 163.5, 32.4	4.35, 4.27, 2.86
4	74.9	CH	4.01	s		2.19
5	30.8	CH_2	2.39/2.19	m	151.2, 74.9	4.01, 2.39, 2.19
6	151.2[b]	C				
7	36.1	CH_2	2.20	m	74.9, 31.0, 23.8	4.01, 2.39, 2.19
8/13	23.8	2 × CH_2	1.27	m	31.9-27.6, 22.0, 16.6, 13.9	1.98, 1.45, 1.27, 0.87
9/14	31.0	2 × CH_2	1.27	m	31.9-27.6, 22.0, 16.6, 13.9	1.98, 1.45, 1.27, 0.87
10/15	22.0	2 × CH_2	1.27	m	31.9-27.6, 22.0, 16.6, 13.9	1.98, 1.45, 1.27, 0.87
11/16	13.9	2 × CH_3	0.87	m	31.0, 23.8, 22.0	1.27
12	33.1	CH_2	1.51	m	74.9, 30.8-31.0	4.01, 2.19, 1.27
17	170.8	C=O				
18	68.4	CH	4.94	q. 7.0	170.2, 16.6	1.35
19	16.6	CH_3	1.35	d. 7.0	170.2, 68.4	4.94
20	170.2	C=O				
21	36.8	CH_2	3.07	d, 7.6	170.2, 134.2, 121.5	5.44
22	121.5	CH	5.44	m	134.2, 36.8, 31.8	5.56, 3.07
23	134.2	CH	5.56	dt, 14.1, 6.9	121.5, 36.8, 31.8	5.44, 1.98
24	31.8	CH_2	1.98	m	134.2, 121.5, 27.8-28.6	5.56, 1.27
25-28	28.6-27.8	4 × CH_2	1.27	m	31.9-28.6, 16.6, 13.9	1.98, 1.45, 1.27, 0.87
29	25.3	CH_2	1.45	m	74.9, 42.9, 28.6-27.8	2.13
30	42.9	CH_2	2.13	m	74.9, 28.6-27.8, 25.3	6.30, 1.45
31	74.9	$CHCl_2$	6.30	m	25.30	2.13

[a]from proton to indicated carbon, [b]extracted from HMBC.

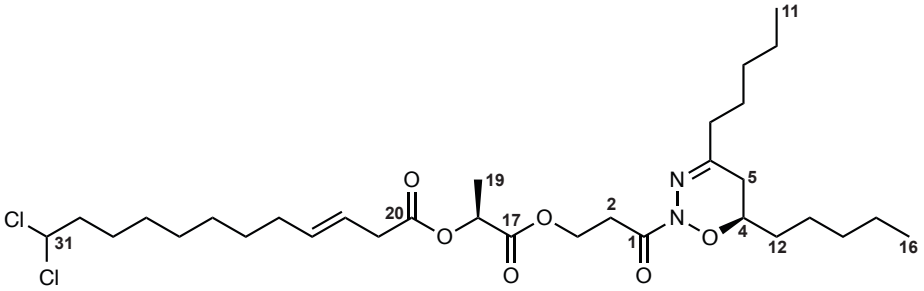

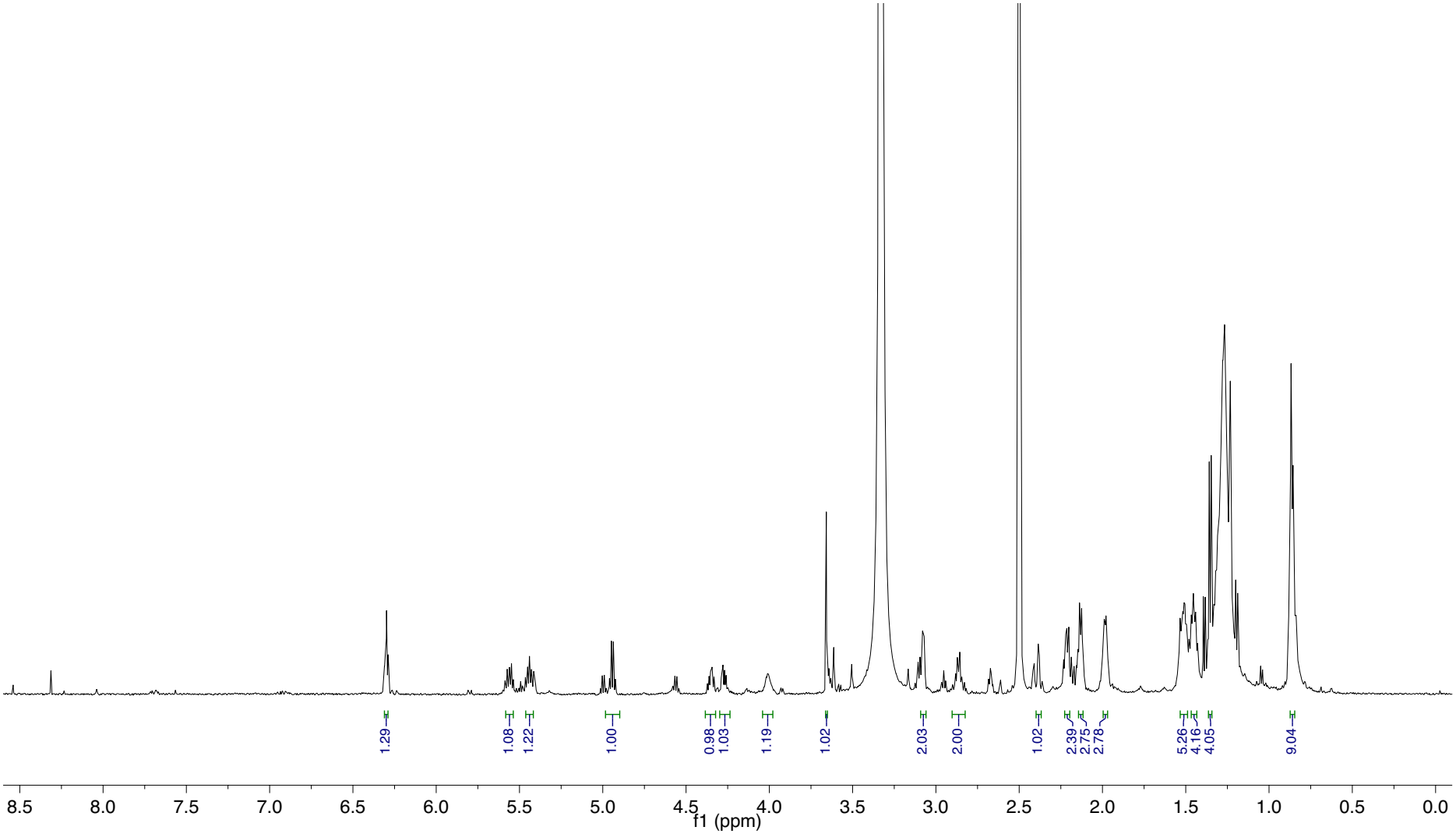

Figure S27. ^{1}H NMR (DMSO-d_6, 600 MHz) spectrum of compound **11**.

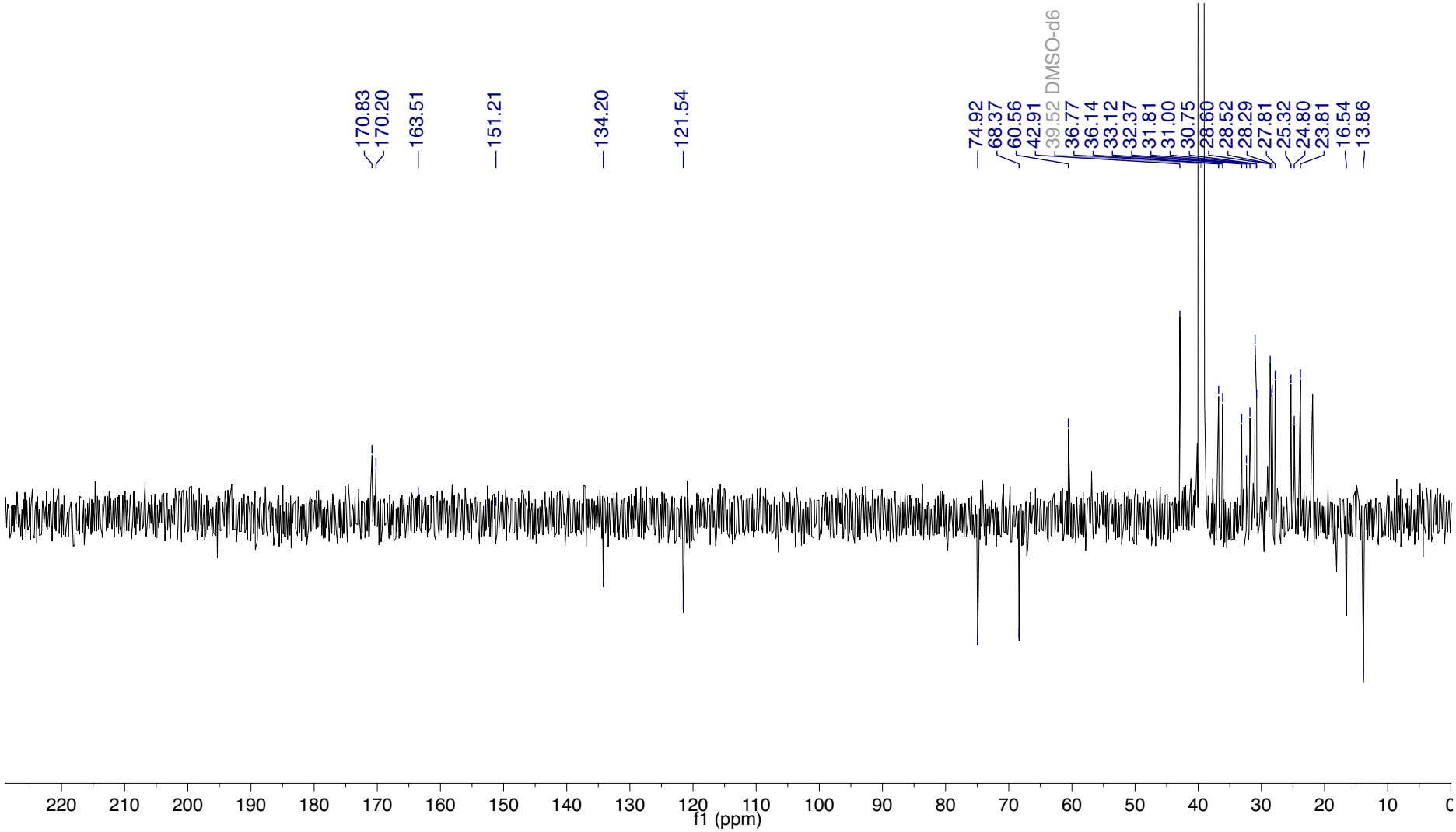

Figure S28. ^{13}C NMR (APT, DMSO-d_6, 150 MHz) spectrum of compound **11**.

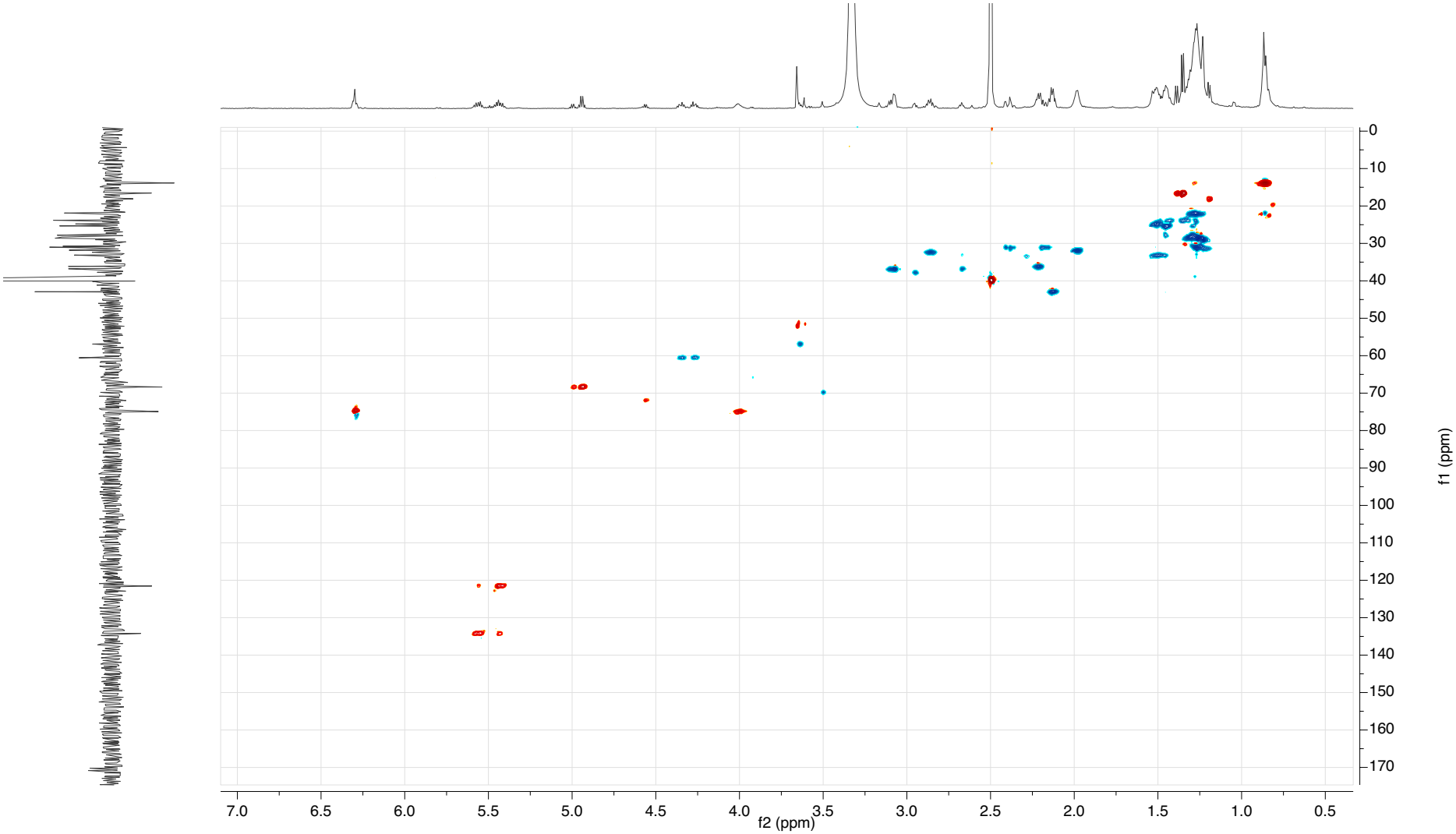

Figure S29. HSQC (DMSO-d_6, 600 MHz) spectrum of compound **11**.

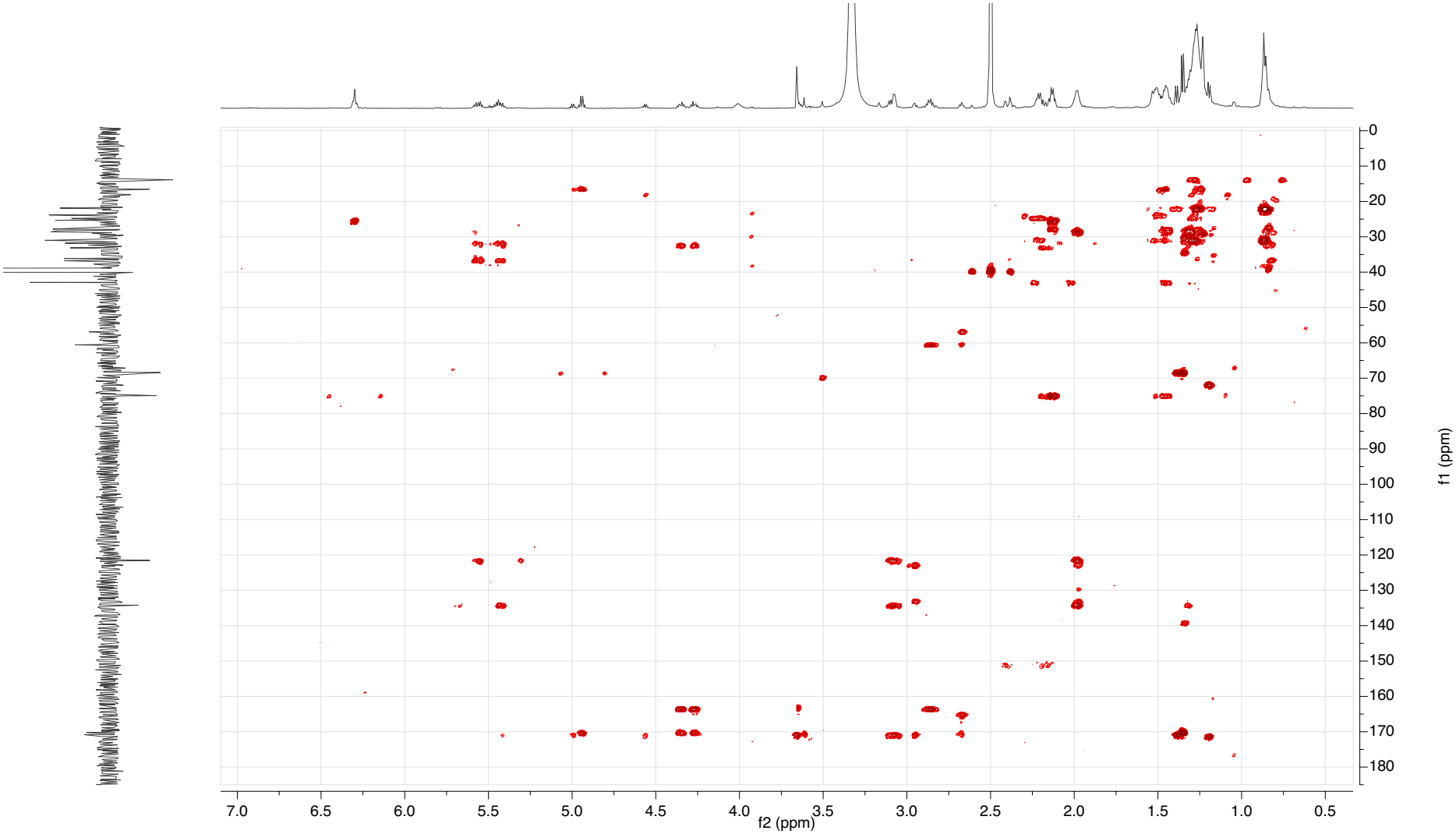

Figure S30. HMBC (DMSO-d_6, 600 MHz) spectrum of compound **11**.

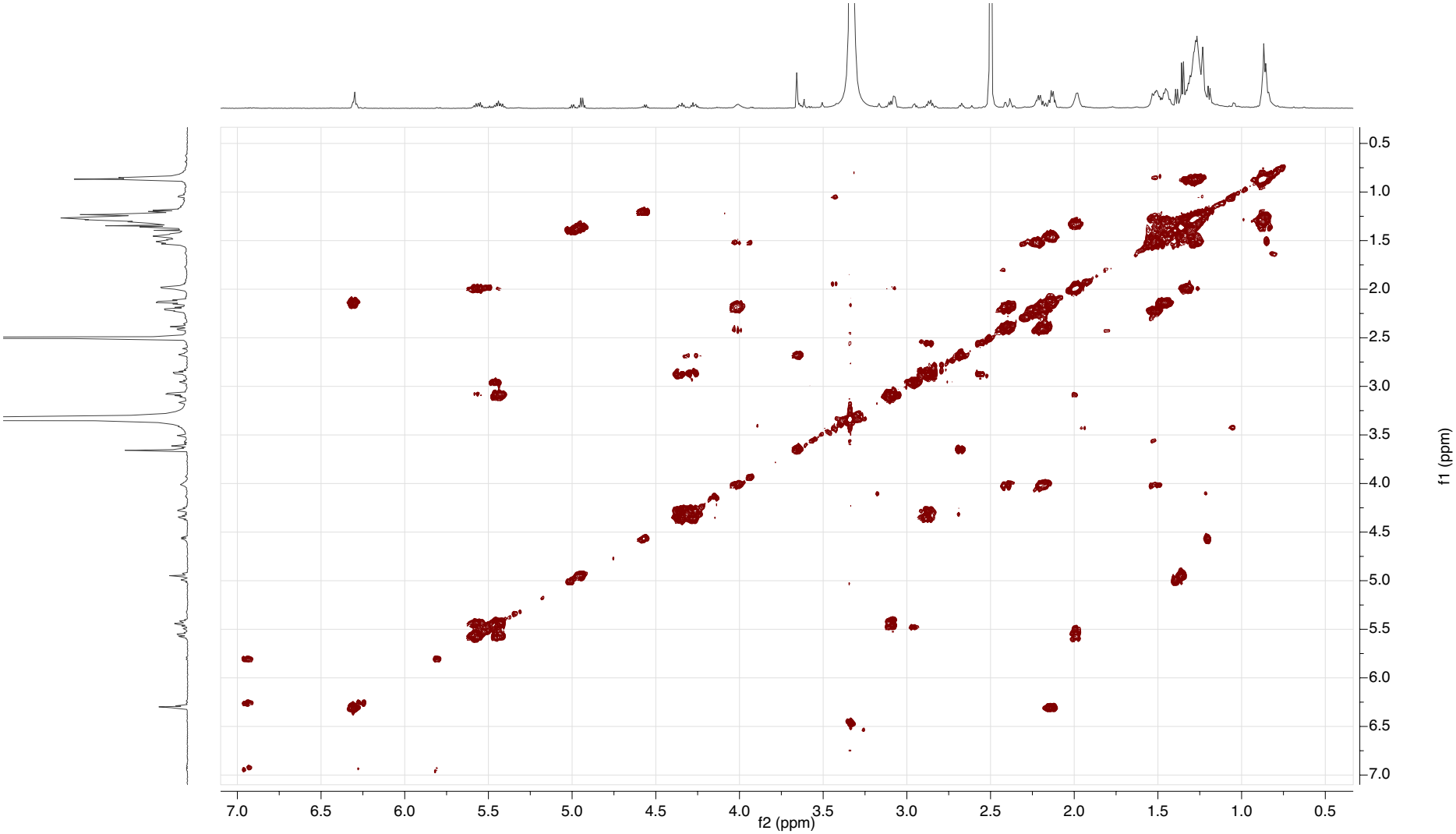

Figure S31. COSY (DMSO-d_6, 600 MHz) spectrum of compound **11**.

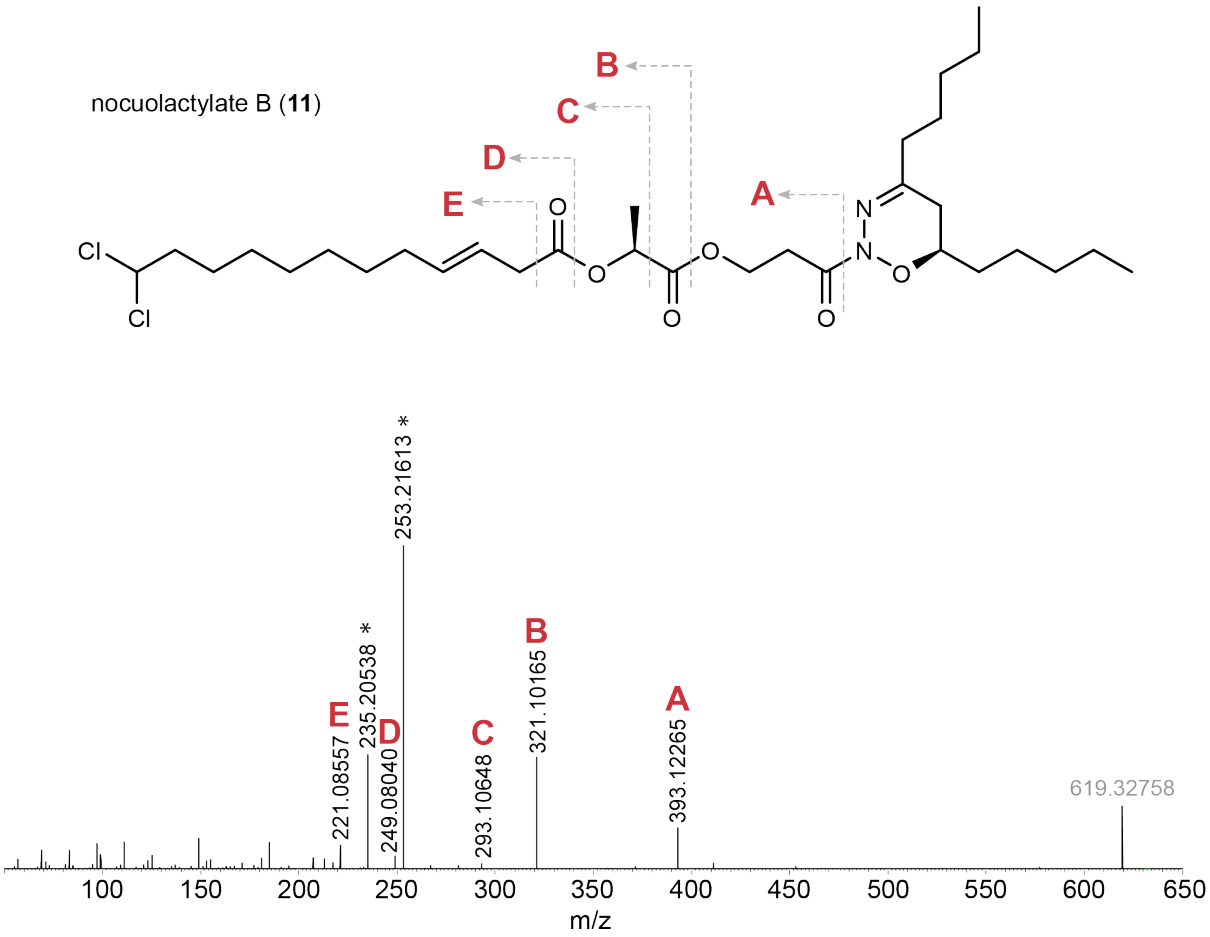

Figure S32. HRESIMS/MS analysis of compound **11**. Asterisks denote major fragments present in all nocuolactylates which result from fragmentation of the **1**-derived portion of the nocuolactylates and likely involve subsequent oxadiazine ring opening, rearrangement and concomitant N_2 loss, as proposed previously for **1**, where these fragmentations were also observed.[28]

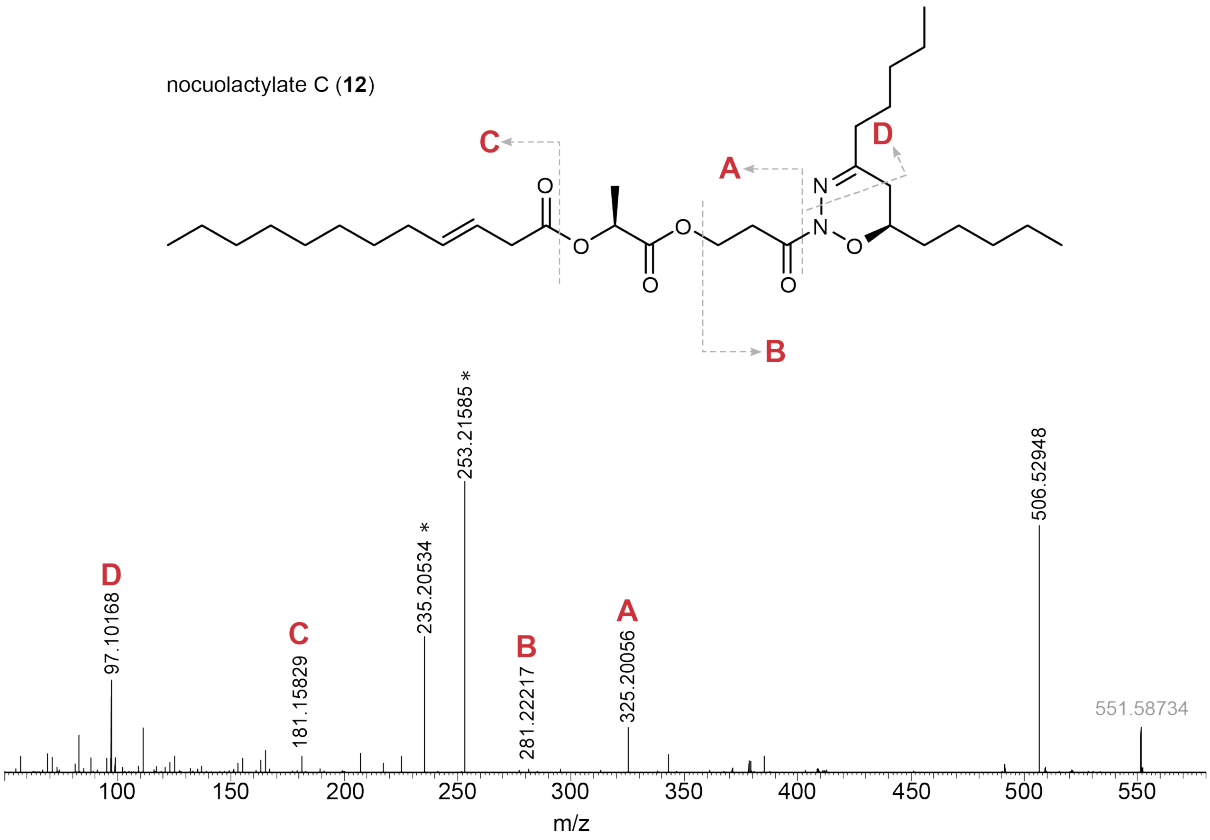

Figure S33. HRESIMS/MS analysis of compound **12**. Asterisks denote major fragments present in all nocuolactylates which result from fragmentation of the **1**-derived portion of the nocuolactylates and likely involve subsequent oxadiazine ring opening, rearrangement and concomitant N_2 loss, as proposed previously for **1**, where these fragmentations were also observed.[28]

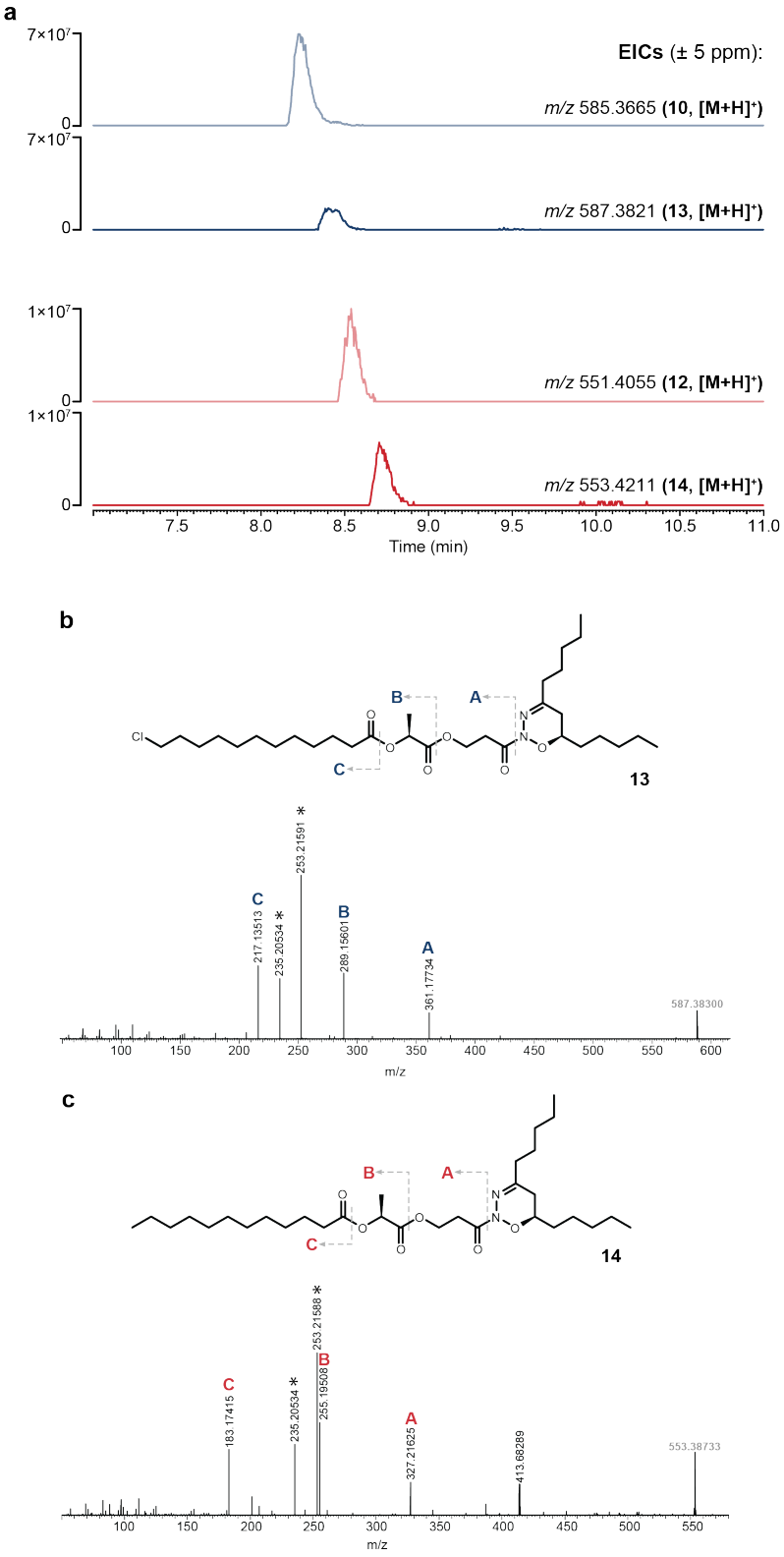

Figure S34. Detection and MS/MS analysis of nocuolactylates D (**13**) and E (**14**). LC-HRESIMS analysis of extracts from *Nodularia* sp. LEGE 06071 cultures (a) indicates the presence of minor saturated analogues of nocuolactylates **10** and **12**, respectively **13** and **14**, as corroborated by analysis of the MS/MS spectra for **13** (b) and **14** (c). Asterisks denote major fragments present in all nocuolactylates which result from fragmentation of the **1**-derived portion of the nocuolactylates and likely involve subsequent oxadiazine ring opening, rearrangement and concomitant N_2 loss, as proposed previously for **1**, where these fragmentations were also observed.[28]

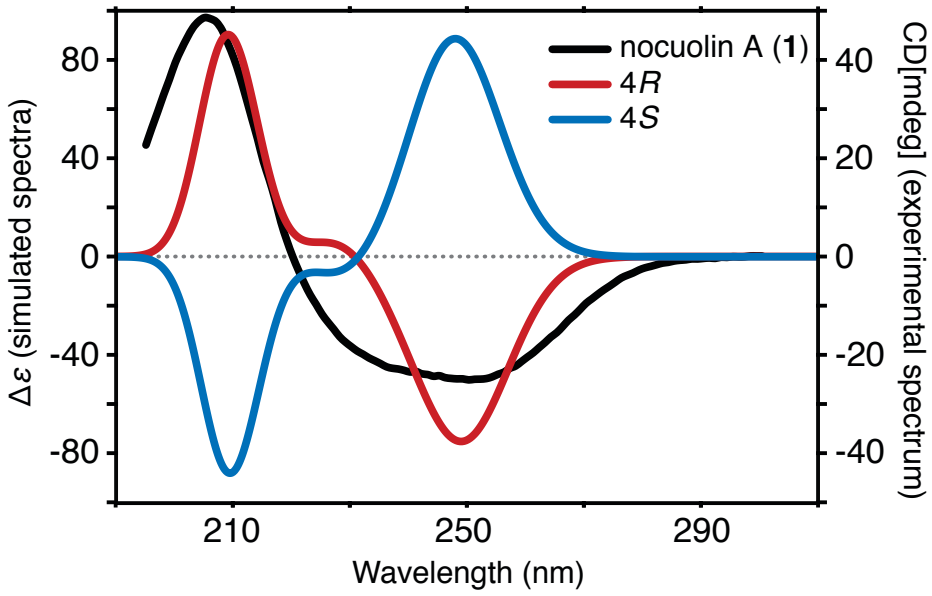

Figure S35. Determination of the absolute configuration of nocuolin A (**1**) using ECD. Experimental ECD spectrum of **1** and simulated ECD spectra of the two possible enantiomers.

Name: ctg19_62_PKS_KR.1
Type: aSDomain
Length: 588
Interval: 45,559 -> 46,146
Bases: GGAGTCTATTTAATCACTGGT...
ASF: KR domain putatively catalyzing L-configuration product formation
ASF: catalytic triad S,Y,N found: True
aSDomain: PKS_KR
aSTool: nrps_pks_domains
database: nrpspksdomains.hmm
detection: hmmscan
domain_id: nrpspksdomains_ctg19_62_PKS_KR.1
evalue: 6.80 × 10 -46
locus_tag: ctg19_62
protein_end: 1,802
protein_start: 1,606
score: 148.2
specificity: KR stereochemistry: (unknown)
specificity: KR activity: active
tool: antismash
translation:
GVYLITGGLGGIGVKIARYLLEHYQARLLLIGRTPLPDESTWENYQEGEDKLSAKIQAYQQLRQLPGS
VLYQAVDIC
NLDDMKQTLNLVSSQWKTQFDGVIHLAGGLPEHLIASETKESLIAGLQQKVMGSWVLHHLLQNQNP
GFFIHFSSVNSFFGGTGVGAYAAA
NSFQEAFSTYQRQHSSWQSYCLSWSMWDET
NCBI Feature Key: aSDomain

Figure S36. Bioinformatics-derived determination of the configuration of the lactyl stereocenter in the nocuolactylates. Stereochemistry of the lactylate portion. Annotation of the KR domain from antiSMASH v.5.0, highlighting the Active Site Finder-tool prediction of an L-configuration for its catalysis product.

Table S6. Cytotoxicity of nocuolactylates A (**10**), B (**11**) and nocuolin A (**1**). IC_{50} and GR_{50} values obtained for two independent assays. Paclitaxel was used as a control.

	IC_{50} (μM)							
	compound 10		**compound 11**		**compound 1**		**Paclitaxel**	
HCMEC	0.77	11.90	4.84	13.90	2.10	1.33	0.0166	0.0559
HCT116	7.15	7.06	4.35	7.74	1.00	1.44	0.0101	0.0153
MCF7	4.15	3.18	2.15	22.20	2.15	0.62	0.1740	0.0172
MG63	8.26	10.60	10.5	6.05	0.74	0.78	0.0705	0.3340

	GR_{50} (μM)							
	compound 10		**compound 11**		**compound 1**		**Paclitaxel**	
HCMEC	6.34	5.46	6.39	5.37	0.78	0.91	0.0028	0.0072
HCT116	3.18	2.62	2.93	4.45	0.69	0.40	0.0062	0.0103
MCF7	1.60	1.87	0.97	3.63	0.34	0.29	0.0262	0.0480
MG63	3.19	6.39	5.25	4.12	0.49	0.69	0.0257	0.0088

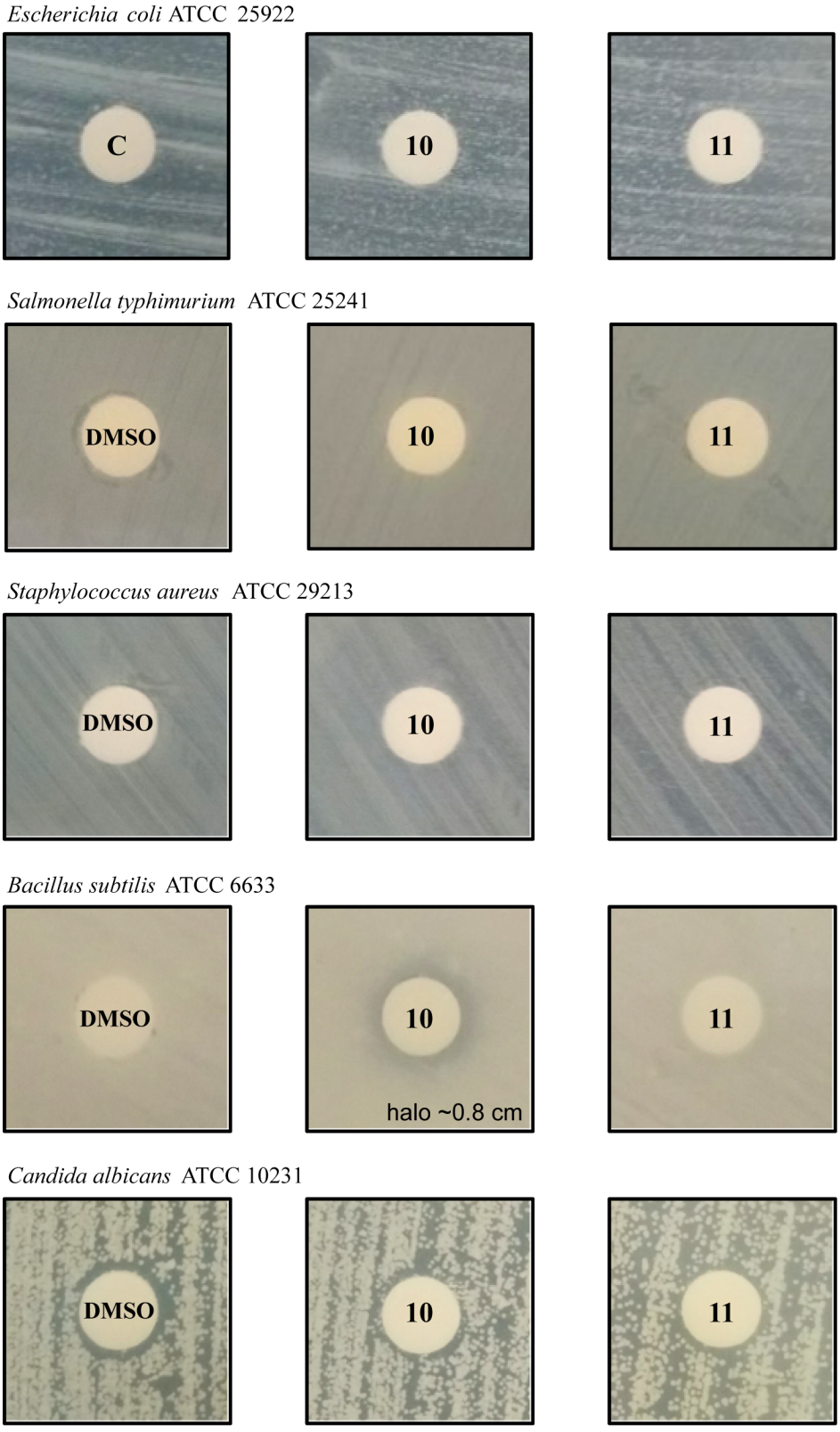

Figure S37. Antimicrobial assays against gram-negative or -positive bacteria and the yeast *Candida albicans*. Fifteen microliters of a 1.0 mg mL^{-1} solution of the test compound (**10** or **11**) were added to the respective disk. For control disks, the same volume of 100% DMSO was added.

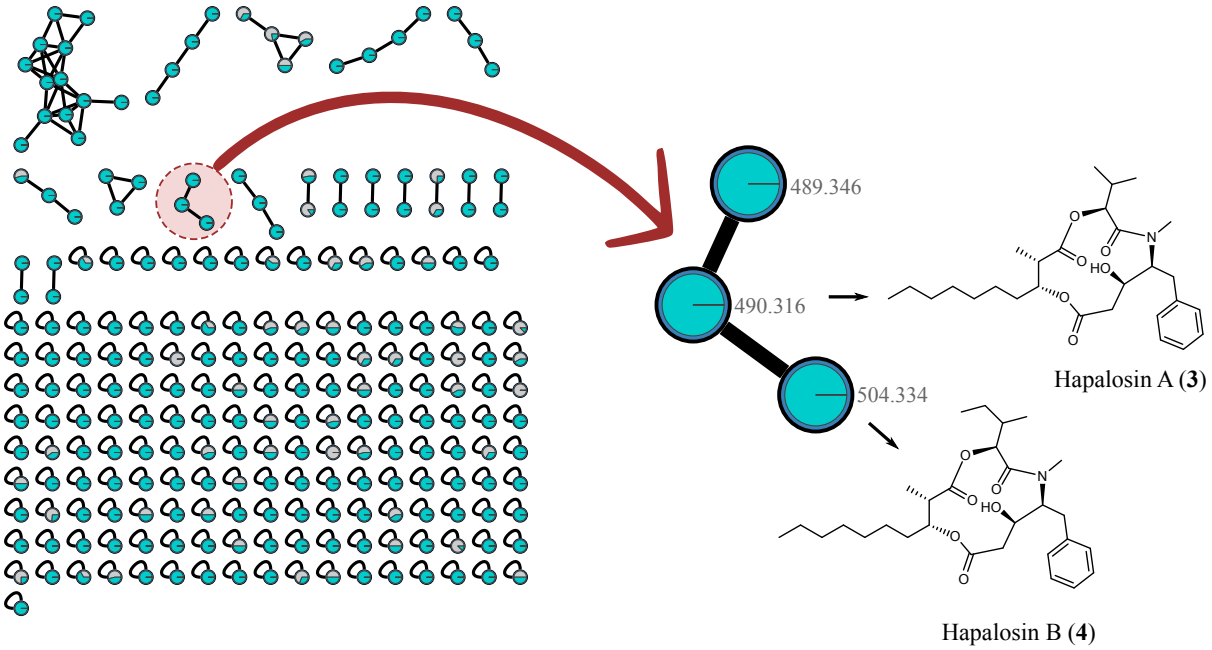

Figure S38. GNPS molecular networking data for a CH_2Cl_2/MeOH (2:1) extract of *Fischerella* sp. PCC 9431. Nodes corresponding to detected hapalosin analogues are highlighted.

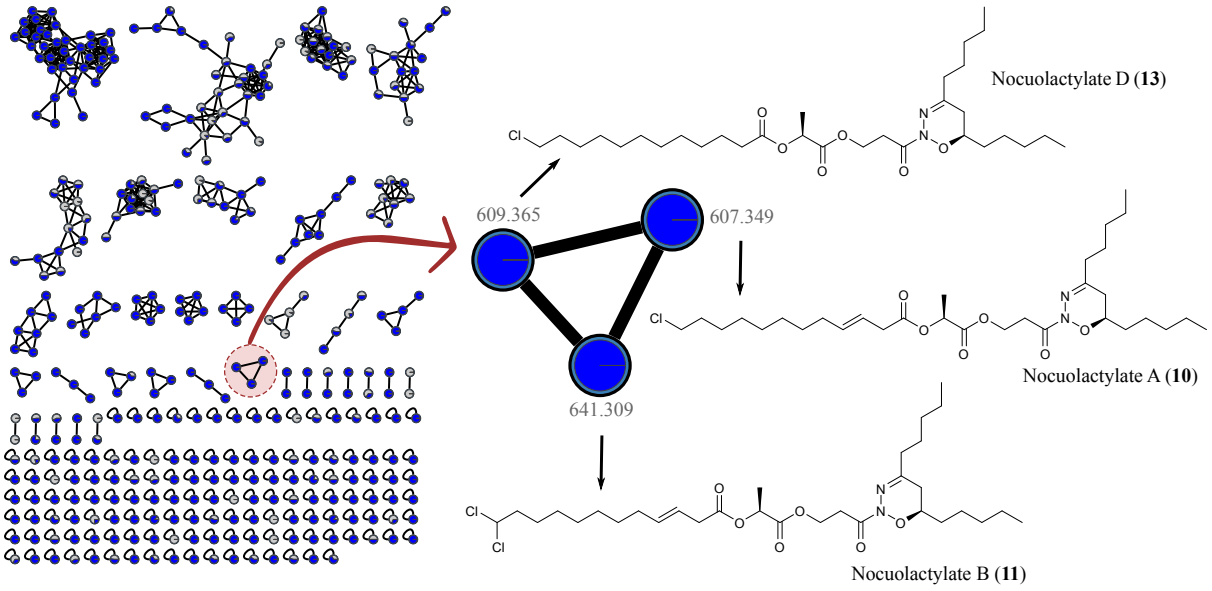

Figure S39. GNPS molecular networking data for a CH_2Cl_2/MeOH (2:1) extract of *Nodularia* sp. LEGE 06071. Nodes corresponding to detected nocuolactylate analogues are highlighted.

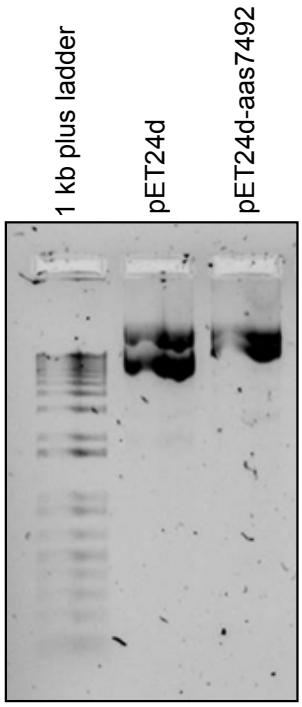

Figure S40. Electrophoresis on agarose gel of isolated plasmid DNA, obtained from *E. coli* BL21 DE3 cells obtained following transformation with either pET24d or pET24d carrying the *aas* gene from *Synechococcus elongatus* PCC 7492.

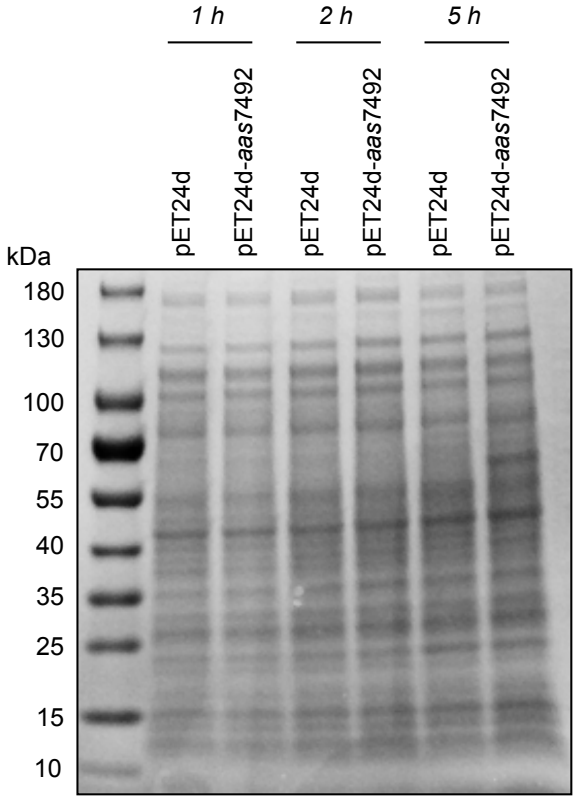

Figure S41. SDS-PAGE analysis of clarified lysates from *E. coli* BL21 DE3 strains harboring pET24d or pET24-*aas*7492. After five hours, overexpression of a protein ~60-70 kDa is observed in *E. coli* cells transformed with pET24-*aas*7492. The *aas*7492 gene encodes a protein of ~71 kDa.

SI References

[1] M. Kanehisa, Y. Sato, M. Kawashima, M. Furumichi, M. Tanabe, *Nucleic Acids Res* **2016**, *44*, D457–D462.

[2] M. Kanehisa, S. Goto, *Nucleic Acids Res* **2000**, *28*, 27–30.

[3] R. C. Edgar, *Nucleic Acids Res* **2004**, *32*, 1792–1797.

[4] M. N. Price, P. S. Dehal, A. P. Arkin, *PLOS ONE* **2010**, *5*, e9490.

[5] D. Kaczmarzyk, M. Fulda, *Plant Physiol.* **2010**, *152*, 1598–1610.

[6] J. C. Meeks, R. W. Castenholz, *Archiv für Mikrobiologie* **1971**, *78*, 25–41.

[7] E. Cequier-Sánchez, R. Covadonga, Á. Ravelo, R. Zárate, *Journal of Agricultural and Food Chemistry* **2008**, *56*, 4297–4303.

[8] T. Pluskal, S. Castillo, A. Villar-Briones, M. Orešič, *BMC Bioinformatics* **2010**, *11*, 1–11.

[9] M. Sud, E. Fahy, D. Cotter, A. Brown, E. A. Dennis, C. K. Glass, A. H. Merrill, R. C. Murphy, C. R. H. Raetz, D. W. Russell, S. Subramaniam, *Nucleic Acids Res* **2007**, *35*, D527–D532.

[10] M. Wang, J. J. Carver, V. V. Phelan, L. M. Sanchez, N. Garg, Y. Peng, D. D. Nguyen, J. Watrous, C. A. Kapono, T. Luzzatto-Knaan, C. Porto, A. Bouslimani, A. V. Melnik, M. J. Meehan, W.-T. Liu, M. Crüsemann, P. D. Boudreau, E. Esquenazi, M. Sandoval-Calderón, R. D. Kersten, L. A. Pace, R. A. Quinn, K. R. Duncan, C.-C. Hsu, D. J. Floros, R. G. Gavilan, K. Kleigrewe, T. Northen, R. J. Dutton, D. Parrot, E. E. Carlson, B. Aigle, C. F. Michelsen, L. Jelsbak, C. Sohlenkamp, P. Pevzner, A. Edlund, J. McLean, J. Piel, B. T. Murphy, L. Gerwick, C.-C. Liaw, Y.-L. Yang, H.-U. Humpf, M. Maansson, R. A. Keyzers, A. C. Sims, A. R. Johnson, A. M. Sidebottom, B. E. Sedio, A. Klitgaard, C. B. Larson, C. A. Boya P, D. Torres-Mendoza, D. J. Gonzalez, D. B. Silva, L. M. Marques, D. P. Demarque, E. Pociute, E. C. O'Neill, E. Briand, E. J. N. Helfrich, E. A. Granatosky, E. Glukhov, F. Ryffel, H. Houson, H. Mohimani, J. J. Kharbush, Y. Zeng, J. A. Vorholt, K. L. Kurita, P. Charusanti, K. L. McPhail, K. F. Nielsen, L. Vuong, M. Elfeki, M. F. Traxler, N. Engene, N. Koyama, O. B. Vining, R. Baric, R. R. Silva, S. J. Mascuch, S. Tomasi, S. Jenkins, V. Macherla, T. Hoffman, V. Agarwal, P. G. Williams, J. Dai, R. Neupane, J. Gurr, A. M. C. Rodríguez, A. Lamsa, C. Zhang, K. Dorrestein, B. M. Duggan, J. Almaliti, P.-M. Allard, P. Phapale, L.-F. Nothias, T. Alexandrov, M. Litaudon, J.-L. Wolfender, J. E. Kyle, T. O. Metz, T. Peryea, D.-T. Nguyen, D. VanLeer, P. Shinn, A. Jadhav, R. Müller, K. M. Waters, W. Shi, X. Liu, L. Zhang, R. Knight, P. R. Jensen, B. Ø. Palsson, K. Pogliano, R. G. Linington, M. Gutiérrez, N. P. Lopes, W. H. Gerwick, B. S. Moore, P. C. Dorrestein, N. Bandeira, *Nat Biotech* **2016**, *34*, 828–837.

[11] R. Adusumilli, P. Mallick, in *Proteomics: Methods and Protocols* (Eds.: L. Comai, J.E. Katz, P. Mallick), Springer, New York, NY, **2017**, pp. 339–368.

[12] P. Shannon, A. Markiel, O. Ozier, N. S. Baliga, J. T. Wang, D. Ramage, N. Amin, B. Schwikowski, T. Ideker, *Genome Res.* **2003**, *13*, 2498–2504.

[13] J. Kotai, *Norwegian Institute for Water Research, Blindern, Oslo* **1972**, *11/69*, 5 pp.

[14] N. M. O'boyle, A. L. Tenderholt, K. M. Langner, *J. Comput. Chem.* **2008**, *29*, 839–845.

[15] Y. Binev, M. M. B. Marques, J. Aires-de-Sousa, *J. Chem. Inf. Model.* **2007**, *47*, 2089–2097.

[16] A. M. Castillo, L. Patiny, J. Wist, *Journal of Magnetic Resonance* **2011**, *209*, 123–130.

[17] S. P. Singh, R. P. Rastogi, D.-P. Häder, R. P. Sinha, *World J Microbiol Biotechnol* **2010**, *27*, 1225–1230.

[18] A. Bankevich, S. Nurk, D. Antipov, A. A. Gurevich, M. Dvorkin, A. S. Kulikov, V. M. Lesin, S. I. Nikolenko, S. Pham, A. D. Prjibelski, A. V. Pyshkin, A. V. Sirotkin, N. Vyahhi, G. Tesler, M. A. Alekseyev, P. A. Pevzner, *Journal of Computational Biology* **2012**, *19*, 455–477.

[19] A. Gurevich, V. Saveliev, N. Vyahhi, G. Tesler, *Bioinformatics* **2013**, *29*, 1072–1075.

[20] T. A. Halgren, *J. Comput. Chem.* **1996**, *17*, 490–519.

[21] J. W. Ponder, *TINKER – Software Tools for Molecular Design*, **1990**.

[22] C. E. Kundrot, J. W. Ponder, F. M. Richards, *J. Comput. Chem.* **1991**, *12*, 402–409.

[23] *Gaussian 09, Revision D.01*, Gaussian, Inc., Wallingford CT, **2009**.

[24] N. A. Clark, M. Hafner, M. Kouril, E. H. Williams, J. L. Muhlich, M. Pilarczyk, M. Niepel, P. K. Sorger, M. Medvedovic, *BMC cancer* **2017**, *17*, 698.

[25] M. L. Micallef, P. M. D'Agostino, D. Sharma, R. Viswanathan, M. C. Moffitt, *BMC Genomics* **2015**, *16*, 669.

[26] J. Yang, Natural Product Anticancer Drug Discovery and Mechanistic Studies on Hapolosin and Silvestrol, thesis, University of Illinois at Chicago, **2013**.

[27] P. M. D'Agostino, T. A. M. Gulder, *ACS Synth. Biol.* **2018**, *7*, 1702–1708.

[28] K. Voráčová, J. Hájek, J. Mareš, P. Urajová, M. Kuzma, J. Cheel, A. Villunger, A. Kapuscik, M. Bally, P. Novák, M. Kabeláč, G. Krumschnabel, M. Lukeš, L. Voloshko, J. Kopecký, P. Hrouzek, *PLOS ONE* **2017**, *12*, e0172850.

[29] M. O. Hunsen, in *Comprehensive Heterocyclic Chemistry III* (Eds.: A.R. Katritzky, C.A. Ramsden, E.F.V. Scriven, R.J.K. Taylor), Elsevier, Oxford, **2008**, pp. 291–299.

[30] Y. Inokuma, T. Ukegawa, M. Hoshino, M. Fujita, *Chem. Sci.* **2016**, *7*, 3910–3913.

[31] E. Danelius, S. Halaby, W. A. van der Donk, T. Gonen, *Nat. Prod. Rep.* **2021**, 10.1039.D0NP00035C.